

# **For Reference**


---

**NOT TO BE TAKEN FROM THIS ROOM**



Ex LIBRIS  
UNIVERSITATIS  
ALBERTAENSIS





Digitized by the Internet Archive  
in 2022 with funding from  
University of Alberta Library

<https://archive.org/details/Park1978>









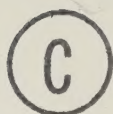




THE UNIVERSITY OF ALBERTA

A VIBRATING SAMPLE MAGNETOMETER AND THE  
ROCK MAGNETIC PROPERTIES OF OLIVINES

by



JOHN K. PARK

A THESIS

SUBMITTED TO THE FACULTY OF GRADUATE STUDIES AND RESEARCH  
IN PARTIAL FULFILMENT OF THE REQUIREMENTS FOR THE DEGREE  
OF MASTER OF SCIENCE

IN

GEOPHYSICS

DEPARTMENT OF PHYSICS

EDMONTON, ALBERTA

FALL, 1978







## ABSTRACT

A vibrating-sample magnetometer for general rock magnetic investigations was designed, constructed, and tested. Its principal features include a geophone drive system, a cubic eight coil detection array cooled by liquid nitrogen, and an oven (0 to 750°C) with forced air cooling system (outside temperature <40°C). It is constructed on a 4" commercial electromagnet presently delivering 5.7 kOe (10 kOe possible). It is capable of measuring natural samples containing magnetite. Measurement of red hematite sediments is not presently practical, but should prove possible with certain improvements.

Tests involving hysteresis and thermomagnetic measurements were conducted. Hysteresis curves obtained for iron and nickel were proved to be valid after the slope method of calibration using a pure iron sample was used to determine the magnetization of an ultrapure nickel sample ( $481 \pm 14$  vs. 484.1 gauss from the literature). Curves of single-domain (sd) magnetite yielded a  $J_r/J_s$  (saturation remanence/saturation magnetization) value of slightly less (0.46 and  $0.47 \pm 0.01$ ) than the theoretical value (0.5). Thermomagnetic tests were conducted using magnetite and nickel. Determined Curie points ( $586 \pm 5^\circ\text{C}$  and  $375 \pm 4^\circ\text{C}$ ) agreed within error with values given in the literature. Sample positioning is not critical. For





samples positioned within  $\pm 0.6$  cm of the centre of the coils the loss of signal is within 1%, and for each  $\pm 0.2$  cm displacement out to  $\pm 0.6$  cm the change in temperature is  $1^{\circ}\text{C}$  or less.

Finely divided synthetic olivines with fayalite components of 30 (FA30), 50 (FA50), and 90% (FA90) were oxidized for effective times of  $\approx 4920$ , 8015, and 8008 minutes respectively in an oxygen atmosphere and 10 Oe field at  $500 \pm 5^{\circ}\text{C}$ ; and magnetic, chemical, X-ray, and optical tests performed to determine the magnetic phases present, their mode of occurrence, and how they changed with time. A chemical remanent magnetization (CRM) was acquired by all three compositions. In the case of FA30 and FA90 the behaviour of the CRM curves was consistent with the growth of magnetite from superparamagnetic to sd, and then to pseudo-single-domain size. Hematite and probable magnetite, but no magnesioferrite, were detected; the hematite increasing with the iron content of the olivine and the magnetite decreasing. Hematite occurs at least (1) as discontinuous rims in FA90 grains with little or no intermixture of magnetite, (2) in the cores of FA50 grains, and (3) sporadically as rims in FA30 grains. Magnetite was tentatively identified in all three compositions by magnetic methods. The overall magnetic stabilities of FA50 are apparently lower than FA30 and much lower than FA90. Magnetic





properties vary locally in FA90. CRM intensities in basic igneous rocks are typically two or three orders of magnitude larger than those produced in the present experiments. These results strongly suggest therefore that the CRM produced at low temperatures ( $<500^{\circ}\text{C}$ ) in nature will not be paleomagnetically important.





## ACKNOWLEDGEMENTS

It is a pleasure to acknowledge the invaluable assistance of the following people.

First, and foremost, I am grateful for the guidance and help given by my thesis adviser, Dr. M.E. Evans.

The following people provided major assistance in this undertaking. Mr. M. Burke provided the original idea for the seismometer drive as well as the seismometer itself, and provided helpful discussion on some electronics topics. Mr. V. Frnoch spent much time with a great deal of patience in photographing the VSM components and the olivine polished sections. Mr. T. Valian gave valuable advice on materials and low temperature topics, loaned his coil-winding apparatus, and kindly joined the wires of my thermocouple. Mr. I. Morrison gave unstintingly of his time in helping to solve some of the electronic noise problems concerning the VSM. Mr. P. Lea of the Technical Services Glass Blowing Shop was responsible for fashioning all the silica parts of the VSM, for constructing most of the oven, and for making the silica holders for the olivine samples. His expert advice on aspects of design was appreciated. I am grateful to Mr. J. Cuthiell for his care and patience in machining the VSM components and calibration samples, and to Mr. N. Riebeek for valuable judgment on





design considerations.

Other people gave of their valuable time and expertise to discrete phases of the work. I am especially grateful to Dr. M.L. Wayman and Mr. B. Snyder of the Mineral Engineering Department, Dr. M. Dudas of the Soil Science Department and Mr. C. Sullivan of the Geology Department. Dr. Wayman supplied and analyzed the nearly-pure iron for the calibration samples, and helped in obtaining scanning electron photomicrographs of the olivine grains. Dr. Dudas kindly analyzed the olivine samples by X-ray diffraction, and offered advice on the D-C-B method of chemical leaching. X-ray diffraction work was also carried out by Mr. Snyder. Mr. Sullivan showed much patience and optimism in making polished thin sections of the extremely fine-grained olivine samples.

The following people kindly loaned equipment. Drs. J.S. Rogers, R.F. Egerton and S.B. Woods loaned electronic equipment for use with the VSM. Dr. Rogers, in addition, made some valuable comments in general discussion. Dr. Woods was responsible for the design of the detection coils on which the present ones were patterned. Dr. J. Takats of the Chemistry Department loaned his centrifuge.

Special materials came from various sources. Dr. P. Thompson kindly supplied the pure nickel used for the





calibration samples. The machinable glass ceramic came from Dr. G.L. Cumming. Dr. G. Hoyer made available his synthetic olivine samples for the olivine work, and also provided insight into experimental procedures.

Other helpful assistance was rendered by Mr. W. Volk, Mr. G. Mannes, Mr. W. Siewert and Mr. B. Haverstock of Technical Services. Dr. P. Davis helped to familiarize me with the VSM set up in one of the undergraduate laboratories.





## TABLE OF CONTENTS

CHAPTER	PAGE
1. INTRODUCTION	1
Purpose of Study	1
Why Construct a VSM as Opposed to other Instruments?	2
Why Study Olivines?	3
Organization of Thesis	5
2. DESIGN AND CONSTRUCTION OF THE VSM	7
Objectives and Constraints	7
General Operation of the VSM	8
Signal Detection System	13
Vibrating Drive Mechanism	18
Vibrating Rod and Sample Holders	27
Heating and Cooling System	31
Pole Covers and Attached Detection Coils	38
3. TESTING AND CALIBRATION OF THE VSM	45
Introduction	45
Monitoring the Signal	45
Testing the Heating and Cooling System	53
Hysteresis and Thermomagnetic Tests	60
Introduction	60
Hysteresis Measurements	63
Thermomagnetic Measurements	73
Measurements of Magnetic Domain State	85
Calibration	87



4. REMANENCE IN OXIDIZED OLIVINES	93
Introduction	93
Early Mineralogical Work	95
The Work of Hoyer	98
Present Work	104
Introduction	104
Procedures, Apparatus, and Experimental Details	105
Grinding of Olivine Samples	105
Oxidation and the Growth of CRM	106
Measurement and Standard Magnetic Procedures	107
Contamination of Samples and their Holders	108
Growth of CRM	114
Model of Oxidized Olivine	117
Identifying the Magnetic Minerals of Oxidized Olivines	118
Optical Microscopy	119
X-ray Diffraction	126
Build-up of IRM	127
AF Demagnetization of CRM	133
Identifying the Mode of Occurrence of the Magnetic Minerals	138
Method of Approach	138
Chemical Treatment using Diammonium Citrate	139
Chemical Treatment by the D-C-B Method	154
Summary of Chemical Work	162





Identifying Changes in the Magnetic Minerals with Oxidation Time	163
Estimates of Quantitative Changes	164
Changes in Stability	167
Changes According to Olivine Composition	170
The Effect of PTRM on the FA50 Samples	175
Verification of Model?	180
Comparison of Present Work with that of Hoyer and Evans	181
5. SUMMARY AND CONCLUSIONS	185
Vibrating Sample Magnetometer	185
Introduction	185
Signal and Sensitivity	185
Hysteresis Tests	188
Thermomagnetic Tests	189
Remanence in Oxidized Olivines	192
Introduction	192
Identity and Occurrence of Magnetic Phases	192
Changes in Magnetic Phases with Oxidation Time	194
Comparison with Work of Hoyer and Evans	196
Application to Paleomagnetism	197

\*\*\*





## BIBLIOGRAPHY

APPENDIX 1.	ELECTROMAGNET	204
APPENDIX 2.	GENERAL USER'S GUIDE TO VSM	205
APPENDIX 3.	DETERMINATION OF $J_r/J_s$ FOR MAGNETITE SAMPLES	211
APPENDIX 4.	CHEMICAL ANALYSIS OF CALIBRATION SAMPLES	221
APPENDIX 5.	CALCULATION OF THE CALIBRATION CONSTANT	222
APPENDIX 6.	BASIC DATA OF NICKEL CALIBRATION SAMPLES	231
APPENDIX 7.	RESUME OF EXPERIMENTAL WORK ON OLIVINES	233
APPENDIX 8.	ESTIMATING THE AMOUNT OF SINGLE DOMAIN HEMATITE IN TERMS OF THE TOTAL POSSIBLE HEMATITE	236



# LIST OF TABLES

Table	Description	Page
1.	Sample Positions During Experimental Runs	52
2.	External Oven Temperature	54
3.	Errors in Temperature Determination	59
4.	Measured Curie Points	83
5.	VSM Calibration Constant ( $K_1$ )	90
6.	Tests of Measurement Repeatability	91
7.	Magnetization of Olivine Prior to Oxidation	109
8.	Composition of Olivine Before and After Oxidation	130
9.	Effect of Diammonium Citrate on the Oxidized Olivine FA30B	143
10.	IRM Properties of Sample FA50C after each Step of Treatment (trt) by the Dithionite-Citrate-Bicarbonate Method	161
11.	Single-Domain Hematite in Sample FA50C	165
12.	Single-Domain Hematite in the Oxidized Olivine Samples of each Composition	166
13.	Magnetic Stability Versus Olivine Composition	173
14.	Remanent Magnetizations of Sample FA50C Produced by Systematic Magnetic Treatments following the Acquisition of CRM at each Oxidation Step	176
15.	Comparison between Magnetic Stabilities of Olivines FA30 (Hoye and Evans) and FA50 (Present Work) with Oxidation Time	178





16.	Comparison between some Magnetic Properties of the Oxidized FA30 Olivine of Hoyer and Evans and that of the Present Work	183
17.	Basic and Derived Data of the Magnetite Samples and Hysteresis Curves used in the Calculation of $J_r/J_s$	216
18.	Chemical Analysis of Calibration Samples	221
19.	Basic and Derived Data of the Iron Calibration Samples and Hysteresis Curves	228
20.	Basic Data of Nickel Calibration Samples	231
21.	Resume of Experimental Work on Olivines	233



## LIST OF FIGURES

Figure	Page
1. General view of the VSM	10
2. Block diagram of the electronic system	12
3. Schematic diagram of the detection coil arrangement and the current produced by changing magnetic flux through the coils as the sample moves from -Z (open arrow) to +Z (solid arrow) during a half cycle	16
4. Outer view of geophone in its holder	20
5. Geophone parts	22
6. Geophone (top), geophone holder (middle), and upper portion of VSM with geophone in place (bottom)	24
7. Schematic longitudinal section of the geophone	26
8. Guide tube/oven (left in top figures) prior to application of Fiberfrax insulation (top left) and after (top right), vibrating rod (right in top figures) without sample holder (top left) and with (top right), regular sample holder (bottom left), and calibration sample holder (bottom right)	29
9. The VSM oven	33
10. Close-up view of lower portion of VSM	37
11. Side views of detection coil holder	40
12. End (top figure) and top (bottom figure) views of the detection coil holder with the coil adjusting screws (M1), adjusting plates (M2), and clamping bolts (M6) labeled	42
13. Single detection coil	44
14. Frequency response of geophone	48





15.	Signal response of detection coils vs. vertical distance (Z) of sample (NI2) from the geometric centre ( $\pm 0.2$ cm) of the detection coil array	51
16.	Temperature gradient in the oven for each of three constant temperatures at the oven centre: (1) 273°C, (2) 410°C, and (3) 585°C	57
17.	Hysteresis loops of three separate magnetite samples: M1 (479 mg), M2 (306 mg), and M3 (28 mg)	65
18.	Hysteresis loop of hematite	67
19.	Hysteresis of nickel calibration samples	69
20.	Hysteresis of iron calibration samples	71
21.	Discontinuous (top) and continuous (bottom) thermomagnetic curves obtained for the magnetite sample, M1	76
22.	Continuous (top) and discontinuous (bottom) thermomagnetic curves obtained for the nickel calibration sample, NI2	78
23.	Comparison of various thermomagnetic curves obtained for magnetite (top) and nickel (bottom)	82
24.	CRM ( $J_r$ , solid curves) as a function of aging time (top) or oxidation time (bottom)	102
25.	IRM build-up curves of sample FA50C for each successive oxidation interval (minutes)	112
26.	Increase of CRM with oxidation time for three olivine compositions	116
27.	Photomicrographs of unoxidized (top) and oxidized (bottom) olivine grains of sample FA30A taken in plane polarized light (top and bottom left) and under crossed nicols (bottom right)	121



28.	Photomicrographs of unoxidized olivine grains of composition FA50 taken in plane polarized light (top) and under crossed nicols (bottom)	123
29.	Photomicrographs of unoxidized (top) and oxidized (bottom) olivine of composition FA90 taken in plane polarized light (left) and under crossed nicols (right)	125
30.	Partial X-ray diffractograms of FA90 olivine: unoxidized (top left), oxidized (middle left), and treated for 29 hours in diammonium citrate following oxidation (bottom left)	129
31.	IRM build-up curves obtained following the last oxidation step on olivines of different compositions	132
32.	AF demagnetization of the CRM of sample FA50C at various stages of oxidation	135
33.	Portions of the curves of AF demagnetization of CRM of sample FA50C (Fig. 32) plotted versus the logarithm of field	137
34.	A model for the chemical leaching of oxidized olivine showing the theoretical effects on the IRM build-up curves of leaching either hematite or magnetite	141
35.	IRM build-up experiment conducted on various parts of the olivine sample, FA90.	145
36.	IRM build-up curves of the oxidized olivine sample FA90A obtained following successive leaching periods in diammonium citrate solution	148
37.	Photomicrographs of the oxidized olivine sample FA30B before (top) and after (bottom) treatment in a diammonium citrate solution for a total of 83.3 hours, taken in plane polarized light (left) and under crossed nicols (right)	151





38.	Photomigraphs of separate portions of the oxidized olivine sample FA90 before (top) and after treatment in a diammonium citrate solution for 6.1 (middle) and 28.8 hours (FA90A, bottom)	153
39.	Scanning electron photomicrographs of separate portions of oxidized FA90 olivine grains before (right) and after (left) treatment in a diammonium citrate solution	156
40.	IRM build-up curves obtained on sample FA50C following successive leaching periods using the dithionite-citrate-bicarbonate method	159
41.	Coercivity of remanence ( $H_{cr}$ ) and median destructive field (MDF) of $^{cr}CRM$ versus oxidation time for the oxidizing olivine sample FA50C	169
42.	IRM (after magnetization in 10 kOe) of oxidized olivine samples versus initial olivine composition	172
43.	The approach to saturation of the normal (solid lines and dots) and reversed (dashed lines, open circles) portions of the hysteresis curves of the magnetite samples (see Fig. 17) as a function of $1/H$	215
44.	Some parameters used in the determination of $J_r$ for the magnetite hysteresis curves	220



## Chapter 1: Introduction

### Purpose of Study

Paleomagnetism is now firmly established as an important branch of the earth sciences; vital for studying global tectonics, the long-term properties of the geomagnetic field, and the earth's core (Nagata 1961, Irving 1964, McElhinny 1973, Stacey and Banerjee 1974). Two fundamental assumptions are implicit in the interpretation of most paleomagnetic data; that the paleomagnetic field through time can be approximated by an axial geocentric dipole, and that the mean direction of the permanent magnetization in rocks at a given site represents the mean direction of the geomagnetic field during the genesis of those rocks. The former assumption involves the macro-evolution of the earth, the latter concerns the micro-evolution of certain rock-forming minerals. The present study is concerned primarily with this latter aspect, and falls naturally into two parts. The first part concerns the design, construction, and testing of an instrument (a vibrating-sample magnetometer or VSM) suitable for studying the magnetic properties of minerals; the second part is an investigation of the remanent magnetic properties of an important class of minerals -- the olivines -- which are paleomagnetically significant but which have been little studied from this standpoint.





## Why Construct a VSM as opposed to other Instruments?

Rock magnetism is concerned with the nature, quantities, and properties of the magnetic minerals occurring in rocks. These characteristics can be determined by a variety of instruments, including VSM's, magnetic balances, and vibrating-coil magnetometers.

The VSM, first constructed by Foner (1956, 1959), works on the principle of the Faraday-Henry Law of electromagnetic induction. A magnetized sample vibrates and induces an e.m.f. in a set of stationary detection coils. Both sample and coils are located between the pole pieces of an electromagnet or within a solenoid. Use of the VSM enables one to determine curves of magnetization ( $J$ ) versus applied field ( $H$ ) (i.e. hysteresis loops). With the addition of an oven and/or low temperature device, curves of  $J$  versus  $T$  (temperature) can also be obtained. Both kinds of measurement provide useful rock magnetic data for mineral identification and for inferring domain states.

The magnetic balance, first constructed by Curie (1895), measures the magnetization induced in a sample located in a magnetic field gradient; the force caused by the gradient being determined by various null methods. Magnetic balances have comparable sensitivities to VSM's, but possess a number of disadvantages; namely, calibration is less easy, sample positioning and centring are generally much more critical, the applied field is less accurately



measurable, they require specially-shaped pole pieces to produce the field gradient, and they are generally less robust, -- for example, they have a fragile suspension system which is very sensitive to draughts. In addition, they are not satisfactory for measuring hysteresis loops. In fact early instruments could only determine Curie points.

The vibrating-coil magnetometer operates on a similar principle to the VSM, but differs in that the detection coils rather than the sample are vibrated. This instrument requires an extremely uniform magnetic field and any effects due to nonuniformities are difficult to allow for. In addition, corrections must be made for the magnetic effects of materials surrounding the stationary sample (Smith 1956, Dwight et al. 1958).

The case for constructing a VSM is therefore quite strong. First, the technology is well known and tested. Second, of those instruments relying on the induction principle, it is the most sensitive. Third, it is reasonably simple to construct. And lastly, it is versatile. It should also be added that constructing one is much less expensive than purchasing the only suitable commercial instrument currently available.

### **Why Study Olivines?**

Basic igneous rocks, which are important carriers of paleomagnetic information, are primarily composed of





pyroxene, plagioclase, and olivine. Pyroxene has been found to contain stable magnetic inclusions which could be deuteric in origin. Evans et al. (1968) showed that the stable remanence of an ancient intrusion in Botswana is carried by exsolved grains of single-domain magnetite in the pyroxene. Hargraves and Young (1969), Murthy et al. (1971), and Wu et al. (1974) presented evidence from other basic rocks that the stable remanence could be carried by ultra-fine single-domain magnetite particles occurring in plagioclase crystals. Mineralogical work by Haggerty and Baker (1967) and Champness (1970) on the olivines has also revealed the presence of small inclusions of magnetite possibly produced by deuteric oxidation at high temperature; however little in the way of accompanying magnetic work was carried out.

One serious problem in determining whether olivine contains a useful stable remanence formed deuterically is that olivine is easily susceptible to later secondary alterations (serpentinization) producing magnetite which could mask the existence of that formed initially. To overcome this difficulty and to control the number of chemical variables involved Hoye and O'Reilly (1973) and Hoye and Evans (1975) carried out magnetic work using synthetic olivines. They studied the properties of various remanent magnetizations in oxidized olivines of composition



(Fe,Mg)<sub>2</sub>SiO<sub>4</sub> (FA30)<sup>1</sup>. They found that the oxidation of non-magnetic olivine produced a magnetic phase which they inferred to be small magnetite inclusions of single- or pseudo-single-domain size, but which they could not identify with certainty. A fuller discussion of the work of these authors -- especially of Hoyer and Evans -- is given in Chapter 4.

The present study extends the work of Hoyer and Evans by using synthetic olivines of other compositions. It seeks to identify the magnetic phase or phases and to describe their nature, occurrence, and properties. Hoyer and Evans concluded that oxidation of olivine-bearing rocks, both deuterically and by later reheating, could produce significant remanent magnetizations in rocks. Therefore it is important to gain a better understanding of the magnetic phases involved.

## Organization of Thesis

The second and third chapters describe the design, construction, and testing of the VSM. Chapter 4 describes the olivine experiments and their results. Chapter 5 evaluates the present VSM and the olivine results and summarizes the conclusions.

---

<sup>1</sup>The (Fe,Mg) series of olivines forms a complete solid solution series between the forsterite (Mg<sub>2</sub>SiO<sub>4</sub>) and fayalite (Fe<sub>2</sub>SiO<sub>4</sub>) end members. In this thesis olivine will be referred to in terms of the molar percentage of fayalite present.



The c.g.s. e.m.u. system has been used throughout. For present purposes this system is most convenient and allows for direct comparison with the referenced works. To convert to S.I. the following convenient relations can be used:

$$1 \text{ e.m.u.} = 10^3 \text{ A/m}$$

$$10^4 \text{ gauss} = 1 \text{ tesla (T)}$$

$$10 \text{ oersted (Oe)} = 10 \text{ gauss (G)} = 1 \text{ mT}$$





## Chapter 2: Design and Construction of the VSM

### Objectives and Constraints

During the construction of this instrument two main objectives were kept in mind: to provide a variable temperature environment up to 750°C and to provide a variable but uniform applied field up to about 10 kOe. Fulfilment of the former objective ideally allows one to determine the Curie (or Néel) points of all the magnetic minerals of interest in paleomagnetic studies. And fulfilment of the latter enables one to obtain hysteresis loops, which are useful for determining the domain state of magnetic minerals. A magnetic field approaching 10 kOe is desirable. Such a field is sufficient to completely saturate magnetite or titanomagnetite -- two major carriers of paleomagnetic information -- but to only partially saturate hematite. Hematite requires from 50 to 100 kOe for complete saturation; but such fields are not practically realized without very large solenoids or superconducting magnets. Nevertheless, a field of 10 kOe does allow one to identify hematite, and such results are useful for comparison with those of other studies which commonly use fields of this magnitude.

The final design was constrained at the outset by the decision to employ a 4 inch electromagnet which was already available in the Physics Department. With this regular but



small size of electromagnet (for details see Appendix 1) a compromise had to be made between a large enough applied field and sufficient working space in the pole gap. The uniformity of the applied field was also a consideration. Tapered pole pieces allow one to obtain a higher field for a given pole gap, but the volume within which the field is uniform is much smaller. Flat, 4 inch (10.16 cm) pole pieces and a pole gap of 1.5 inches (3.81 cm) were chosen as a final compromise.

In what follows a general description of the instrument is first given, and then the various parts and their design are discussed in more detail.

### General Operation of the VSM

Most major parts of the VSM are labelled in Fig. 1 and referred to by letter in the text. A block diagram of the electronic system is shown in Fig. 2. A magnetic sample located in a sample holder at the lower end of a rod (A) is vibrated at a fixed frequency by means of a geophone (B) hooked up to an oscillator and power amplifier (Fig. 2). The vibrating sample induces an e.m.f. in the detecting coils. Signal output from the detecting coils passes to a synchronous detector where harmonics and high frequency noise are attenuated and the fundamental wave amplified and fullwave rectified. A portion of the signal from the oscillator, acting as a reference signal, passes into the







Fig. 1. General view of the VSM. Labeled parts are:

(A) vibrating rod (Fig. 8), (B) geophone drive (Figs. 4, 5, 6 and 7), (C) drive holder (Figs. 4 and 6), (D) support plate, (E) positioning rail, (F) VSM support structure, (G) guide tube (Fig. 8), (H) heating element extension wires, (I) forced air cooling system, (J) electromagnet spacer bars, (K) oven (Fig. 9), (L) pole cover, (M) detection coil holder (Figs. 11 and 12), (N) liquid nitrogen tubes, (O) oven and guide tube support stand (Fig. 10).

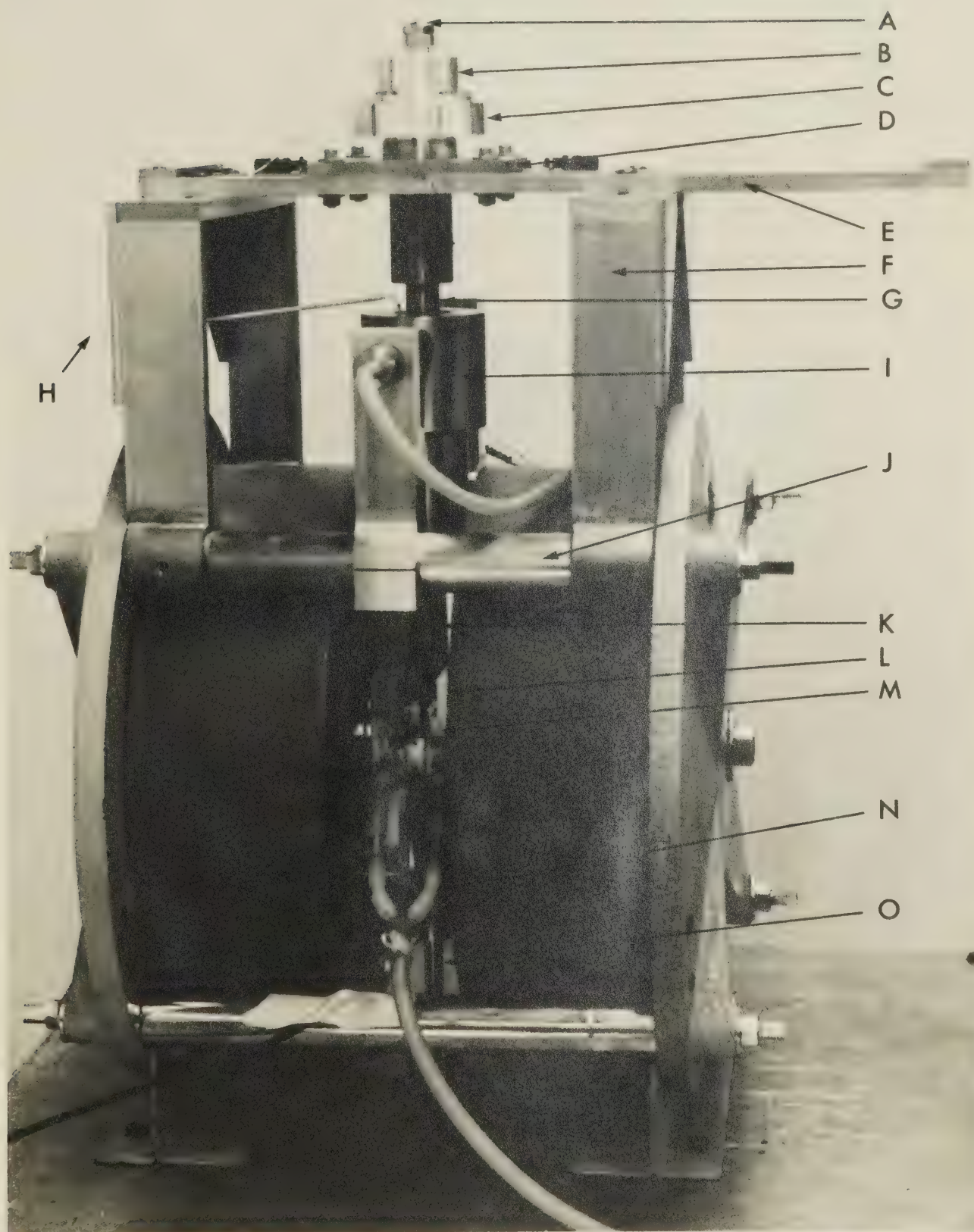
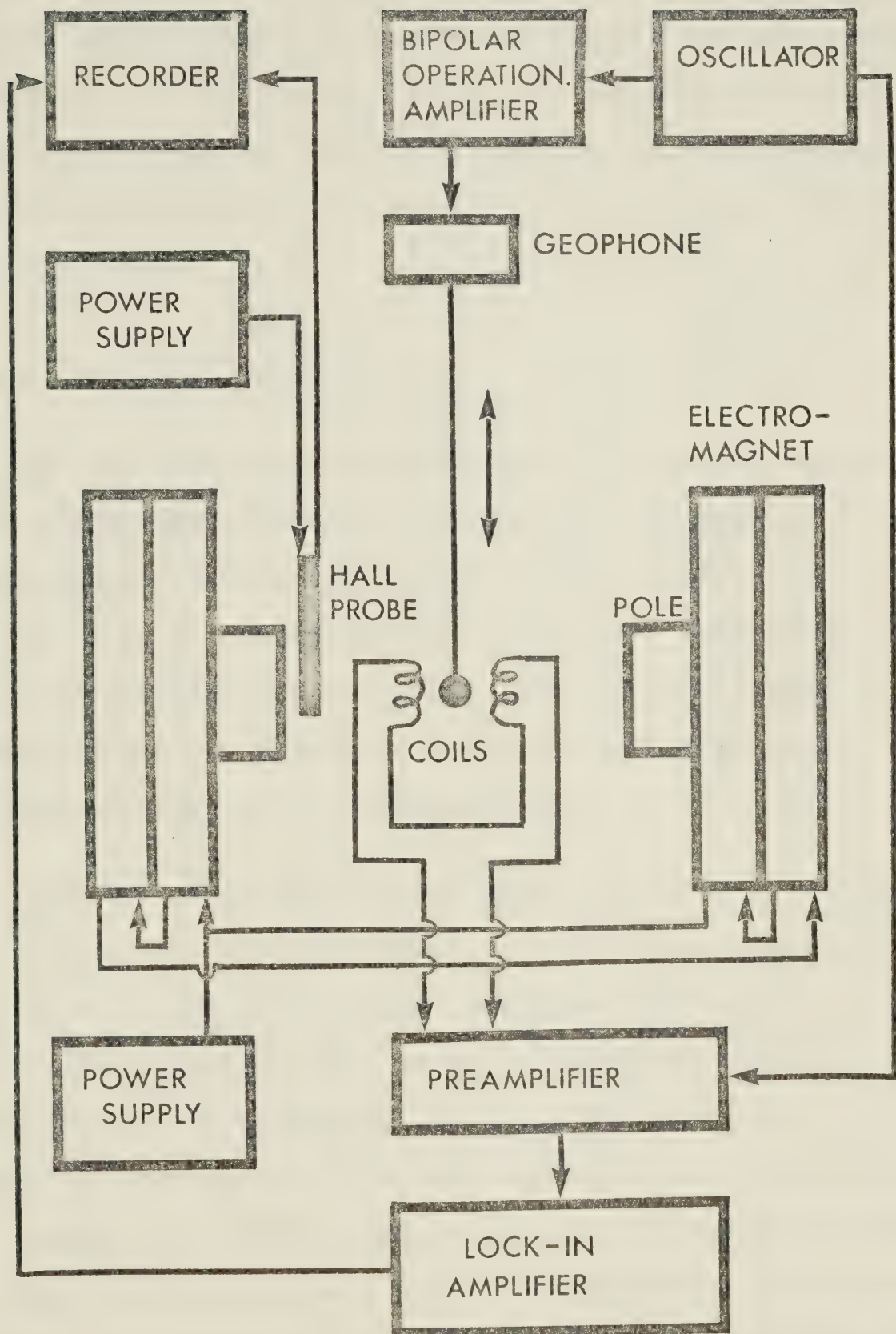








Fig. 2. Block diagram of the electronic system.





synchronous detector (within the lock-in amplifier, Fig. 2). The mean value of the resulting signal, being proportional to the input signal and thus to the magnetic moment of the sample, is fed to one axis of an x-y recorder. The other axis of the recorder is attached either to a Hall probe, measuring the applied field, or to a thermocouple placed near the sample.

### Signal Detection System

In any detecting coil arrangement it is desirable to have a good signal-to-noise ratio and a sensitivity commensurate with the magnitude of the signal to be measured. It was expected that samples for analysis would not only contain magnetite, but also the more weakly magnetic mineral, hematite; hence an instrument with a reasonably high sensitivity was aimed for.

One way of increasing the signal-to-noise ratio is to use a special coil arrangement. The use of but one coil can give a very high sensitivity, but there are decided advantages to using pairs of coils in series arranged either symmetrically or antisymmetrically about the sample. In a symmetric arrangement coils are located at  $+r$  and  $-r$  from the sample centre, are parallel to one orthogonal direction, and are wound in the same sense. Antisymmetric coils are wound in the opposite sense. The net output signal obtained at the geometric centre of either coil arrangement has a





zero voltage gradient. It also possesses saddle points, wherein the signal amplitude remains relatively constant. The antisymmetric coil array has the additional advantage that any background noise caused by magnetic field instability and/or mechanical vibrations of magnet and coils is largely eliminated.

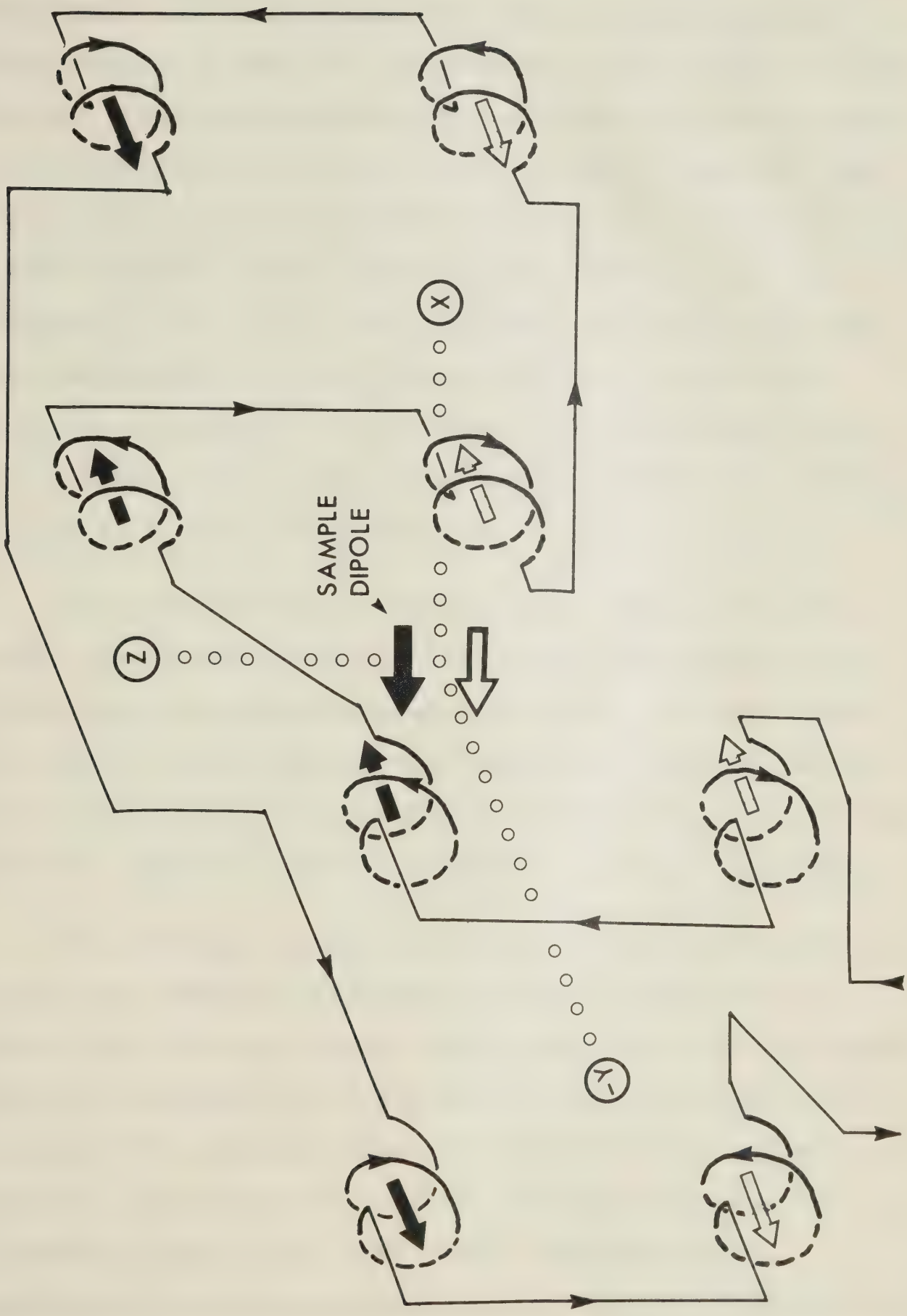
Bowden (1972) investigated three coil configurations which he considered to be the only suitable ones for the VSM. Each has some advantages, but he concluded that a cubic arrangement of eight coils positioned perpendicular to both the applied field and vibrating rod was the most satisfactory. With this configuration the signal does not change sign in any octant; all the directional derivatives of the same degree are equal at the saddle point; there are saddle points for the three principle directions, each component of the signal being about equal in amplitude; and the region about the saddle points at which the signal response is nearly constant is relatively broad compared to other configurations, perhaps an order of magnitude wider. This latter point means that sample positioning is less critical. It was therefore decided to use this coil configuration, which is illustrated schematically in Fig. 3.

There are generally a number of ways to further reduce the noise and enhance the signal. Foner (1974) notes that the best way to gain considerable improvement in sensitivity is to maximize the filling factor, -- the "ratio of the





Fig. 3. Schematic diagram of the detection coil arrangement and the current produced by changing magnetic flux through the coils as the sample moves from -Z (open arrow) to +Z (solid arrow) during a half cycle. X is the applied field direction, Y is parallel to the coil axes, and Z is the direction of sample vibration.







sample volume to the effective coil volume". To increase this ratio one can decrease the coil size, increase the sample size, or move the coils closer to the sample. In the present case the coil size had been fixed very early; being patterned after an earlier instrument which uses the cubic coil configuration. The maximum sample size was fixed by the inside diameter of the vibrating rod; namely, 1 cm. The distance of the coils from the sample was dictated by what was considered to be the minimum diameter of oven which could be installed at the centre of the coil system. Since this diameter was 2.5 cm, the distance between coil centres in the X, Y, and Z directions was set at 2.86 cm.

Two further ways of reducing noise are to cool the coils and to affix them rigidly to the pole pieces (Foner 1974). Both have been carried out and are discussed below. The latter method ensures that mechanical coupling between the vibrating system and coils is essentially eliminated and that the coils do not move relative to the applied field.

The reference signal is obtained directly from the oscillator. However, the VSM was initially designed to obtain its reference signal from a reference coil and magnet system. A reference coil had therefore been incorporated into the VSM design immediately below the drive magnet, where it would coaxially enclose the vibrating rod. The reference signal could then either be induced by a cylindrical reference magnet inserted into the vibrating rod



or obtained directly from the oscillating magnet of the geophone.

### Vibrating Drive Mechanism

Several different drive mechanisms are in use today, including loud speakers and motor drives. Loud speakers have been frequently employed, but these are only suitable for small samples. A particularly successful VSM marketed by Princeton Applied Research (PAR, Princeton, N.J.) uses a transducer consisting of the field magnet and voice coil of a high quality loudspeaker. This mechanism has the following useful advantages: it maintains a constant frequency, it allows sample access through its centre by means of a hole bored through the magnet, and it produces an electromagnetic field which can be used for deriving the reference signal.

The present mechanism is adapted from a very low frequency land geophone (L-1 model, Mark Products, Inc., Houston, Texas). It is shown assembled and disassembled in Figs. 4, 5, and 6, with a schematic cross section depicted in Fig. 7. In normal operation the central magnet mass, outer casing (B3 and B8), and the cylindrical magnet keeper (B4) of the geophone remain stationary, while the intervening coil (B6) vibrates in response to seismic activity. This operation is similar in principle to that of the PAR transducer in which the voice coil is driven by an oscillator/amplifier circuit. In the present operation of





Fig. 4. Outer view of geophone in its holder.



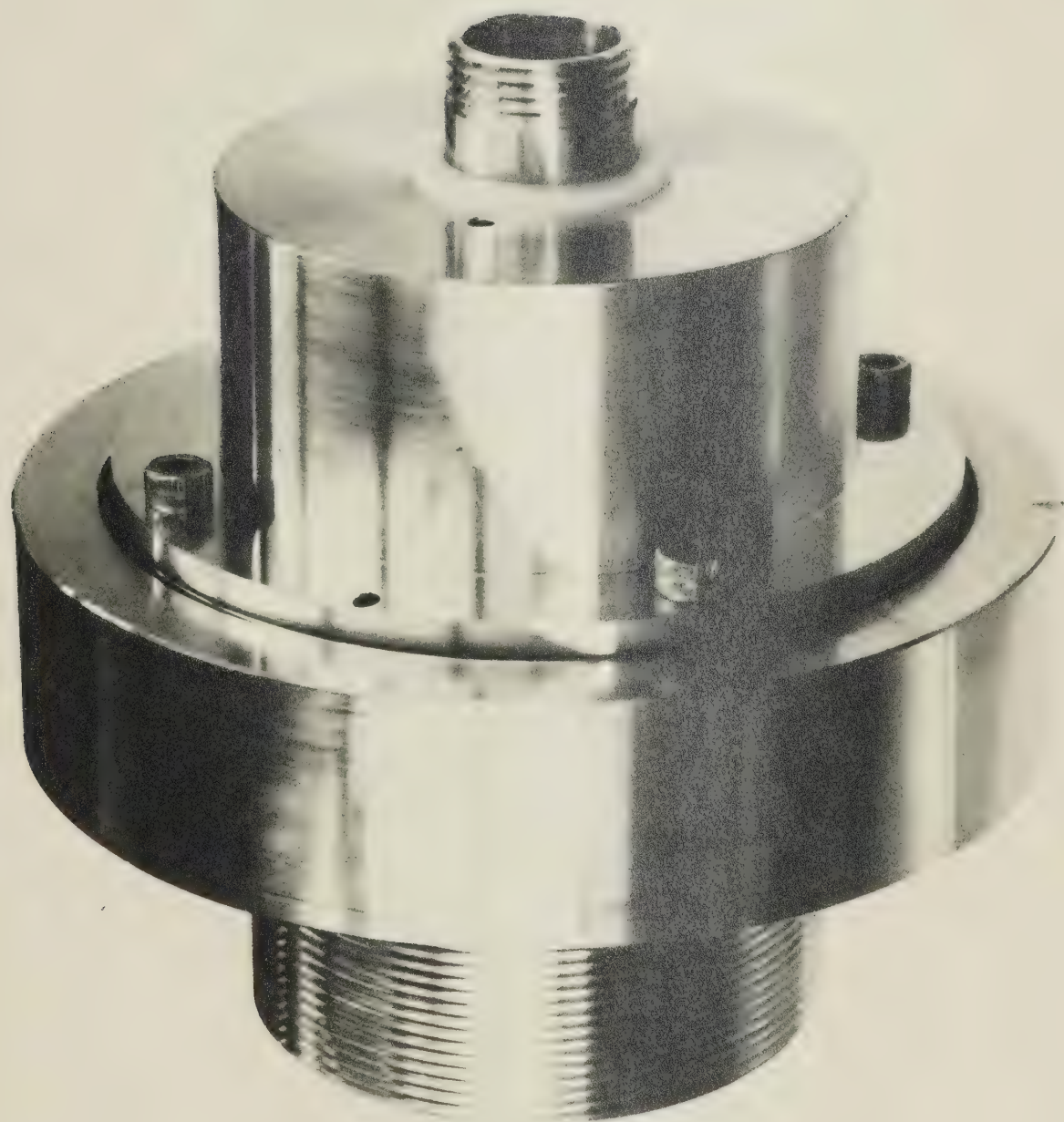






Fig. 5. Geophone parts: teflon bearing (B2), upper housing (B3), magnet keeper (B4), teflon insulators (B5), coil (B6), lower teflon bearing (B7), and lower housing (B8). The magnet is hidden within the coil.

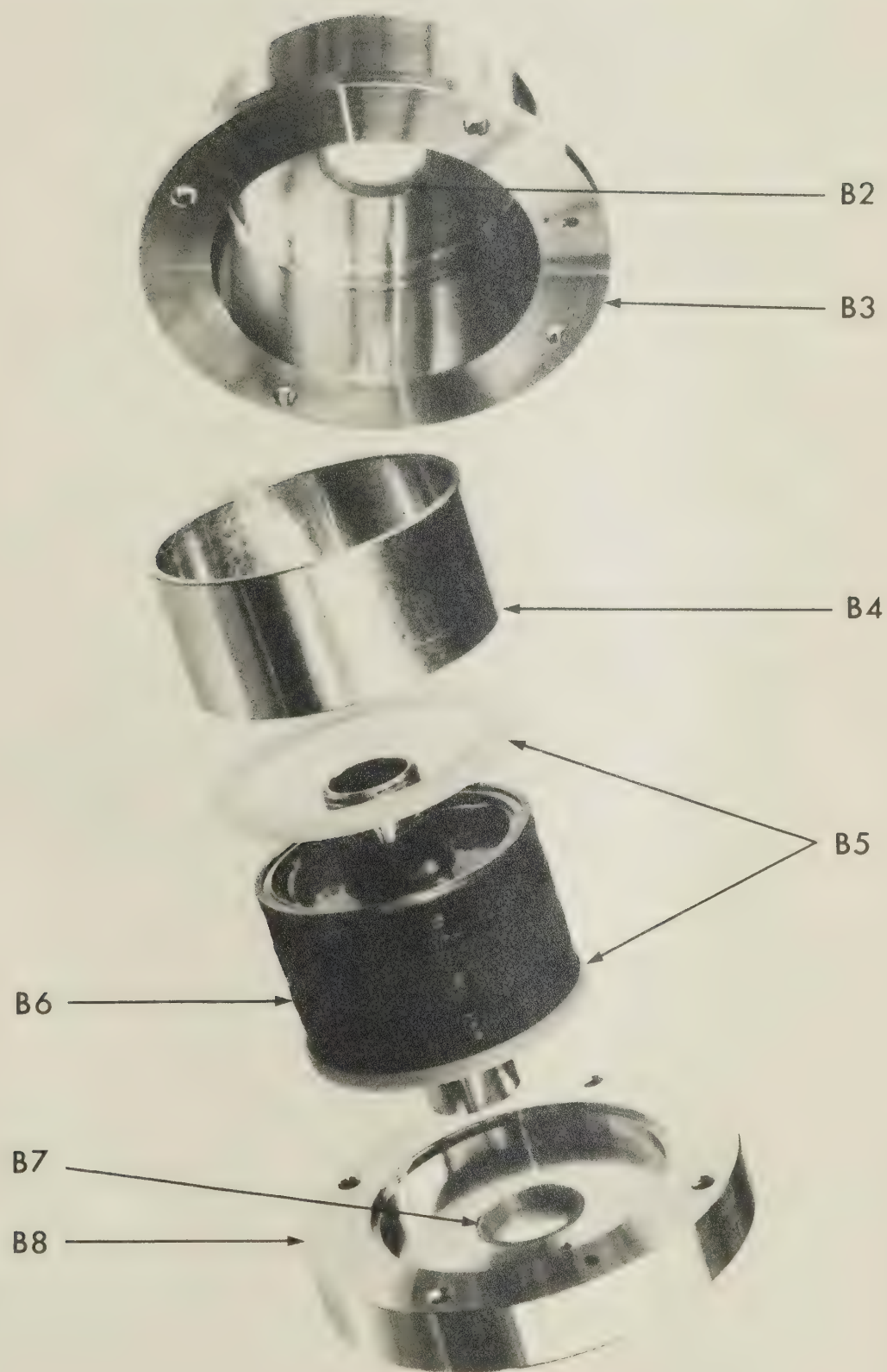








Fig. 6. Geophone (top), geophone holder (middle), and upper portion of VSM with geophone in place (bottom). Visible components of the geophone are as follows: aluminum tube (B1), upper teflon bearing (B2), upper housing (B3), lower housing (B8), and level adjustment screws (B9). The geophone sits in the holder snugly secured by the o-rings (C1). In the lower figure the labeled parts are: top of vibrating rod (A), geophone (B), geophone holder (C), square support plate (D), positioning rail (E), and rail crosspiece (F1).

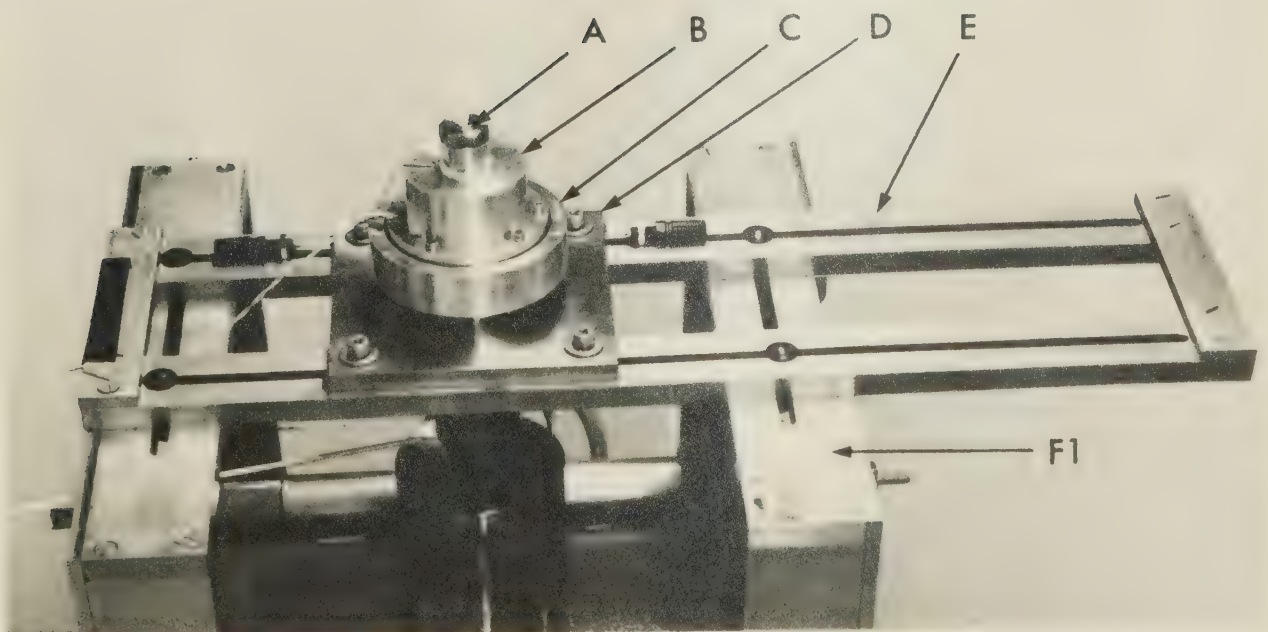
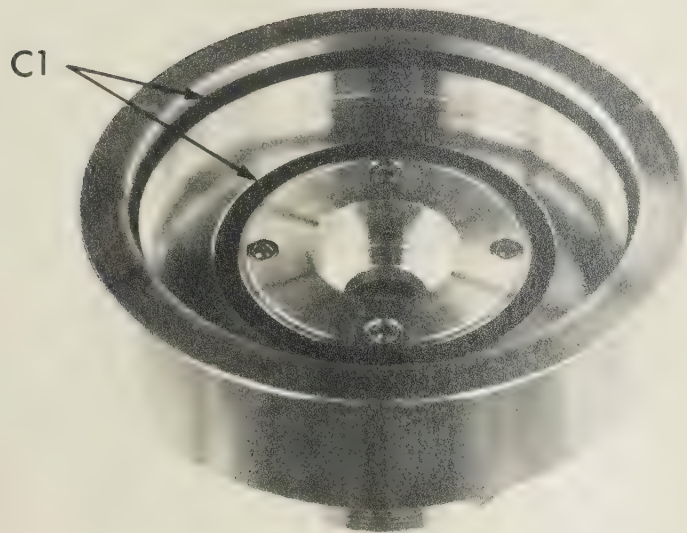
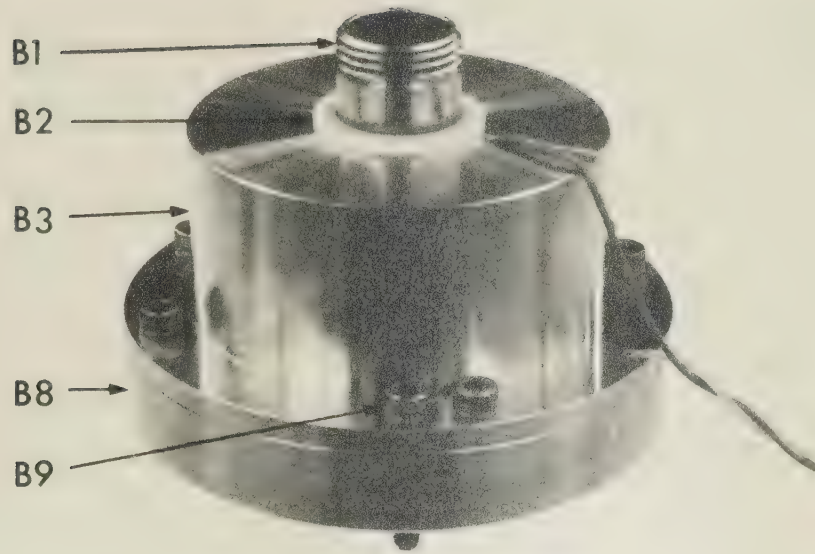




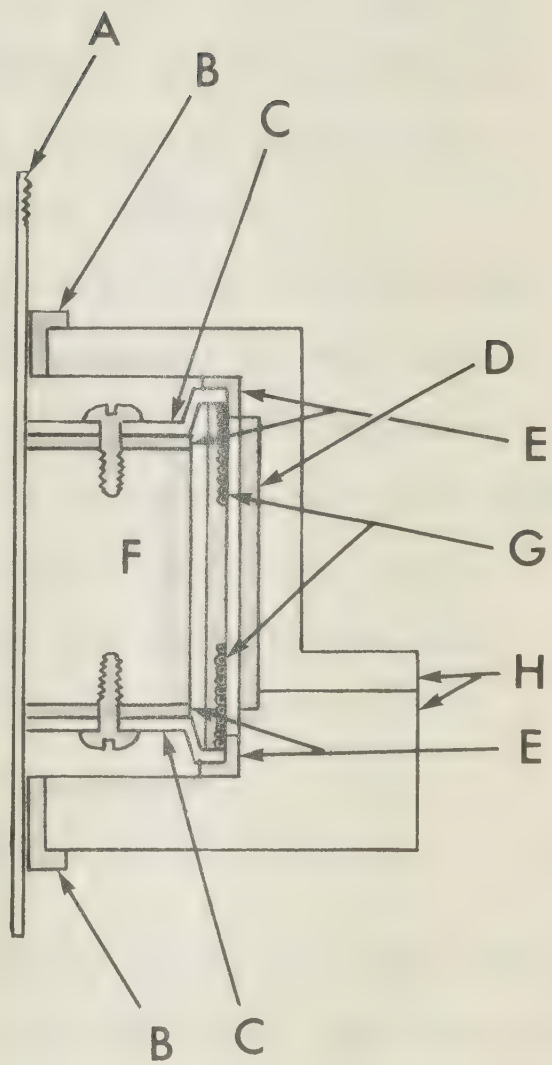
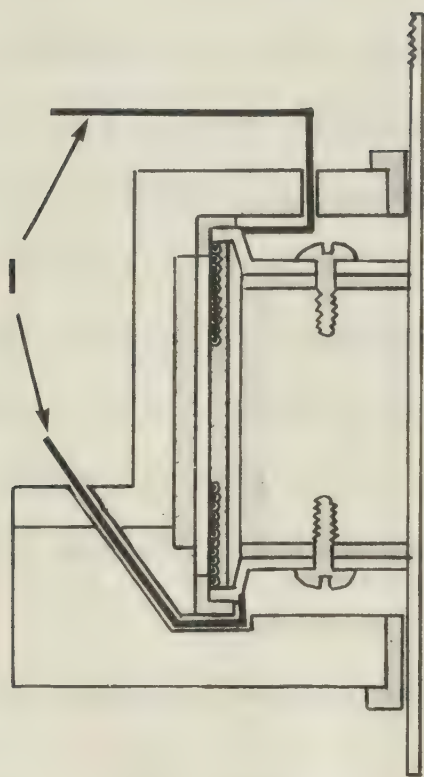


Fig. 7. Schematic longitudinal section of the geophone.

The various components are as follows:

aluminum tube (A), teflon bearing (B), spring (C), magnet keeper (D), insulator (E), magnet (F), coil (G), outer casing (H), and electrical connections (I). Parts acting as electrical insulators are shaded in solid gray.







the geophone only the magnet is free to move; and this in response to an oscillator signal fed to the fixed coil (B6). The normal central pillar from which electrical connection was formerly made has been removed, and this allows one a maximum top access diameter of 1.59 cm. The mass of the magnet is large (124.5 g) and comparable to the mass it supports (about 110 g). The frequency can be varied from several hertz to 50 kHz or more, and amplitudes up to several millimetres can be produced. However, at progressively higher frequencies an increasing amount of vibrational energy is lost to the surrounding equipment. PAR uses a special system of weighted springs and antishock vibration mounts to eliminate energy loss to the rest of the equipment. Such a system is difficult to design and to adjust properly (according to the PAR manual), and was therefore avoided in the present instrument.

### Vibrating Rod and Sample Holders

The rod (A, Fig. 1) is depicted in Fig. 8. There were several important considerations in designing this unit. It had to be able to pass through the magnet of the geophone. It had to provide easy access for the introduction of a thermocouple (see below). And it had to withstand temperatures up to 750°C in its basal section. Each of these points is discussed in order below.

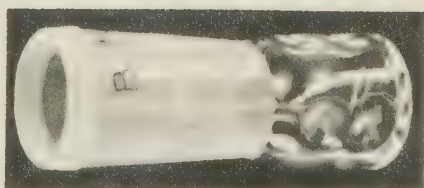
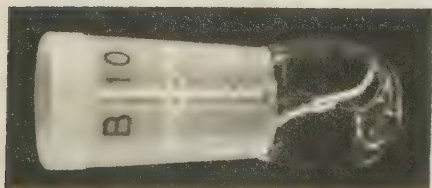
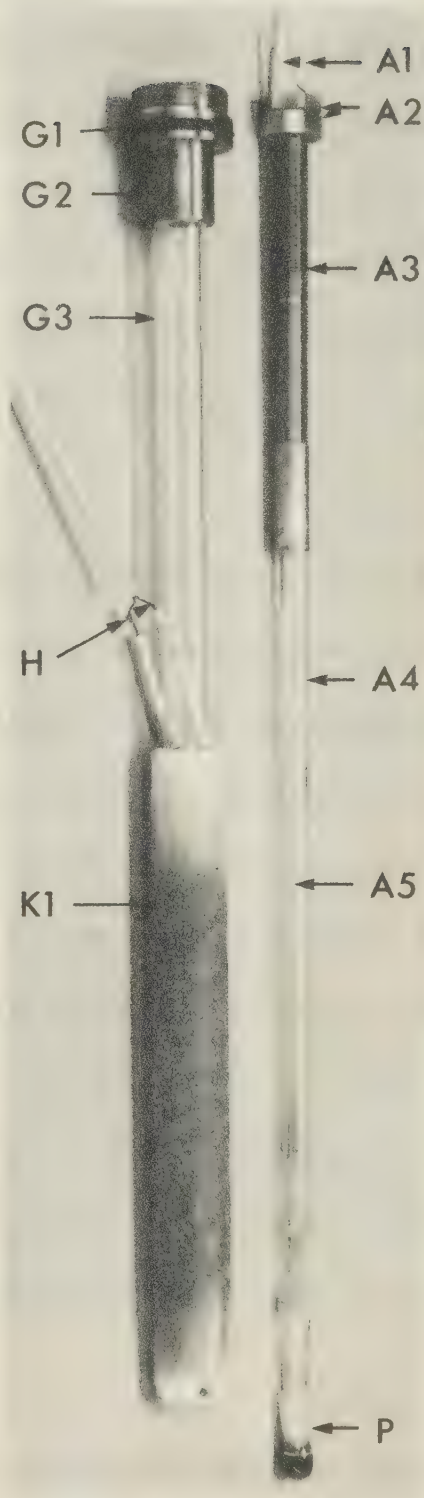
The diameter of the access hole within the magnet





Fig. 8. Guide tube/oven (left in top figures) prior to application of Fiberfrax insulation (top left) and after (top right), vibrating rod (right in top figures) without sample holder (top left) and with (top right), regular sample holder (bottom left), and calibration sample holder (bottom right). Parts labeled on the guide tube and oven are: O-ring (G1), brass section (G2), quartz section (G3), heating element (H), and Fiberfrax insulation (K1). Components of the vibrating rod are: thermocouple wires (A1), locking nuts (A2), upper brass section (A3), lower quartz section (A4), inner quartz tube (A5), and sample holder (P).







centre is 1.59 cm. Besides the rod this hole also had to accommodate a small cylindrical aluminum tube (B1, Fig. 6) which when press-fitted into the hole provides for a rigid link between magnet motion and rod by means of a cap (A2, Fig. 8) threaded onto both tube and rod. With the tube in place a maximum rod diameter of 0.96 cm is conveniently accommodated, which allows the thermocouple easy access into the rod.

In order to withstand 750°C temperatures the lower section of the vibrating rod (Fig. 8) was constructed of quartz tubing (A4). This was glued into a thin-walled brass upper section (A3) with high temperature Sauereisen cement (Sauereisen Cements Co., Pittsburgh, Pa). Some of the design features incorporated into the lower section were first described in a paper by Sill and Drensky (1975); for instance, a slight flare in the silica tube at top and bottom for centring purposes, and a small diameter silica tube (A5) for separating the thermocouple leads (A1). Upper leads in the brass tube are insulated from one another by Teflon spaghetti (Ibid.).

Affixing the sample holders to the end of the silica part of the vibrating rod was a problem. A possible method was to make threaded connections; however, quartz cannot be threaded using standard tools and techniques. It was decided to affix the sample holders by a press-fit method using commercial ground quartz cone and socket joints. A cone



piece was consequently fused onto the end of the rod and a hollow socket piece onto the sample holder (Fig. 8) .

Two types of silica sample holder were constructed, both utilizing the cone and socket method of attachment. One holder is roughly spherical in shape to hold ordinary samples and the other is roughly cylindrical to contain calibration samples (Fig. 8) . The latter internally contains dimple protrusions to accept a press fit cylindrical matrix (0.8 cm in diameter) containing a spherical calibration sample. Ordinary powder samples are held in place by a special machinable glass ceramic piece glued into the end of the rod (see below).

### Heating and Cooling System

The oven consists in part of a quartz tube doubling as a guide tube, which surrounds the vibrating rod and sample (Figs. 8 and 9). It is non-inductively wound; individual coils being separated by a filler of asbestos cement. The whole is covered by a layer of asbestos paper to ensure uniform distribution of heat and by several layers of Fiberfrax insulation (The Carborundum Co., Niagara Falls, N.Y.).

The thermocouple is composed of bare 36 gauge Platinel II wire which offers high thermopower, low magnetic susceptibility, resistance to oxidation, and which is noted for its mechanical strength (Kinzie 1973) -- an important

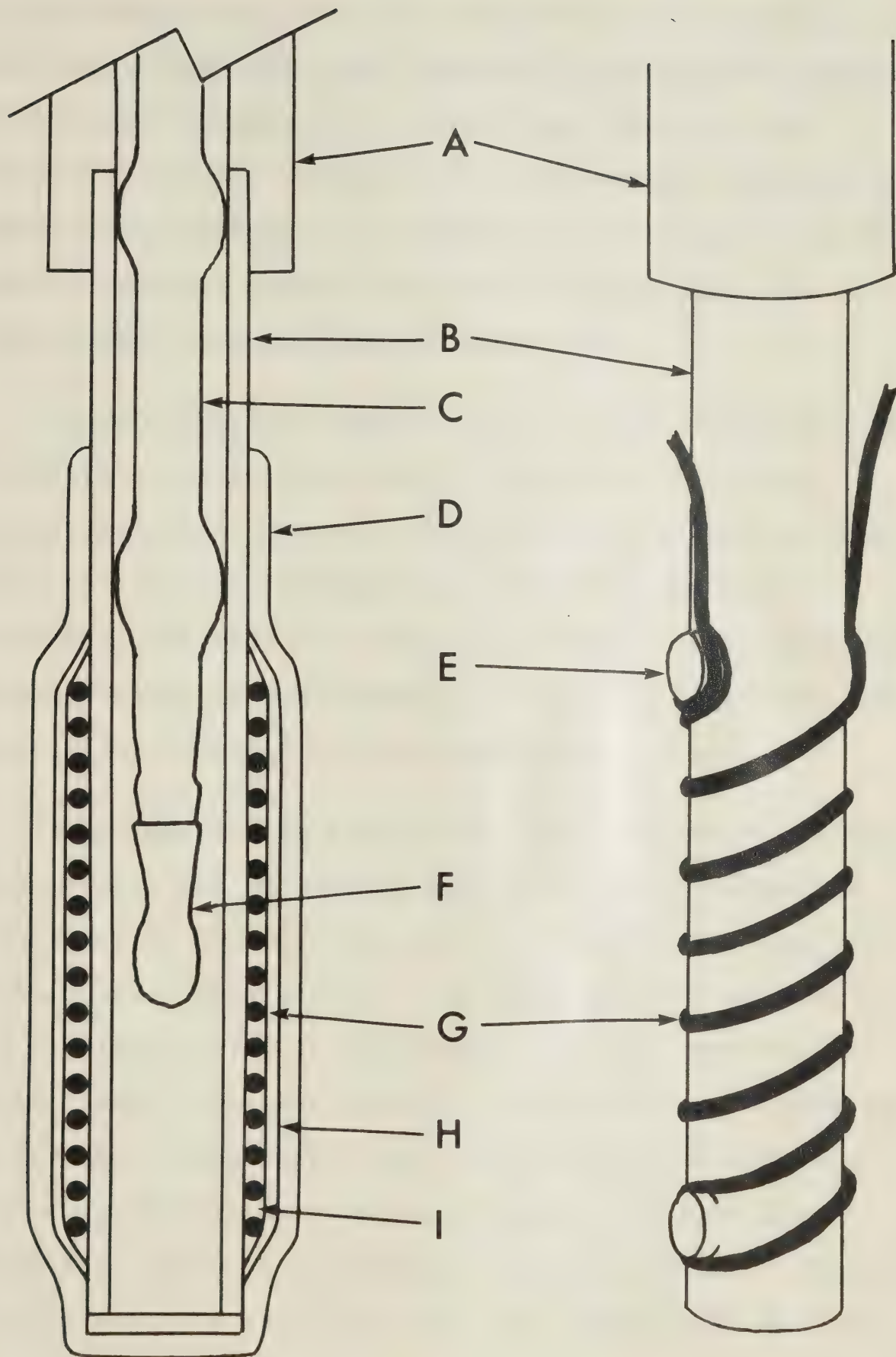








Fig. 9. The VSM oven. On the left is a longitudinal section showing the sample holder (F) and the vibrating rod (C) positioned within the oven. The right-hand figure is a view of the oven prior to the application of insulation. The oven parts are labeled as follows: quartz guide tube (B), Fiberfrax insulation (D), quartz binding post (E), heating element (G), asbestos paper (H), asbestos cement (I). 'A' is the middle brass section into which the guide tube is cemented.





property for vibrating systems. It is centrally positioned at the bottom end of the vibrating rod about 1 cm from the sample by a specially made piece of glass ceramic (Corning Glass Works, Corning, N.Y.) glued into the rod with Sauereisen cement. To facilitate thermocouple replacement -- should the need arise, -- a small glass ceramic screw can be removed from the base of the glass ceramic piece and the thermocouple removed from the bottom end.

Three conditions had to be met in the construction of the heating and cooling system: rapid heating, rapid cooling, and the protection of instrument parts from heat. Rapid heating and cooling helps to ensure the last condition, but these are also desirable in order to minimize chemical alteration of samples, which is a well-known and ever-present problem in rock magnetism.

Rapid heating is achieved by good insulation. In the present case due to space restrictions the thickness of insulation is limited. The asbestos cement and paper has a limited insulating effect. Main insulation is achieved by the overlying layer of Fiberfrax, a ceramic fiber paper. Further heat retention could be achieved by evacuating the guide tube, which would essentially eliminate heat loss occurring through convection. Provision was made for evacuation by the incorporation of o-ring seals at critical points, but this option has not been implemented to date.





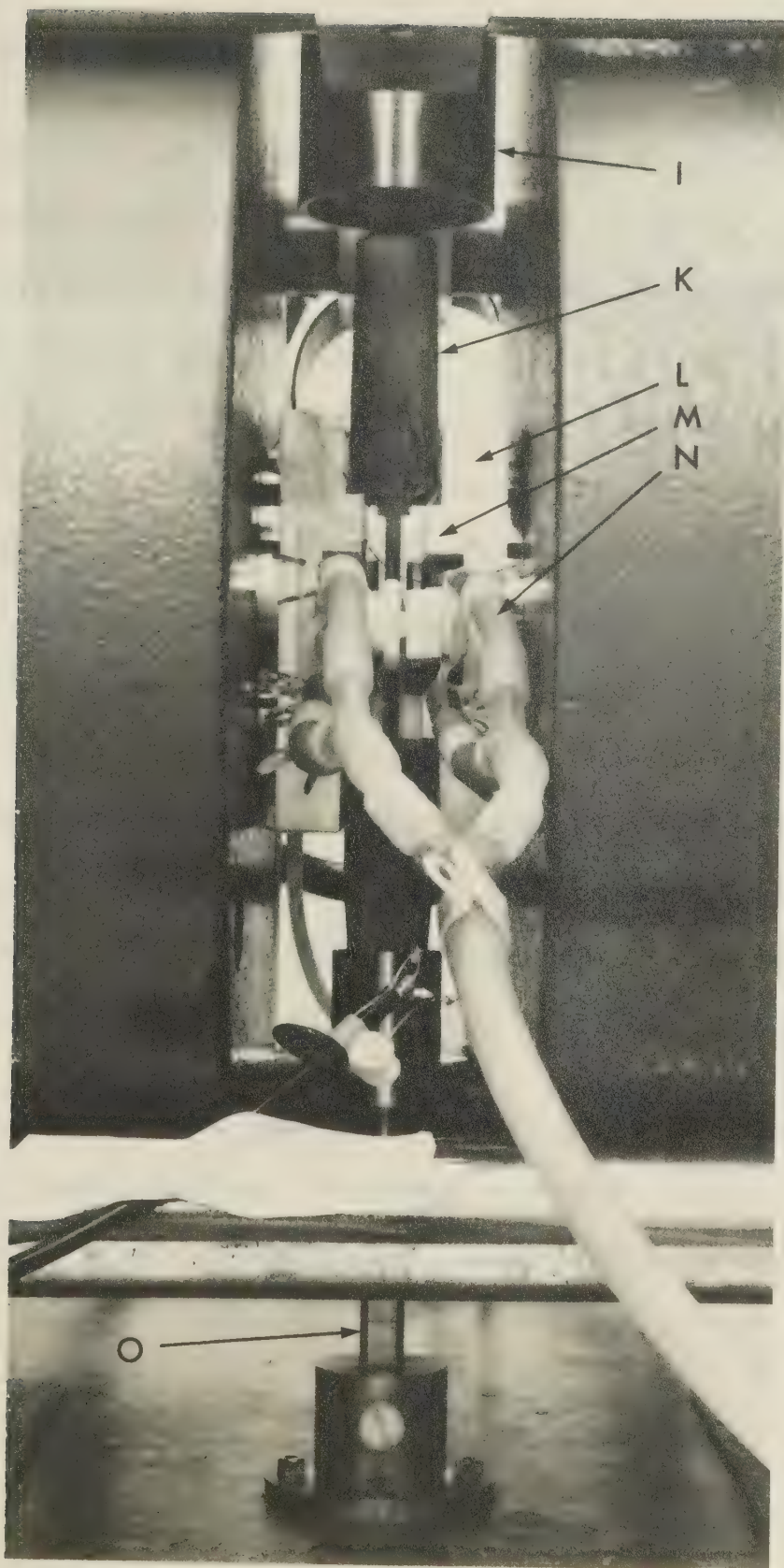
Rapid cooling of the oven is a problem. The usual cooling system for VSM's is a water jacket surrounding the oven. This has been dispensed with in the present instrument in order to position the detecting coils closer to the sample and to reduce the pole gap. Instead, a forced air system is employed in which a stream of air or 'liquid' nitrogen is continuously trained on the oven and the surrounding parts (Fig. 10). This can lead to noise problems by the movement of coil leads, but care has been taken to minimize this effect.

The protection of VSM parts from heat is important. This can be partly effected by the previously-mentioned ways of achieving rapid heating and cooling. Outside the oven the vital parts to be protected are the detection coils and the pole pieces. The detection coils are cooled to liquid nitrogen temperature. As for the pole pieces, they are covered by a layer of Teflon up to 0.63 cm thick (see below, and Fig. 10). Teflon can be exposed to a maximum continuous temperature of 280°C, but the calculated outside surface temperature of the oven assuming a maximum inside temperature of 750°C, a maximum thickness of Fiberfrax insulation (0.40 cm), and a still air temperature of 21°C, will be 360°C. This temperature will be somewhat lower at the adjacent Teflon parts due to the slight air gap and the presence of air currents. Forced air circulation dramatically decreases the temperature outside the furnace and ensures adequate protection for all parts (Table 2,





Fig. 10. Closeup view of lower portion of VSM. Labeled parts are detailed in Fig. 1.







Chapter 3).

### Pole Covers and Attached Detection Coils

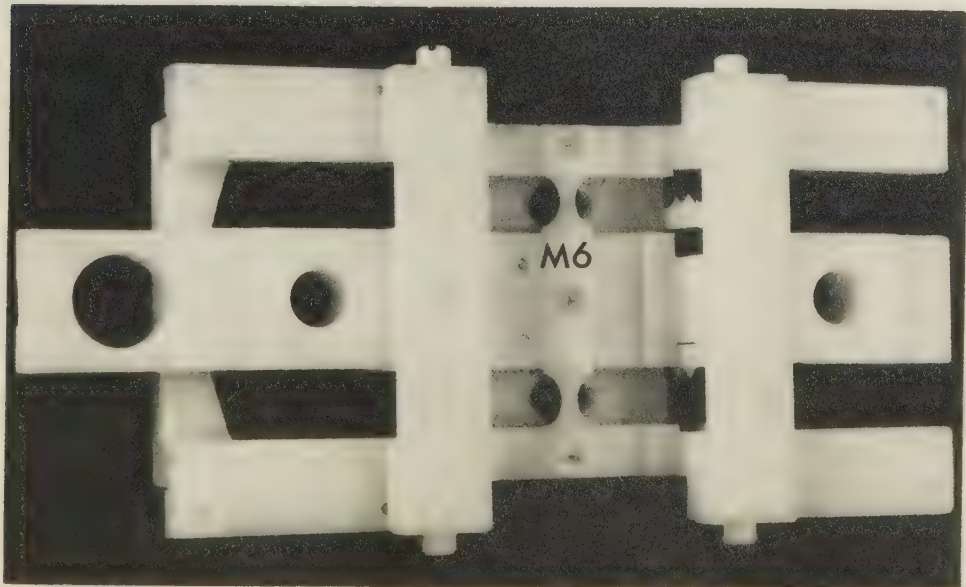
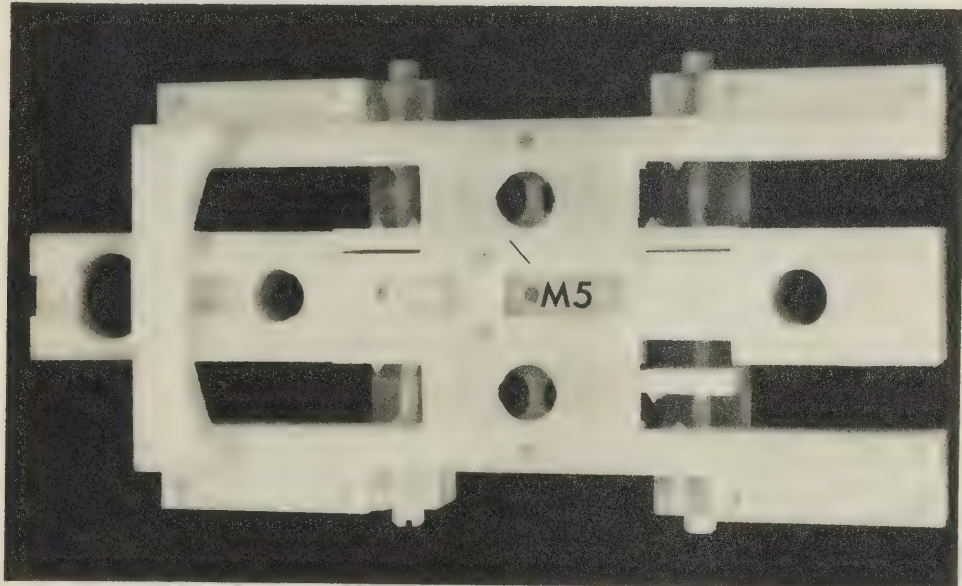
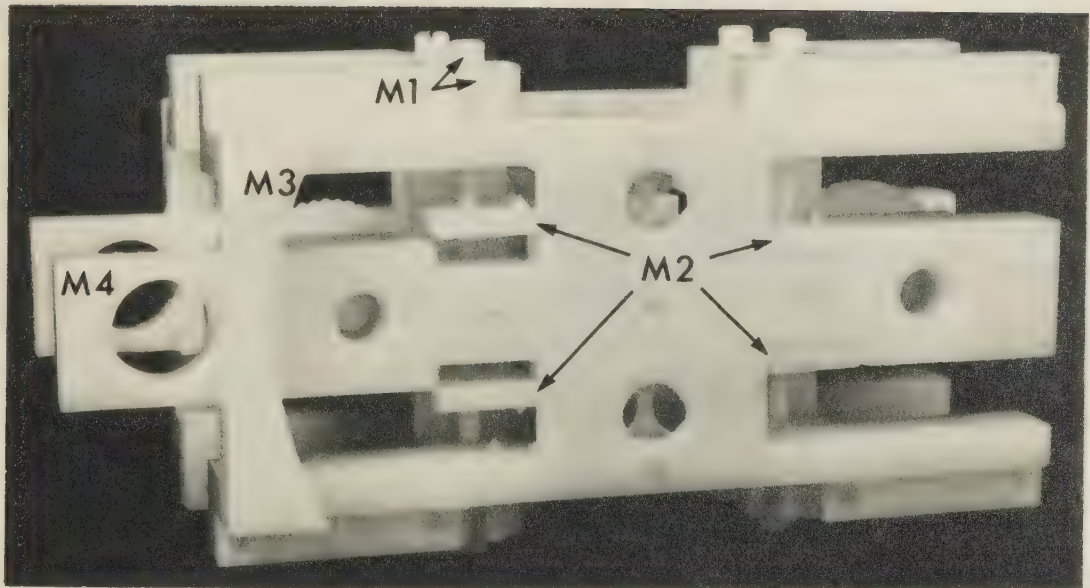
The cover on each pole face consists of fixed and sliding pieces. Both pieces are made of Teflon to provide heat protection for the poles. The fixed pieces (Fig. 10) also act as guides to the sliding pieces (Figs. 11 and 12), which in turn serve as mounts for the detection coils (one shown in Fig. 13) and the Hall probe. The sliding pieces and their assembly are slid into position and held firmly against the fixed pieces and hence the pole faces, by means of two Teflon bolts (M6, Fig. 12). The detection coils are mounted so as to achieve as little thermal contact as possible with other parts of the instrument. This is accomplished by means of the 'cone and socket' arrangement shown in Figs. 11 and 12 (M2). Adjustable screws (M1) position and secure the coils in the vertical (Z) direction.

The coils are threaded by tubes carrying liquid nitrogen as shown in Fig. 10. Good thermal bonding between tube and coil former is achieved through the use of a commercial thermal compound.





Fig. 11. Side views of detection coil holder ( $\times 1$ ). Top figure is the outer view showing coil adjusting screws (M1), adjustable plates (M2), piece that abuts cylindrical pole piece (M3), and handle for withdrawing holder (M4). Middle figure is the outer view of the opposite side showing the Hall probe slot (M5). Lower figure is an inner view. M6 is the strap which holds two of the liquid nitrogen tubes away from the oven.



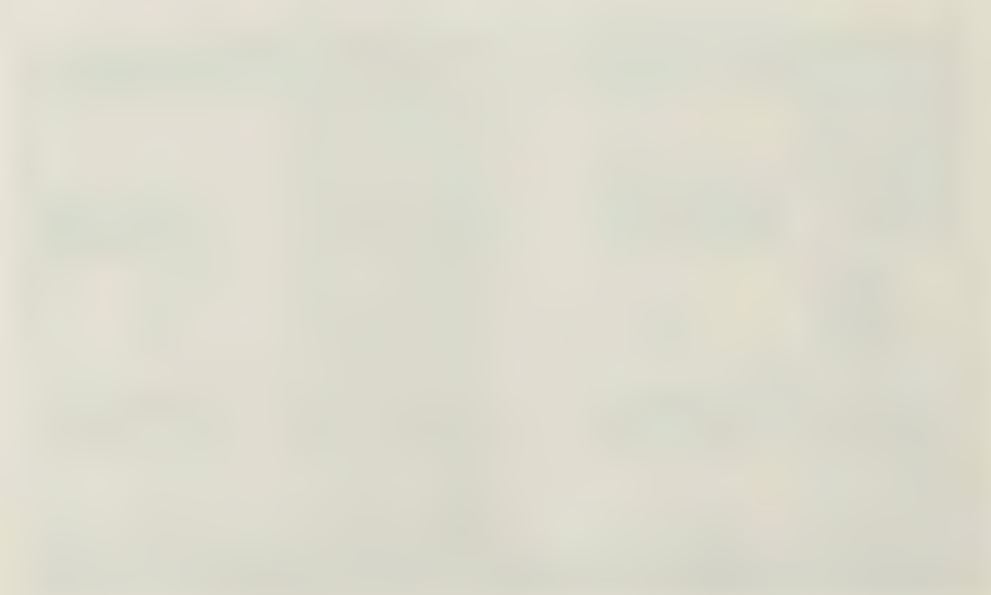
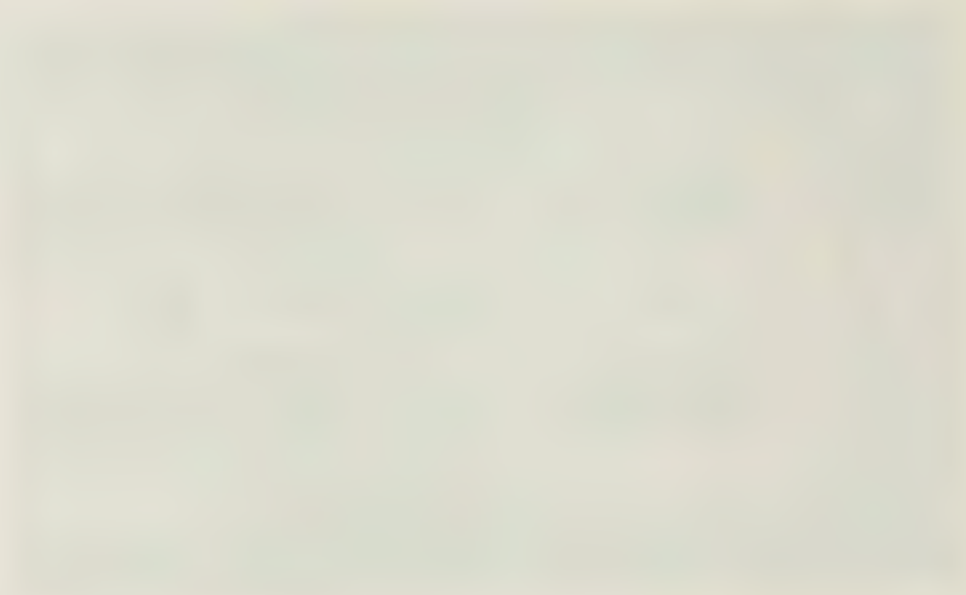
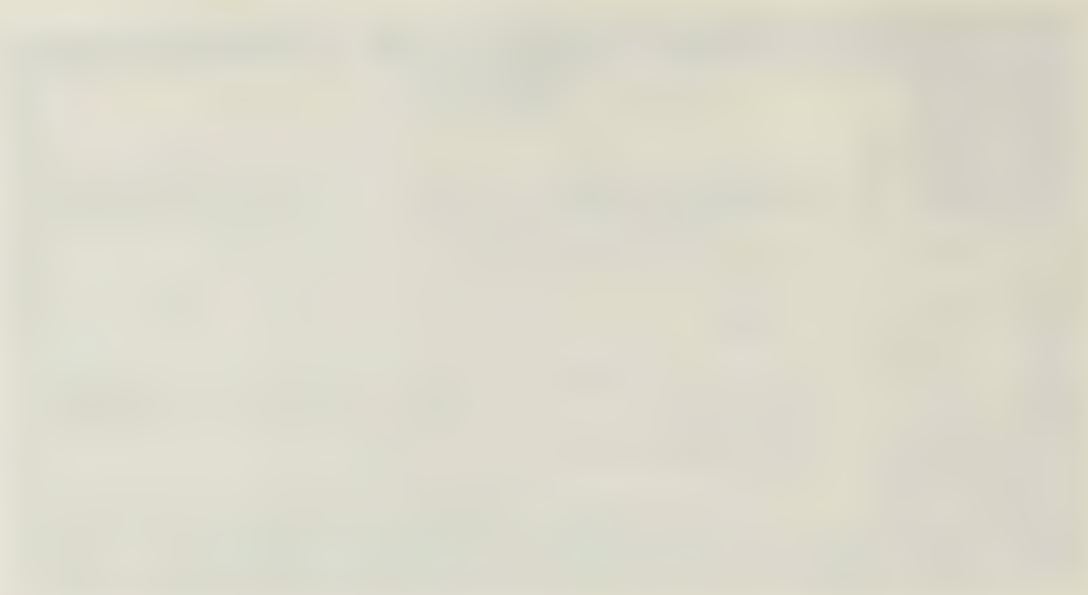
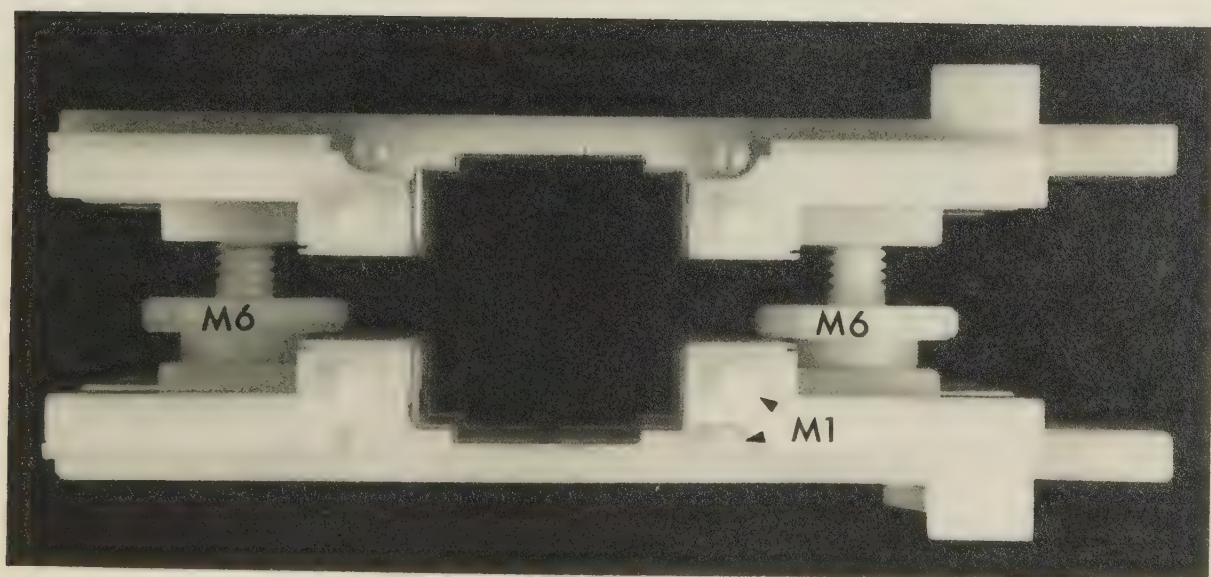
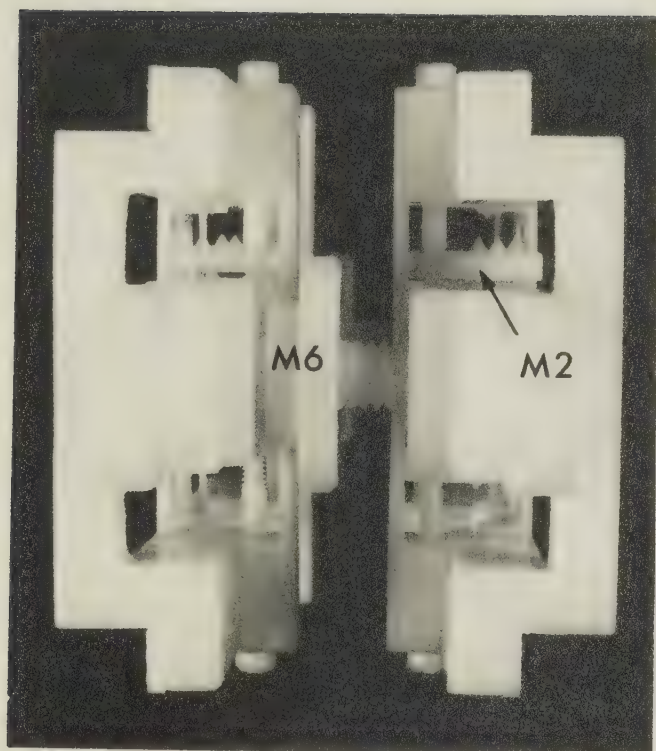






Fig. 12. End (top figure) and top (bottom figure) views of the detection coil holder with the coil adjusting screws (M1), adjusting plates (M2), and clamping bolts (M6) labeled.



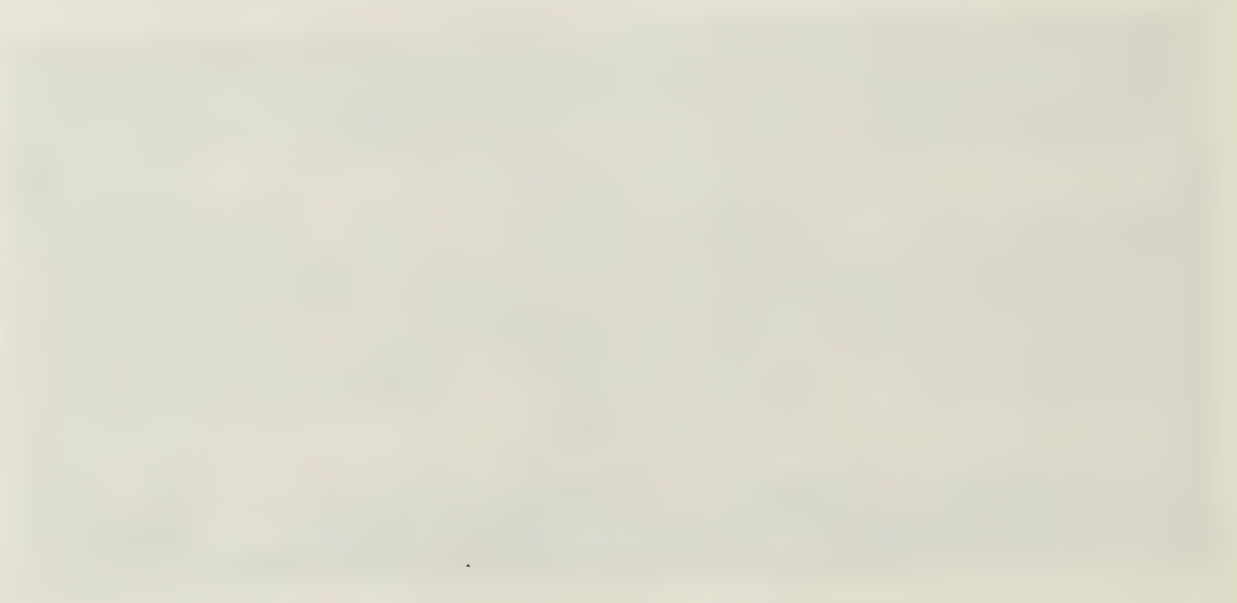
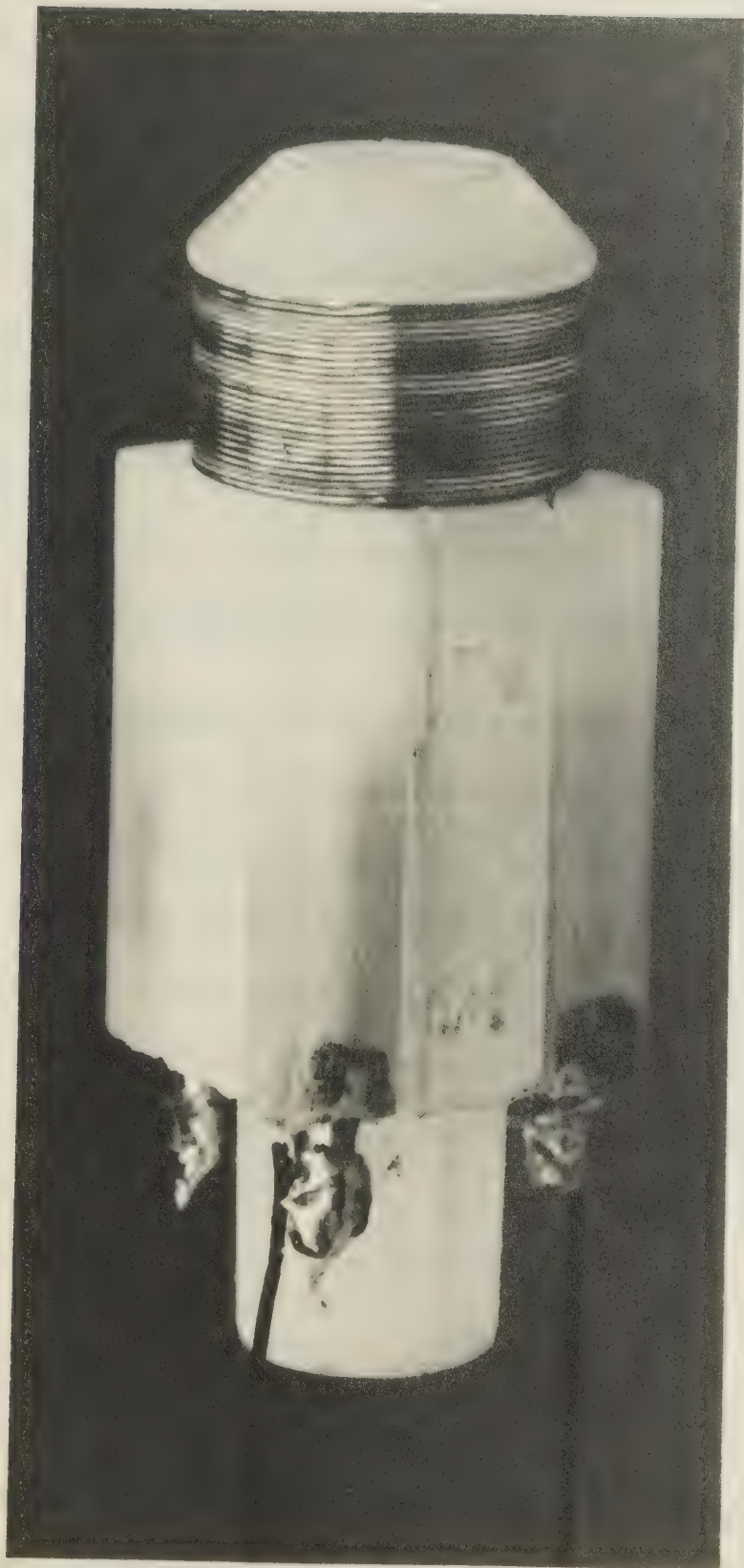




Fig. 13. Single detection coil (X3).







## Chapter 3: Testing and Calibration of the VSM

### Introduction

In Chapter 2 several desirable characteristics for inclusion in a VSM suitable for rock magnetic studies were noted. Also mentioned were the physical constraints associated with the present system, and the way in which these affected the incorporation of the most desirable characteristics in the VSM. Once construction of the VSM was completed it remained to determine how well the instrument measured up to the compromised original expectations.

The first important tests involved the signal: in particular its strength and noise component. In the process most aspects of the signal detection and processing system were tested. Next the heating/cooling system was considered. Once these major systems were proved to be operating satisfactorily tests were conducted involving the primary uses of the instrument; that is, for obtaining hysteresis and thermomagnetic curves. These topics are discussed below followed by a discussion of the calibration.

### Monitoring the Signal

This section mainly discusses signal behaviour under varying conditions such as amplification, processing, frequency, noise, and sample position.



The raw signal from an iron calibration sample with a mass of 130 mg vibrating at a frequency of 27 Hz in a field of about 4.8 kOe was found to be 10  $\mu$ V. This signal could be additionally amplified by the inclusion of a transformer (x100) and a pre-amplifier (PAR model 112;x100), but the amount of additional amplification could not be determined since there was no impedance matching in the circuit. At the time the advantages of this expedient were not realized. It was important then in later experiments -- and especially for calibration -- to have the same transformer and/or preamplifier in the circuits of those experiments which were being compared, or else there was no relationship between the measured voltages.

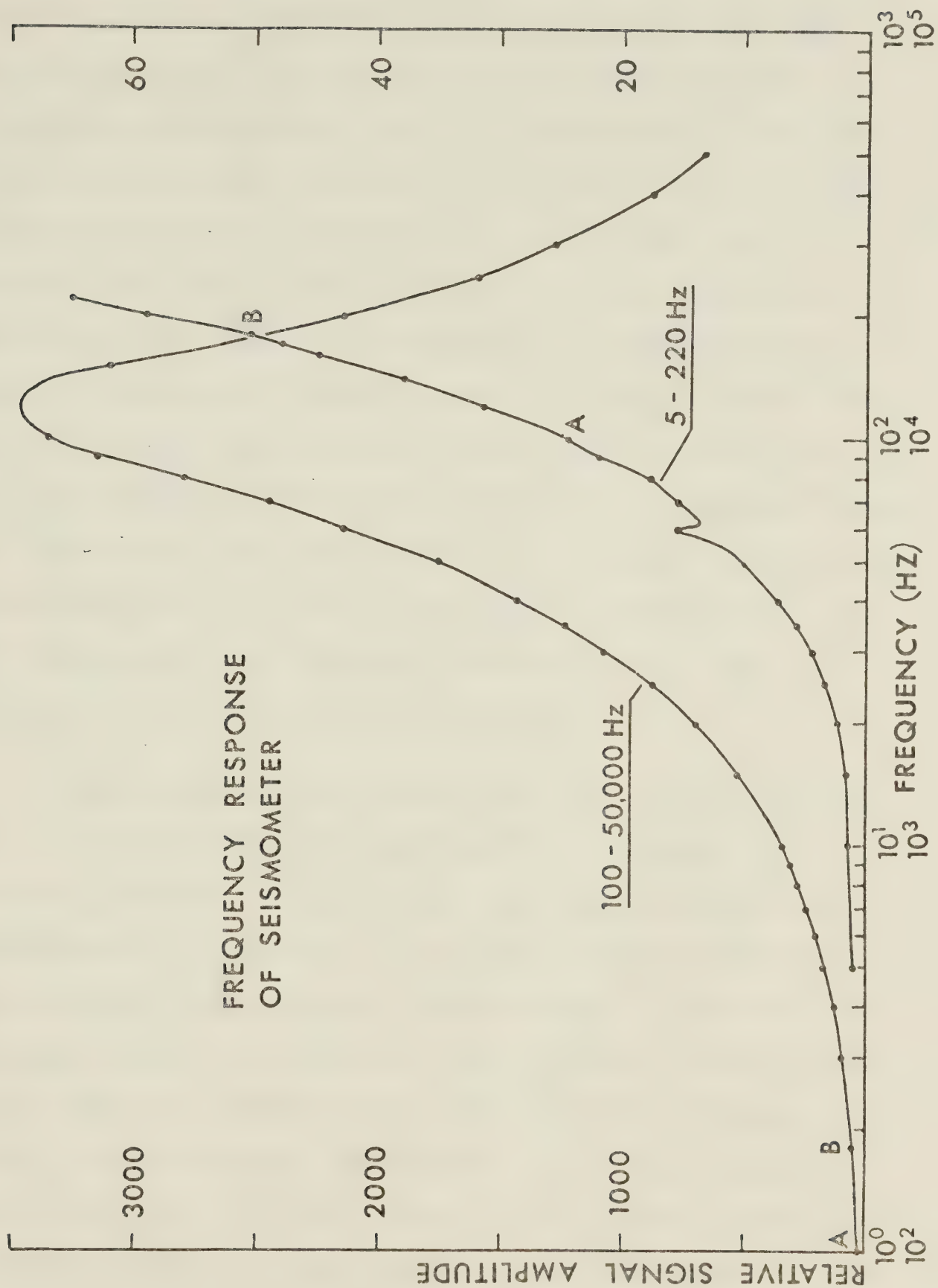
The amplified signal was measured as a function of frequency and sample position. A plot of frequency response at constant oscillator output is shown in Fig. 14. The geophone drive allowed a frequency which varied from 5 Hz to at least 50 kHz. At low frequency the amplitude of vibration of the sample was one to two millimetres, above which the geophone reached the physical limit of its range. With increasing frequency the physical amplitude decreased, but the signal amplitude increased 7000 times to reach a peak at about 12 kHz, thereafter decreasing. Superimposed is a noise signal not eliminated by the lock-in amplifier, grounds, shields, etc. which has at least three observable components. The major noise component increases fourfold between 5 Hz (where it constitutes 50% of the signal) and







Fig. 14. Frequency response of geophone. A and B  
represent the same points on the two curves.





about 100 Hz, and remains steady to at least 600 Hz. This noise is somewhat distorted between 30 and 140 Hz, due apparently to the main line signal as evident in the frequency response curve (Fig. 14). Harmonics of the main line frequency were observed at 120 and 180 Hz. The third noise component was a steady higher frequency signal constituting 10% of the total noise at 5 Hz. The choice of operating frequency for the subsequent experiments was mainly a matter of trial and error. Frequencies at or near the main line frequency were avoided. The frequency had to be high enough to avoid sticking of the vibrating rod within the guide tube, but not so high as to transmit most of the signal energy to the rest of the VSM. A frequency of 35 Hz was chosen, but any frequency between about 10 and 100 Hz (except 60) would probably be suitable.

Signal amplitude vs. sample position was plotted (Fig. 15) in order to find the exact centre of the coils and to ascertain whether the coils were properly connected. The measurements are somewhat noisy due to sticking problems involving the vibrating rod. That portion of the curve measured appears to conform to the expected response of an eight coil j-th sensing arrangement as given in Bowden (1972). Unfortunately, the complete curve could not be measured, since the sample could not be lowered beyond a few millimetres past the coil centre as an independent determination revealed (Table 1). Therefore the indicated centre of the coils shown in the signal response curve is







Fig. 15. Signal response of detection coils vs. vertical distance ( $Z$ ) of sample (NI2) from the geometric centre ( $\pm 0.2$  cm) of the detection coil array. Plotted points are each the results of from one to five determinations. Errors are standard deviations except in six cases where the absolute error (ranging from 0.01 to 0.02 cm) is plotted. Using the dimensions of the coil array ( $x = 2.86$  cm,  $y = 2.86$  cm,  $z = \sim 3.02$  cm) the theoretical signal response has been calculated from the appropriate equation given in Bowden (1972), and plotted in the inset. The centre of the upper set of coils is denoted by 'C'. 'A' is the probable range within which the experimental response curve was determined, but the position of the geometric centre may be in error (see above).

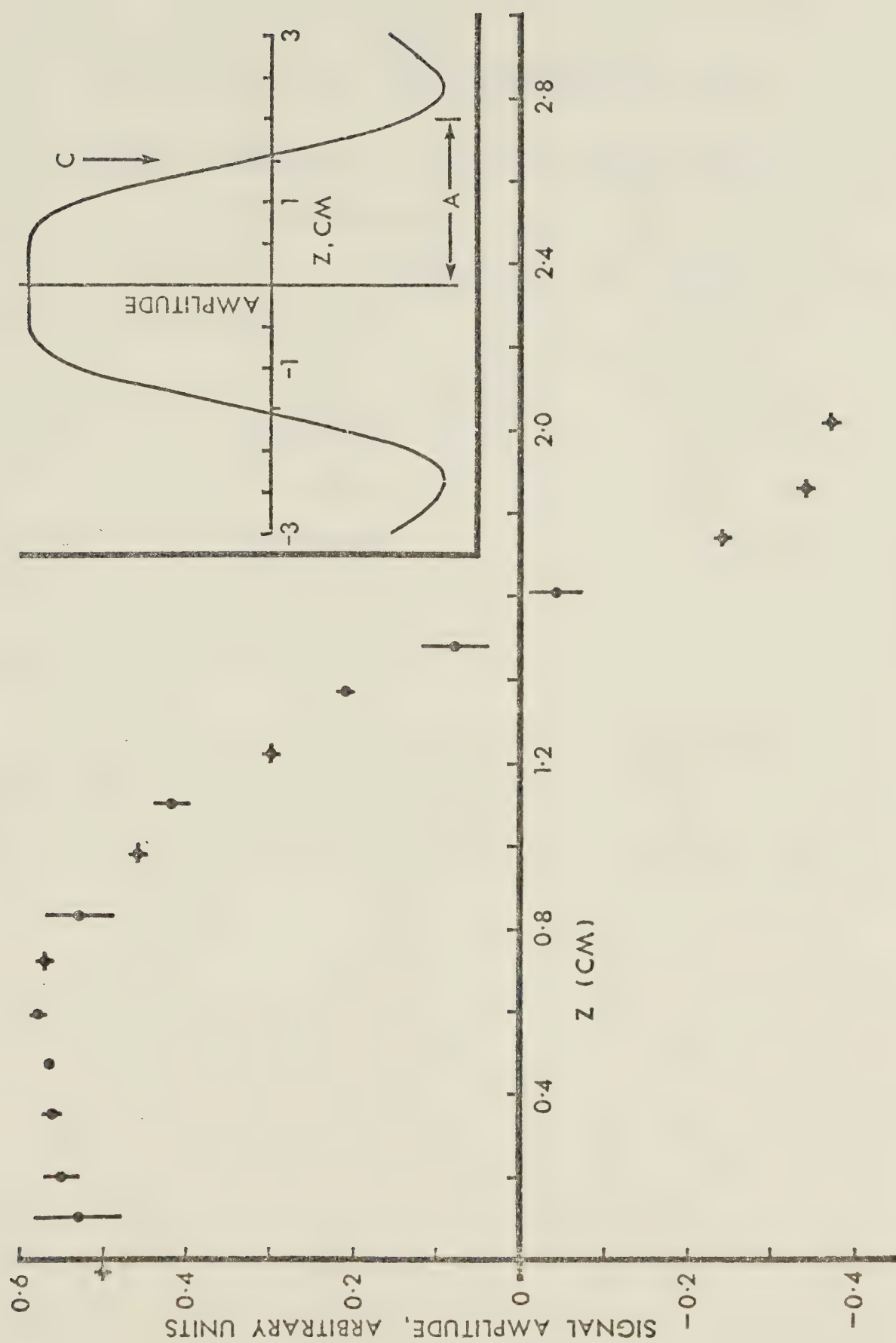




TABLE 1.  
SAMPLE POSITIONS DURING EXPERIMENTAL RUNS

Sample	Experimental run	Position(a) (cm)
NI1; FE1,2,3	hysteresis	$0.16 \pm 0.11$
NI2	hysteresis, $J_s$ -T	$0.12 \pm 0.17$
M1	hysteresis, $J_s$ -T	$0.14 \pm 0.16$
M2	hysteresis	$0.18 \pm 0.15$
M3	hysteresis	$0.14 \pm 0.16$

NOTE:

The position of the sample centre determined by length measurements is given as distance with absolute error (a) below the geometric centre of the coil array.





possibly in error by 1 to 2 mm. The theoretical curve given in the inset indicates that the amplitude at the centre remains constant to within 1% variation within  $\pm 6$  mm from the centre or to within 0.5% within  $\pm 2$  mm from the centre. According to Table 1 samples were generally located within the bounds of this latter positioning error. It is apparent that positioning is not critical, and that samples can vary in position within reasonably wide limits to obtain a signal which is close to maximum and which will be directly comparable to that of other samples whose positions may vary by as much as 1 cm relative to the sample under consideration.

### Testing the Heating and Cooling Systems

The oven was monitored both internally and externally. Externally it was important to ascertain whether the heat would present any problems for the surrounding apparatus. During the initial heating runs conducted away from the VSM the oven was heated to various temperatures and the temperature of the outer surface monitored at several points (Table 2). At the highest temperature the thermometer attached 1mm away from the outer surface of the oven centre -- that part which would be closest to the detection coils -- recorded a temperature of  $205 \pm 3^\circ\text{C}$ . This reading emphasized the importance of efficient cooling. The same thermometer was monitored during succeeding tests with the oven installed in the VSM. With forced air cooling the



TABLE 2. EXTERNAL OVEN TEMPERATURE (T, °C)

INTERNAL	EXTERNAL			
	Cold junction	Oven <sup>1</sup> bottom	Oven Centre <sup>2</sup>	
			no cooling	cooling <sup>3</sup>
314±9	23.5	30	90±5	39±2
527±3	24.5	58	151±3	39±2
~739	24.5	77	205±3	--

<sup>1</sup> 0.1 cm from outer surface, 9 cm from oven centre.

<sup>2</sup> 0.1 cm from outer surface.

<sup>3</sup> forced air cooling.



temperature outside remained essentially constant at the much lower temperature of about 40°C for internal temperatures to at least 585°C.

The next tests involved measuring the temperature gradient in the oven for each of several constant temperatures at the oven centre (273, 410, and 585°C; Fig. 16). During each run the position of the sample was raised and lowered in steps, and allowed to reach thermal equilibrium at each step before measurements were taken. Several measurements were taken at each step in order to average out temperature fluctuations due to the inexactness of maintaining constant temperature at the centre by manual control. The temperature difference ( $\Delta T_{st}$ ) between the sample centred in the oven and the thermocouple 0.93±0.11 cm above ( $\Delta L_{st}$ ), only varies by about 2°C between the bottom ( $\Delta T_{st} = 4^\circ$ ) and top ( $\Delta T_{st} = 6^\circ$ ) curves. The difference measured on the centre curve appears to be rather anomalous ( $\Delta T_{st} = 10^\circ$ ). This curve (solid) is the average of readings taken on raising and lowering the sample (dashed curve). In view of the observed discrepancy between the two dashed curves -- probably due to not maintaining the correct temperature at the centre when lowering the sample -- the top dashed curve, which yields a  $\Delta T_{st} = 5^\circ\text{C}$  similar to the other curves, is taken to be the correct curve. The average  $\Delta T_{st}$  from these three curves (5°) with a possible error of ±1°, due to the error in determination of  $\Delta L_{st}$ , is used in constructing the temperature scale of the thermomagnetic

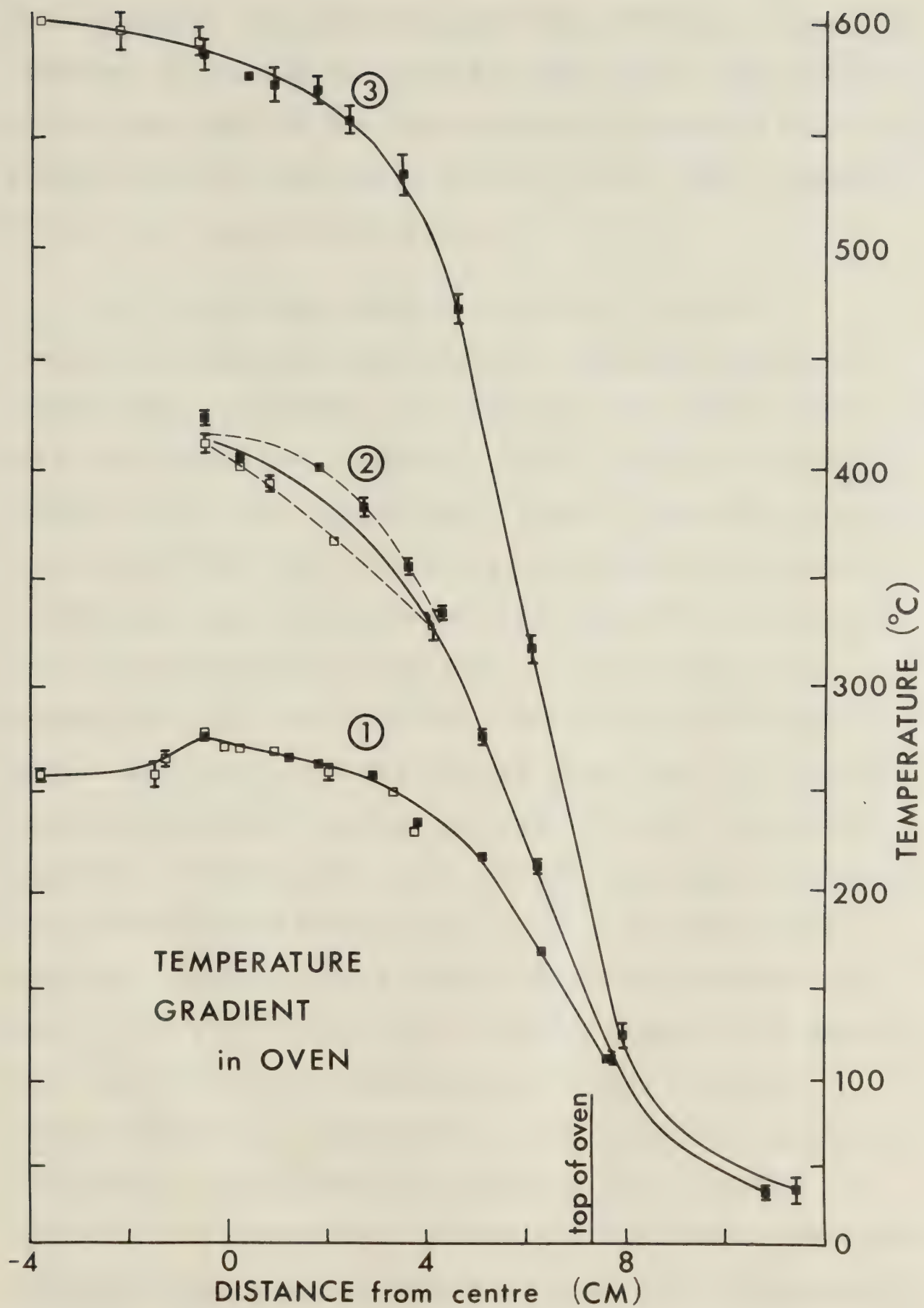






Fig. 16. Temperature gradient in the oven for each of three constant temperatures at the oven centre: (1) 273°C, (2) 410°C, and (3) 585°C.

Individual points on the curve are usually averages of several readings taken at various times while raising (solid squares) or lowering (open squares) the sample. The sample was allowed to reach thermal equilibrium at each position. In curve (2) the discrepancy between the 'raising' and 'lowering' curves is probably due to a drop in temperature at the oven centre during readings taken while lowering the sample.





curves discussed later. Again, exact sample positioning is not critical;  $\Delta T_{st}$  increasing by about  $1^{\circ}\text{C}$  for each 0.2 cm increment of the sample above the oven centre out to 0.6 cm and by less than  $1^{\circ}\text{C}$  for corresponding increments below. The gradient of the lower curve does not change out to about 2 cm, and so  $\Delta T_{st}$  does not change.

What can be said about the possible error in temperature determinations? Several possible errors have already been mentioned; now these and other major sources of error are summarized (Table 3). First, there is the error associated with the thermocouple itself. According to Olsen and Freeze (1964) the error from any undamaged Platinel II thermocouple will not exceed  $\pm 2$ ,  $\pm 3$ , and  $\pm 6^{\circ}\text{C}$  at 260, 538, and  $1371^{\circ}\text{C}$  respectively. Second, this particular error assumes that the cold junction has been maintained at  $0^{\circ}\text{C}$ . When it has not, as in the present case, then, due to the e.m.f.-temperature function not being linear, the simple expedient of adding the e.m.f. reading corresponding to room temperature to the measured e.m.f. will produce an error. How large an error is not known, but it is expected to be small. A test was conducted to compare temperatures measured with the Platinel II thermocouple to those measured concurrently at the same level in the oven with a platinum - 13% rhodium vs. platinum thermocouple. The agreement is within  $2^{\circ}$  for temperatures between 230 and  $740^{\circ}\text{C}$ . (Both were corrected for the cold junction being at room temperature). The third error is that associated with the changing



TABLE 3. ERRORS IN TEMPERATURE DETERMINATION

Source	Type	Errors in Temperature (°C)				
		300	400	500	600	700
Thermocouple <sup>1</sup>	a	(±2.1)	(±2.5)	(±2.9)	(±3.2)	(±3.6)
$\Delta T_{st}$ <sup>2</sup>	a	-1	0	(+0.5)	+1	(+2)
$\Delta L_{st}$ <sup>3</sup>	a	(±0.5)	±0.8	(±1.0)	±1.1	(±1.3)
Thermal inequilibrium <sup>4</sup>	$\sigma$	±2.0	±2.5	±2.9	±3.4	±3.9
Observer <sup>5</sup>	a	±0.5	±1.0	±1.0	±1.0	±1.0
Total		+5	±7	±8	+10	±10
		-6			- 9	
r.m.s.		±3	±4	±4	± 5	± 6

NOTES: a = absolute error,  $\sigma$  = standard deviation.

Figures in parentheses are interpolated values.

<sup>1</sup> Largest possible error on any uncalibrated Platinel II thermocouple (Olsen and Freeze 1964).

<sup>2</sup> Error results from taking the difference in temperature between sample and thermocouple ( $\Delta T_{st}$ ) as a constant.

<sup>3</sup> Error resulting from error in determination of sample to thermocouple distance.

<sup>4</sup> Error associated with the calculation of temperature scale. It may include other sources of error.

<sup>5</sup> Error in reading the millivoltmeter.





temperature gradient for different temperatures of the sample. This results in a  $\Delta T_{st}$  error of about  $\pm 1^\circ\text{C}$  for  $\Delta T_{st}$  assumed constant as in the present case. Superimposed on this is a fourth error of  $\pm 1^\circ\text{C}$  due to the error in  $\Delta L_{st}$ . The fifth possible error results mainly from thermal inequilibrium between sample and thermocouple. A measure of this is the standard deviation associated with the calibration of the temperature scale. It is an increasing error which for nickel amounts to  $\pm 1.5^\circ\text{C}$  at the Curie temperature ( $\theta$ ) (see below) for the discontinuous curve and  $\pm 2.4^\circ\text{C}$  at  $\theta$  for the continuous curve. The corresponding values for magnetite at its  $\theta$  are  $\pm 1.9$  and  $\pm 3.3^\circ\text{C}$ . A sixth source of error is that associated with reading the millivoltmeter, and amounts to  $\pm 0.5^\circ\text{C}$  below about  $365^\circ\text{C}$  and  $\pm 1^\circ\text{C}$  above this temperature. Finally, an error of about  $1^\circ\text{C}$  is incurred for each increment of 0.2 cm displacement between sample centre and oven centre over distances of at least  $\pm 0.6$  cm. As summarized in Table 3 the absolute error varies from 5 to  $12^\circ\text{C}$  between 300 and  $700^\circ\text{C}$ . But since in general the errors will not be additive, the r.m.s. error of from 3 to  $6^\circ\text{C}$  depending on temperature (see Table 3) is a reasonable estimate.

## Hysteresis and Thermomagnetic Tests

### Introduction

The basic data produced by the VSM's are hysteresis



curves (magnetization vs. field) and thermomagnetic curves (magnetization vs. temperature). Each allows a variety of calculations and deductions to be made concerning the magnetic materials present. Trial runs using known substances to produce the curves, and subsequent analysis, provides the most effective test of the capability and performance of the instrument. Below, hysteresis and thermomagnetic measurements are described, followed by a calculation of the important parameter ( $J_R/J_S$ ) involving the hysteresis curves.

Before describing these measurements it is useful to review some of the theory and terminology that will be used in this and following Chapters. The basic relation which describes the magnetization of materials in the c.g.s. e.m.u. system of units is

$$B = H + 4\pi J \quad (1)$$

where  $B$  is the magnetic induction in gauss,  $H$ , the applied field in oersteds, and  $J$ , the magnetization in gauss.

Magnetization is ultimately dependent on the magnetic moments of individual atoms due to the orbital motion and spin of electrons. Three fundamental types of magnetism arise according to the response of electrons to an external field and to their interaction with adjacent atoms. The quantity which distinguishes the behaviour of each type of



magnetism, the susceptibility ( $k$ ), is defined by the relation

$$k = J/H. \quad (2)$$

When this quantity is negative, with magnitude about  $10^{-6}$ , the material exhibits diamagnetism. All substances display this property due to the precession of the orbital motion of electrons in the presence of an external field. If the susceptibility is positive of about the same magnitude, the material displays paramagnetism. This phenomenon arises due to the weak interaction of atomic moments in an external field.

The third fundamental type of magnetism, -- ferromagnetism -- is ordinarily measured by the VSM. It is exhibited by materials which have a high positive susceptibility of the order of 10 to  $10^5$  arising from strong magnetic interaction between adjacent atoms. These interactions result in spontaneous magnetization, wherein atomic moments are aligned parallel within tiny regions called magnetic domains. In the absence of an external field domain moments are initially randomly oriented and the net moment is zero. Another quantity which allows one to characterize ferromagnetics is the permeability ( $\mu$ ) described by the relation

$$\mu = B/H. \quad (3)$$





Ferromagnetic substances have high permeabilities, which are dependent on field strength and previous magnetic history. All ferromagnetic properties disappear when the substance is heated to the Curie temperature ; and the substance thereafter becomes paramagnetic.

In paleomagnetism the important magnetic minerals, magnetite and hematite, display ferromagnetic characteristics. Both are composed of two interpenetrating atomic sublattices, which have magnetic moments that are essentially antiparallel to one another. This magnetic phenomenon is labelled antiferromagnetism. In the case of magnetite the sublattice magnetizations are unequal, and the phenomenon is termed ferrimagnetism. In hematite the sublattice moments are equal but probably not quite parallel, thus resulting in a weak ferromagnetism.

### Hysteresis Measurements

The measurement of hysteresis loops is important for identifying the magnetic material present and possibly inferring something about its domain state ( $J_r/J_s$  calculation: see below). In addition, the hysteresis loops of certain magnetic materials (eg. Fe, Ni), can be used for calibrating the VSM (see below).

Hysteresis loops for magnetite, hematite, nickel, and iron are displayed in Figs. 17 to 20. These are the actual





Fig. 17. Hysteresis loops of three separate magnetite samples: M1 (479 mg), M2 (306 mg), and M3 (28 mg). The vertical scale has been normalized to the saturation magnetization ( $J_s$ ) calculated by the method of Bean and Jacobs (1960); see text.

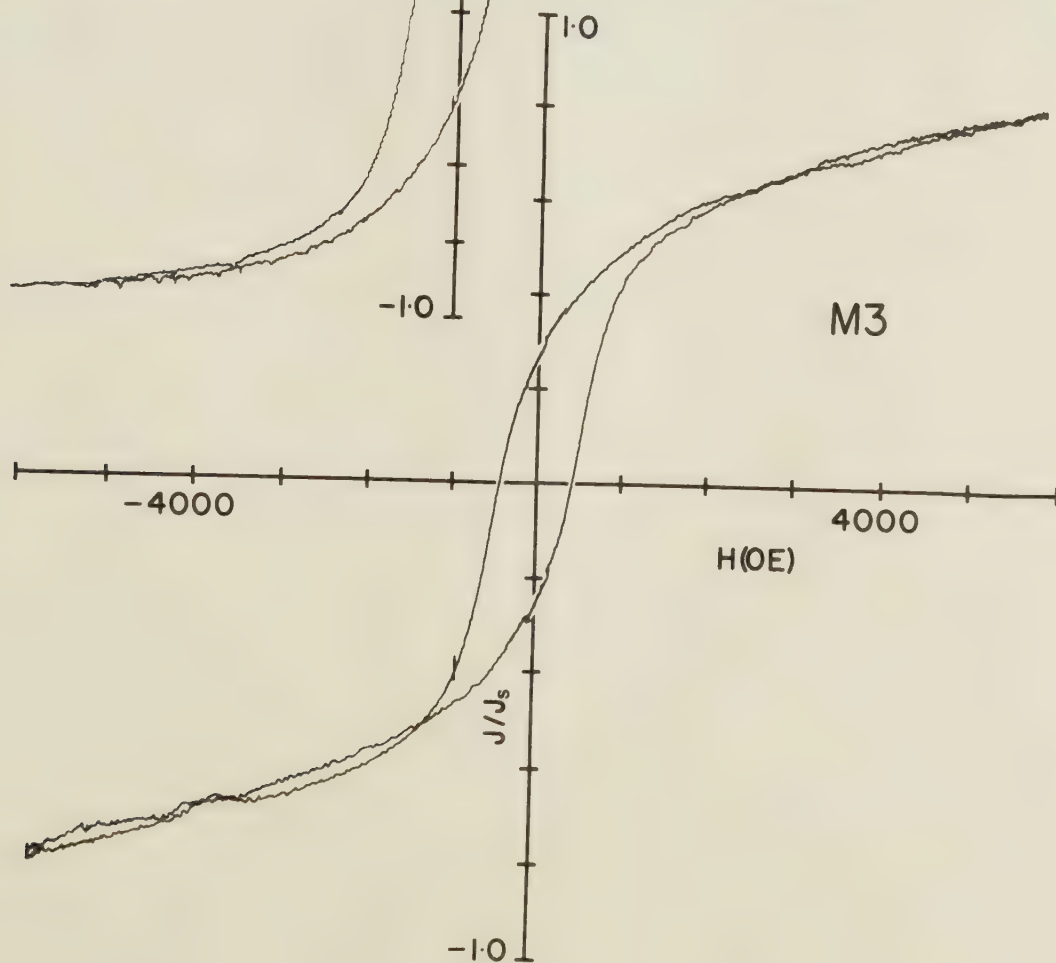
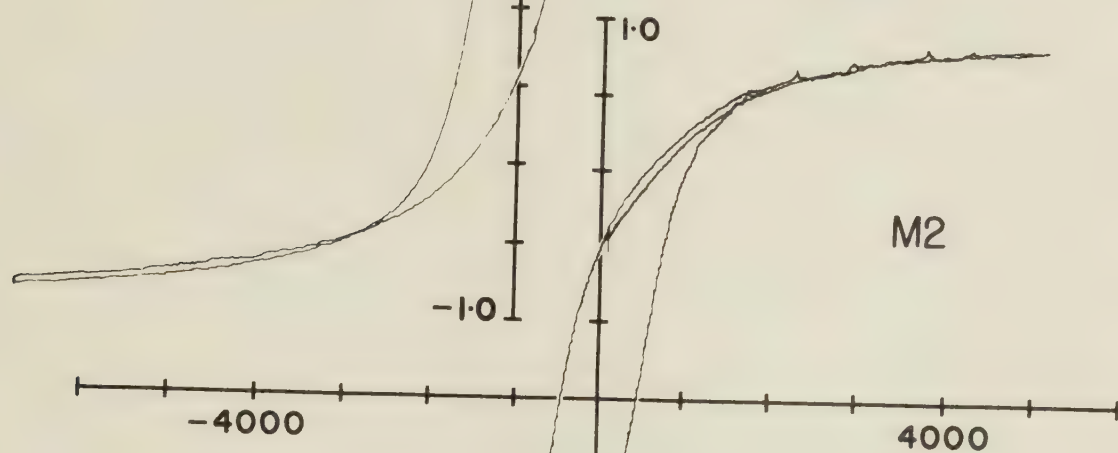
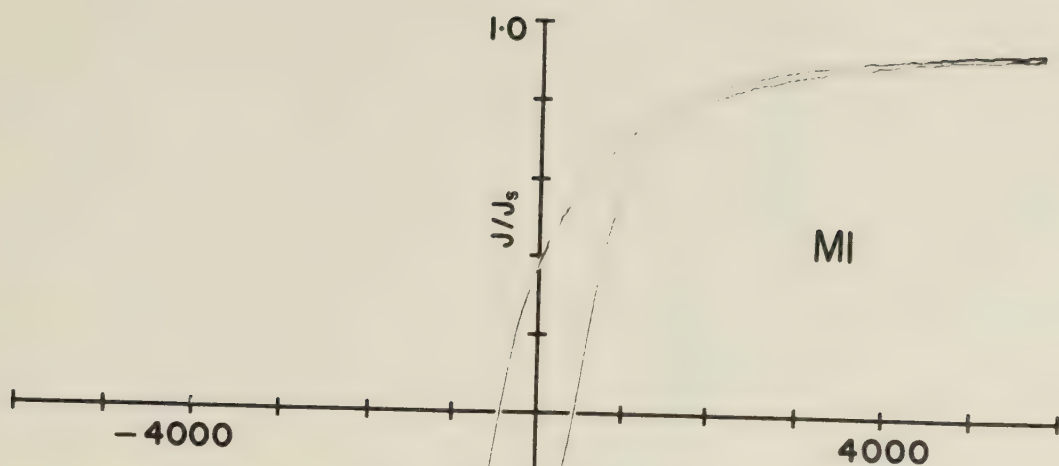








Fig. 18. Hysteresis loop of hematite (red anhydrous  
form from Fisher Scientific Co. Ltd.;  
mass:  $1.016 \pm 0.004$  g).

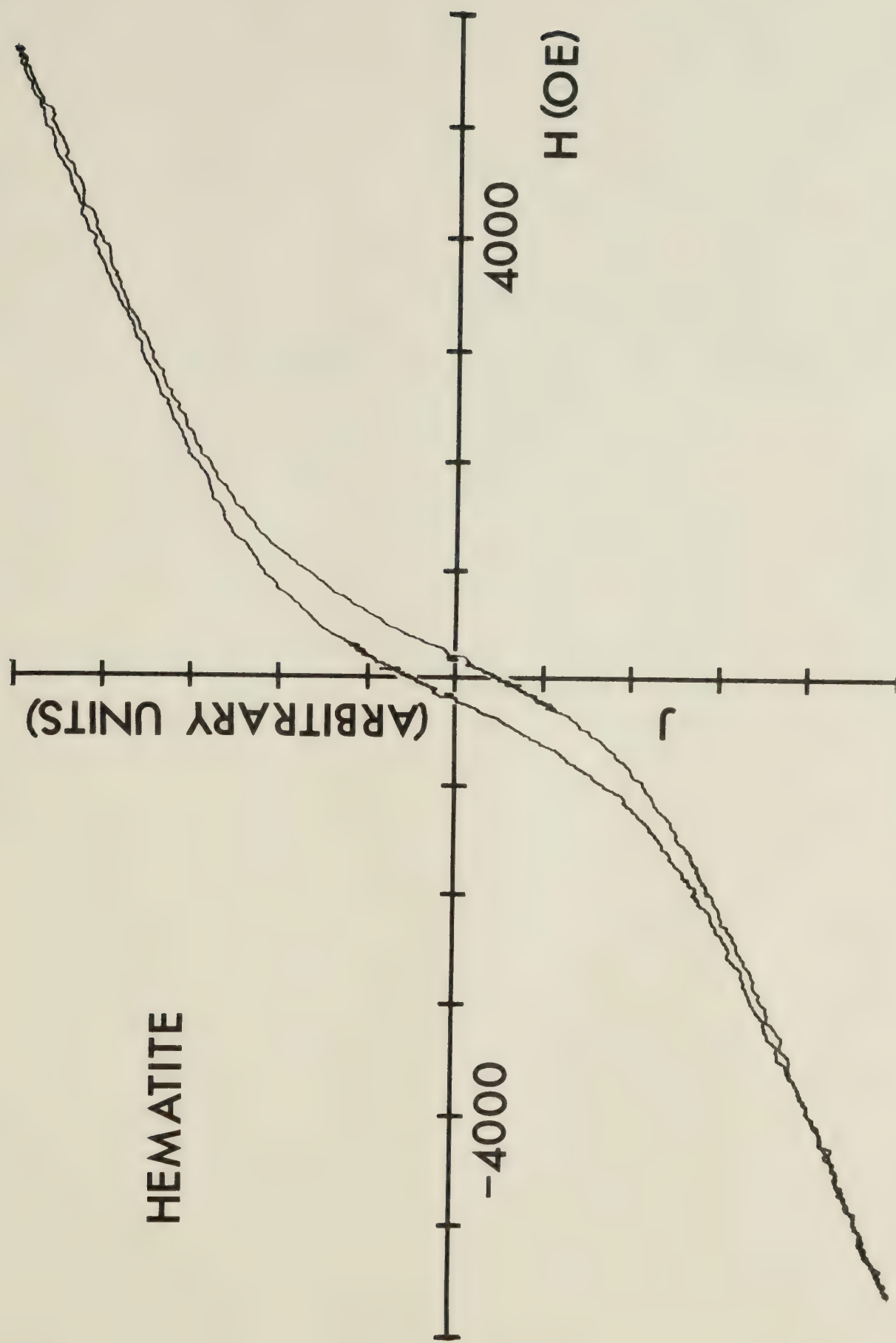






Fig. 19. Hysteresis of nickel calibration samples. All instrument settings remained constant for both curves.

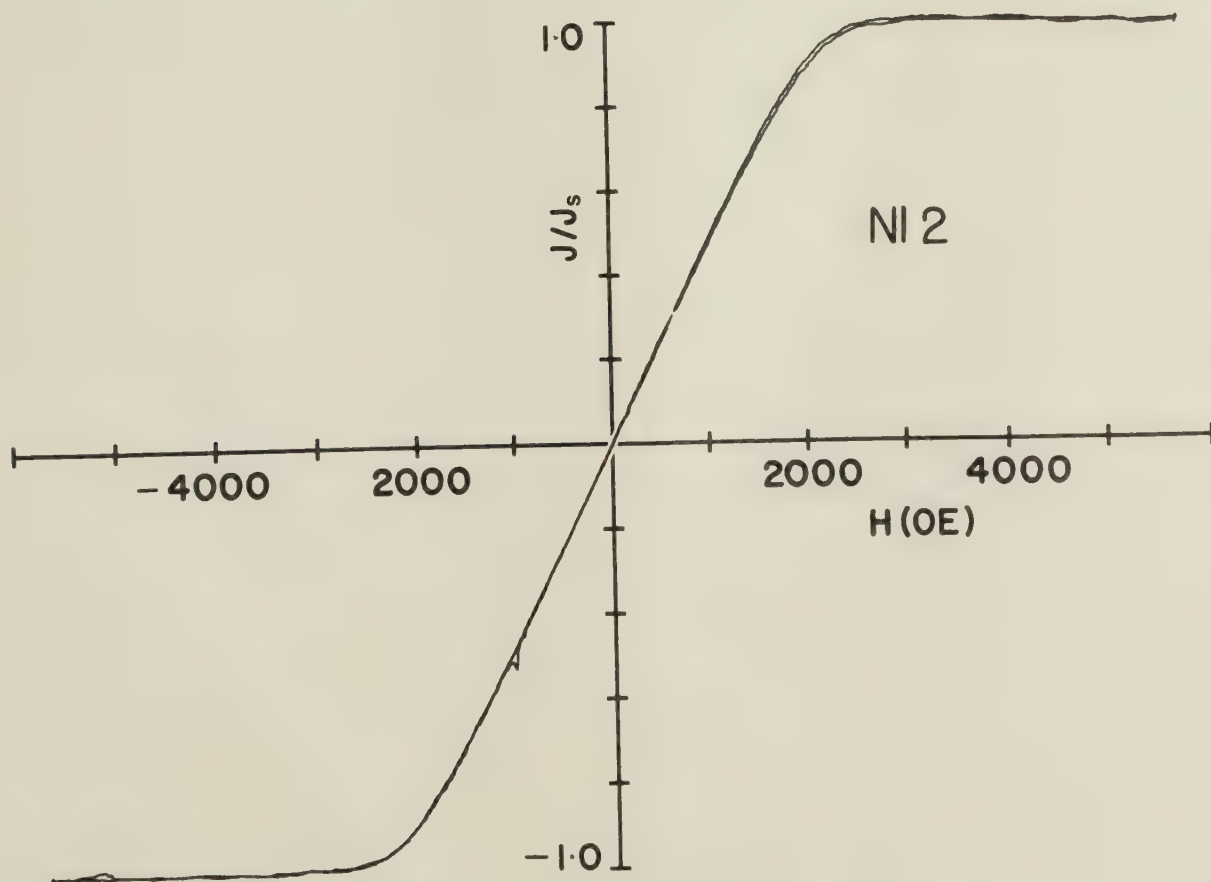
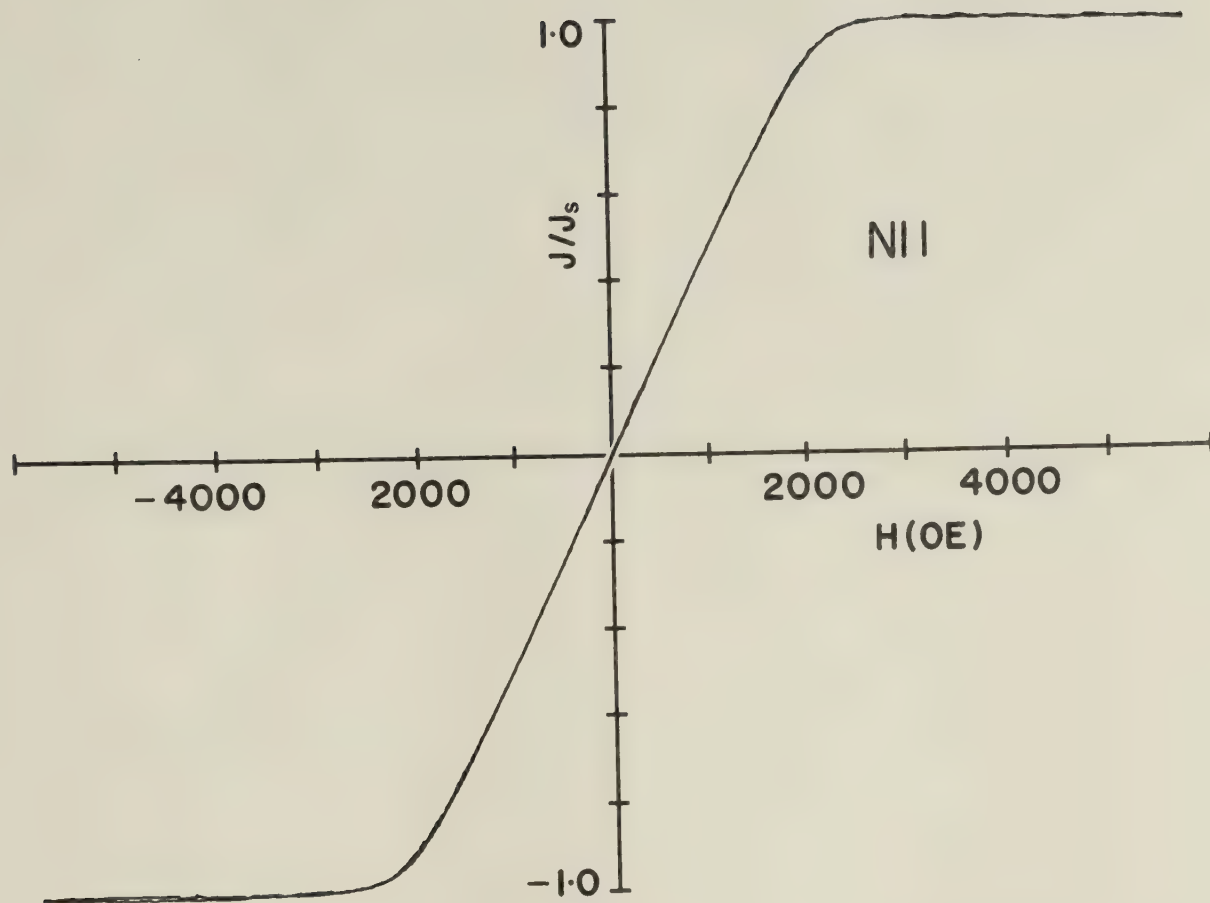
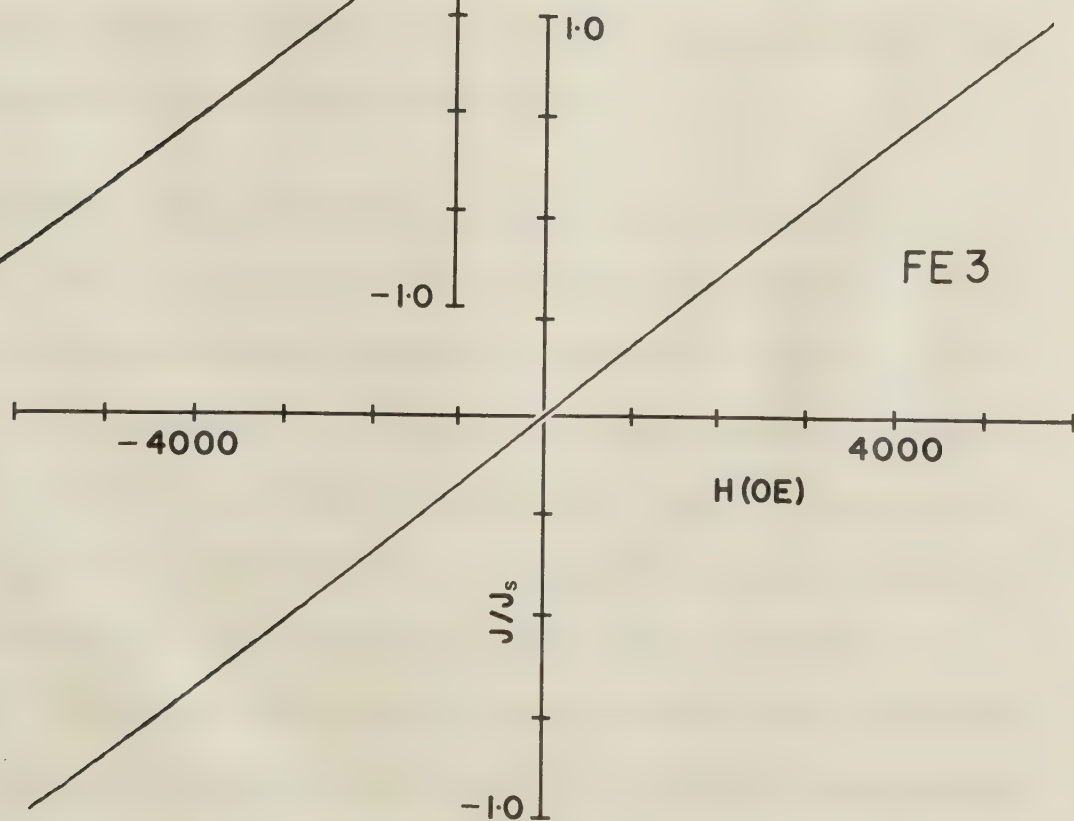
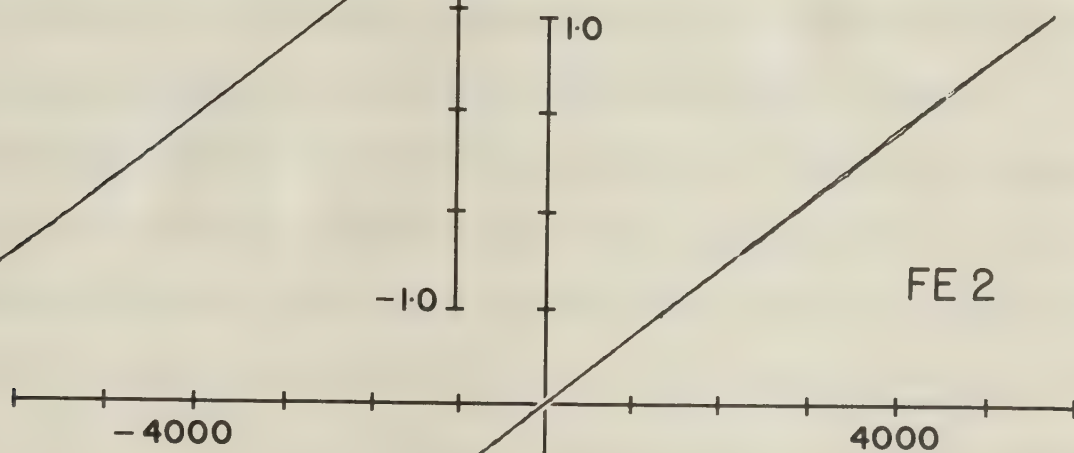
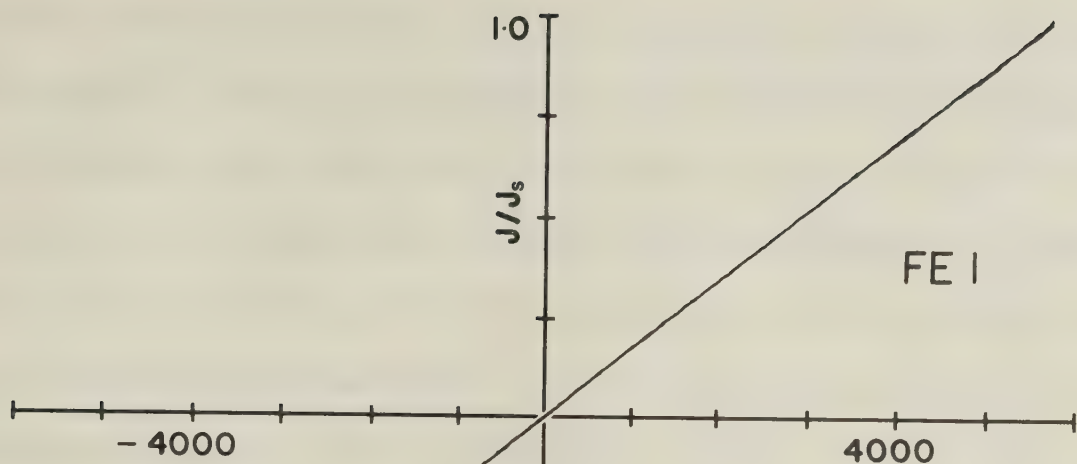








Fig. 20. Hysteresis of iron calibration samples. The vertical scale has been normalized to the highest magnetization attained. In this case therefore  $J_s$  is not the saturation magnetization. All instrument settings remained constant for all three curves.





curves drawn by an x-y plotter. The axes have been added later. Inconsistencies in the expected smooth curves are variously due to noise and possible slight sticking of the rod inside the guide tube (M1 and M3, Fig. 17). The noise appears to be greatest in the weakest samples as expected (M3, Fig. 17; Fig. 18). The observed curves at face value are those characteristic of the substances tested. Nickel curves display a slight negative slope at apparent saturation. It was first thought that this effect was due to the diamagnetism of the sample holder, but a rough calculation showed that the contribution from that source should be ten times smaller. Another possibility is that the magnetic field may pull the sample, and therefore the rod, slightly to one side. With increasing field this action will result in increasing friction between rod and guide tube, consequently reducing vibrational amplitude and hence the signal received by the detection coils.

Measurement of hysteresis curves for magnetite and hematite is most important from the paleomagnetic point of view. One of the present magnetite samples, diluted to 5% (28 mg) to correspond to a typical concentration in basic igneous rocks, had hysteresis which was easily measurable (Fig. 17). Since magnetite has a saturation magnetization of about 92 e.m.u./g, the moment of the sample should correspond to about 2.58 e.m.u. On the other hand hematite is much weaker than magnetite, and its present measurement (Fig. 18) allows a qualitative judgement to be made about



the sensitivity of the instrument. Considering the curve of isothermal remanent magnetization for single-domain hematite powder in Roquet (1954; given in Irving 1964) the magnetization of hematite measured in the present applied field of 5.7 kOe should be 0.026 e.m.u./g. It may be twice as large if the maximum saturation value of 0.5 e.m.u./g quoted in Irving (1964) is used. Hence, the moment of the present 100% sample (1.016 g; red anhydrous form from Fisher Scientific Co. Ltd.) should be at least 0.02 e.m.u., which is approximately 1.0% of that calculated for the 5% magnetite sample. The measured voltage readings on the lock-in amplifier for the two samples show a similar relationship wherein the hematite reading is 1.4% of the magnetite reading. There is some doubt as to whether the preamplification circuit corresponded in both runs, and so the relationship between the measured voltages, though appearing to conform to the magnetization calculations, is in doubt. If the measured relationship is true, then the instrument in its present form is capable of measuring magnetite in natural rocks in concentrations of at least 0.05%. The VSM, however, would not be capable of measuring the hysteresis of hematite found in red sediments which has typical proportions of 1 to 3% (Van Houten 1973) unless the hematite were concentrated by some method.





## Thermomagnetic Measurements

A thermomagnetic (or  $J_S$ -T) curve is a plot of magnetic moment ( $J_S$ ) (or intensity) versus temperature (T). At the Curie temperature of a ferromagnetic substance the spontaneous magnetization of a domain in zero field, disappears, and the substance becomes paramagnetic. Thus Curie point determinations are another useful aid in identifying the magnetic minerals present in a sample.

The Curie points of two known substances -- magnetite and nickel -- were determined. The curves are depicted in Figs. 21 and 22. Both continuous and discontinuous heating and cooling curves were measured, with the upper set of curves in each Figure being obtained first. These are the same samples for which the hysteresis was measured prior to heating.

For the continuous  $J_S$ -T curves the specimens were heated to  $<50^\circ\text{C}$  above their respective Curie points in 5 to 15 minutes, and then cooled to room temperature in a somewhat longer period of time (25 minutes for nickel) by means of a stream of evaporating liquid nitrogen trained on the outside of the oven. Due to thermal inequilibrium between sample and thermocouple, the heating curves lie to the left of the cooling curves in the critical higher temperature range. In the lower temperature ranges the cooling curves lie below the heating curves. In the case of magnetite much of this difference can be accounted for by an





Fig. 21. Discontinuous (top) and continuous (bottom) thermomagnetic curves obtained for the magnetite sample, M1. Vertical scales have been normalized to the magnetization at 25°C. A baseline shift occurred during the cooling cycle of the bottom experiment. All instrument settings remained the same for the two experiments.

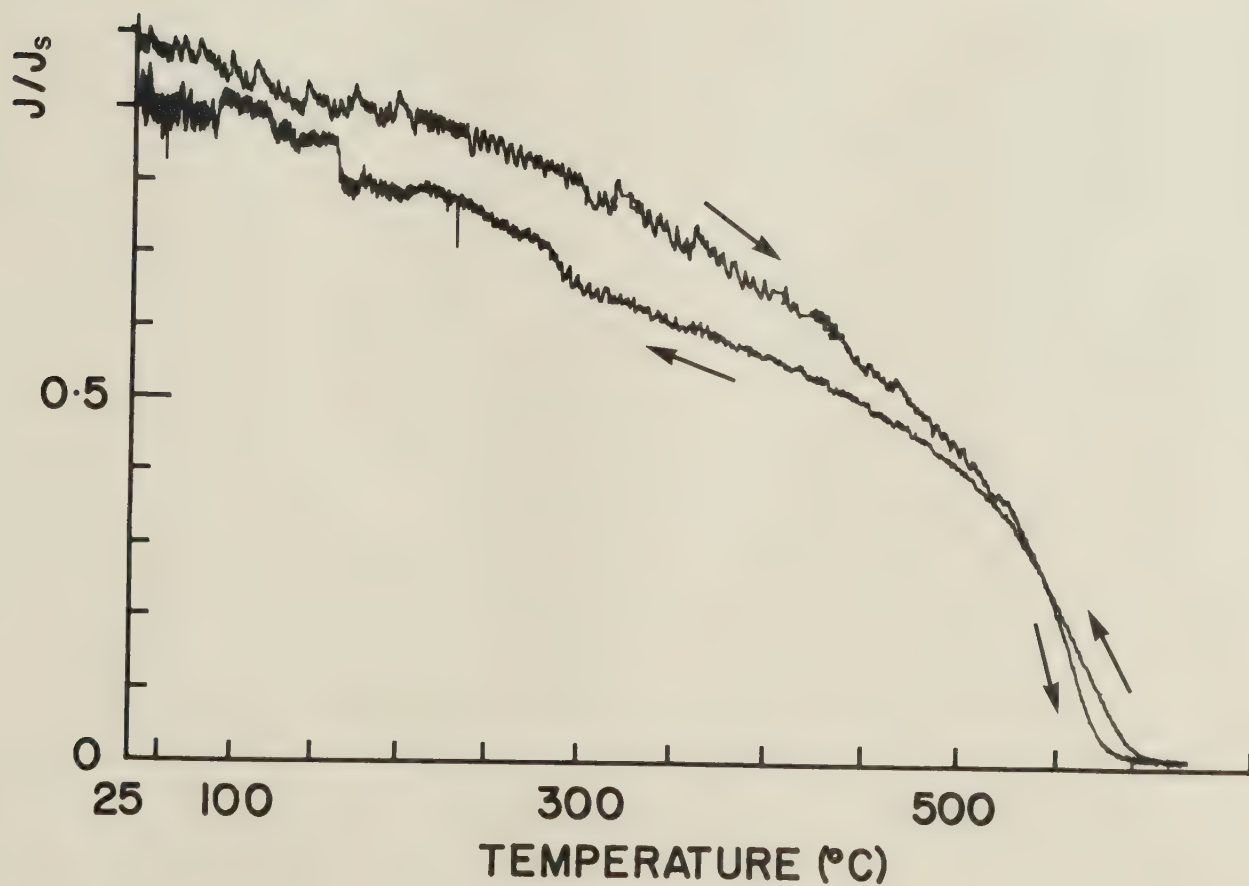
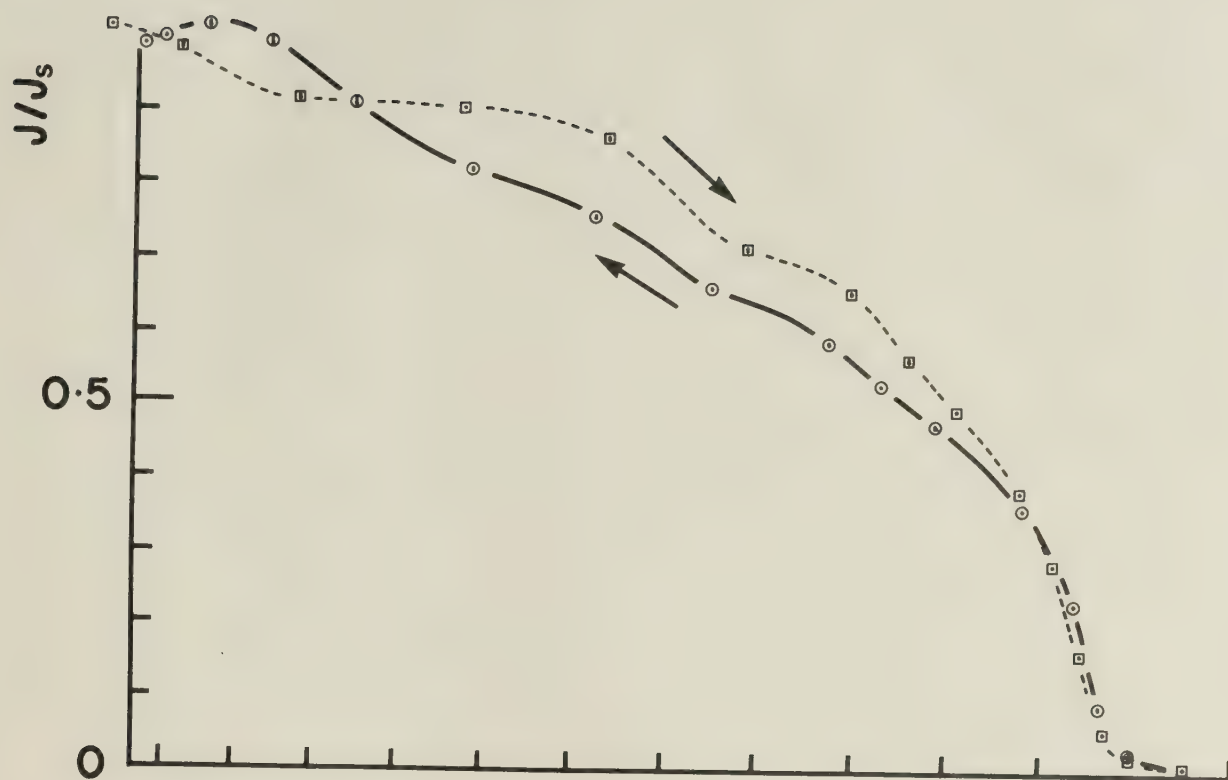
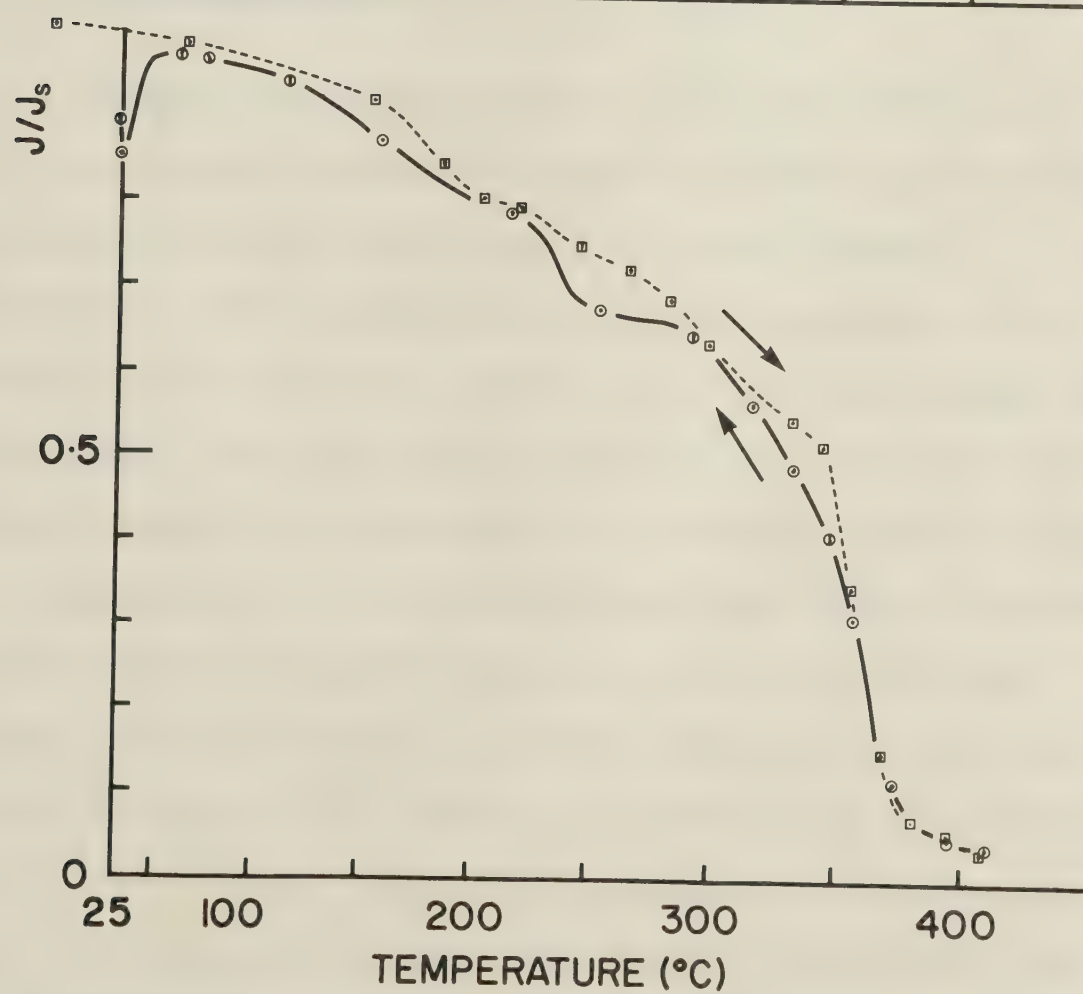
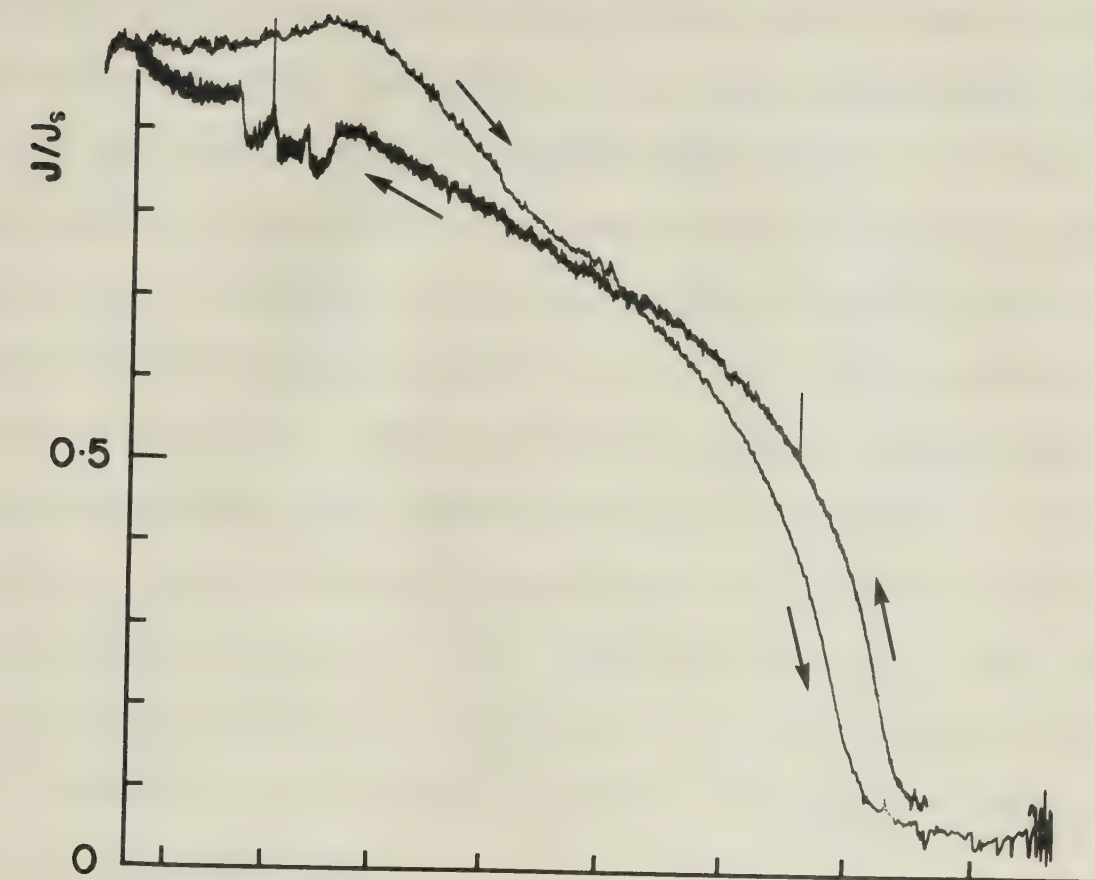








Fig. 22. Continuous (top) and discontinuous (bottom) thermomagnetic curves obtained for the nickel calibration sample, NI2. Vertical scales have been normalized to the magnetization at 25°C. In the top figure the apparent baseline shift in the latter portion of the cooling curve is due to a brief interval at which the time constant of the lockin amplifier was changed from 30 ms to 1 s. The spikes in the same curve are due to movements of the tubes carrying liquid nitrogen vapour through the detection coils. All instrument settings are the same for both runs, except as noted.





unexplained baseline shift determined from a check before and after the run. For nickel, the major differences may be due to annealing. Case and Harrington (1966) point out that the removal of small strains induced during the grinding process by the method of annealing can result in large changes in the magnetization curves of nickel depending on the treatment used. The initial increase in magnetization of the nickel curve may indeed have this explanation, for the result of heat treatment (annealing) is to increase the magnetization (Ibid.). Other inconsistencies in both nickel and magnetite curves are variously due to vibration of the coil leads and to periods of slight sticking of the rod within the guide tube.

To obtain the discontinuous  $J_s$ -T curves (Figs. 21 and 22), the oven was heated for short intervals (30 seconds to 2 minutes duration) and allowed to reach thermal equilibrium. This equilibrium condition appeared to be maintained for 20 to 30 seconds. Just as the voltage began to decrease the chart pen was lowered to the paper briefly (points enclosed by symbols) and a reading taken. Cooling was accomplished in the manner described above. The total duration of the magnetite run was one hour and fifty minutes. As expected the agreement between heating and cooling curves is much better, especially in the critical Curie point region, since the samples have been allowed to reach thermal equilibrium. Some inconsistencies in the nickel curves are probably explained by the sticking



problems mentioned above. There is a rather consistent difference between the heating and cooling curves of magnetite (Fig. 21). This may be explained by the oxidation of a small portion of the magnetite to hematite as evidenced by a layer of red matter on the top surface. When the baseline shift is taken into account in the continuous curve done later, the effect is less noticeable; evidently the surficial oxide acts as a barrier to further oxidation.

For comparison the continuous heating curve and discontinuous curves for magnetite are normalized, and plotted together with a theoretical  $J_S$ -T curve (Fig. 23). The same procedure was followed for the nickel curves, except that the continuous cooling rather than heating curve is used. Both nickel and magnetite theoretical  $J_S$ -T curves were plotted from tables of values normalized to J at 0°K and T at  $\theta$  (Ni: American Institute of Physics Handbook, p. 5-145). The Curie points of these theoretical curves were plotted assuming values of 580 and 358°C for magnetite and nickel respectively. The continuous cooling curves (that for magnetite not shown) agree with the discontinuous curves for both substances. Evidently, the slower process of cooling has allowed the samples to attain thermal equilibrium; that is,  $\Delta T_{st}$  is a minimum.

Curie points were obtained for all the experimental curves (Table 4).  $\theta$  may be derived empirically -- for example, by determining the point of inflection on the







Fig. 23. Comparison of various thermomagnetic curves obtained for magnetite (top) and nickel (bottom). All curves have been normalized to their respective magnetizations at 25°C. The magnetite curves compared are the discontinuous heating (1) and cooling (2) curves (Fig. 21), the continuous heating (3) curve (Fig. 21), and a theoretical curve (4). Nickel curves compared are the continuous cooling curve (5) (Fig. 22), the discontinuous heating (6) and cooling (7) curves (Fig. 22), and a theoretical curve (normalized values given in American Institute of Physics Handbook, p. 5-145).

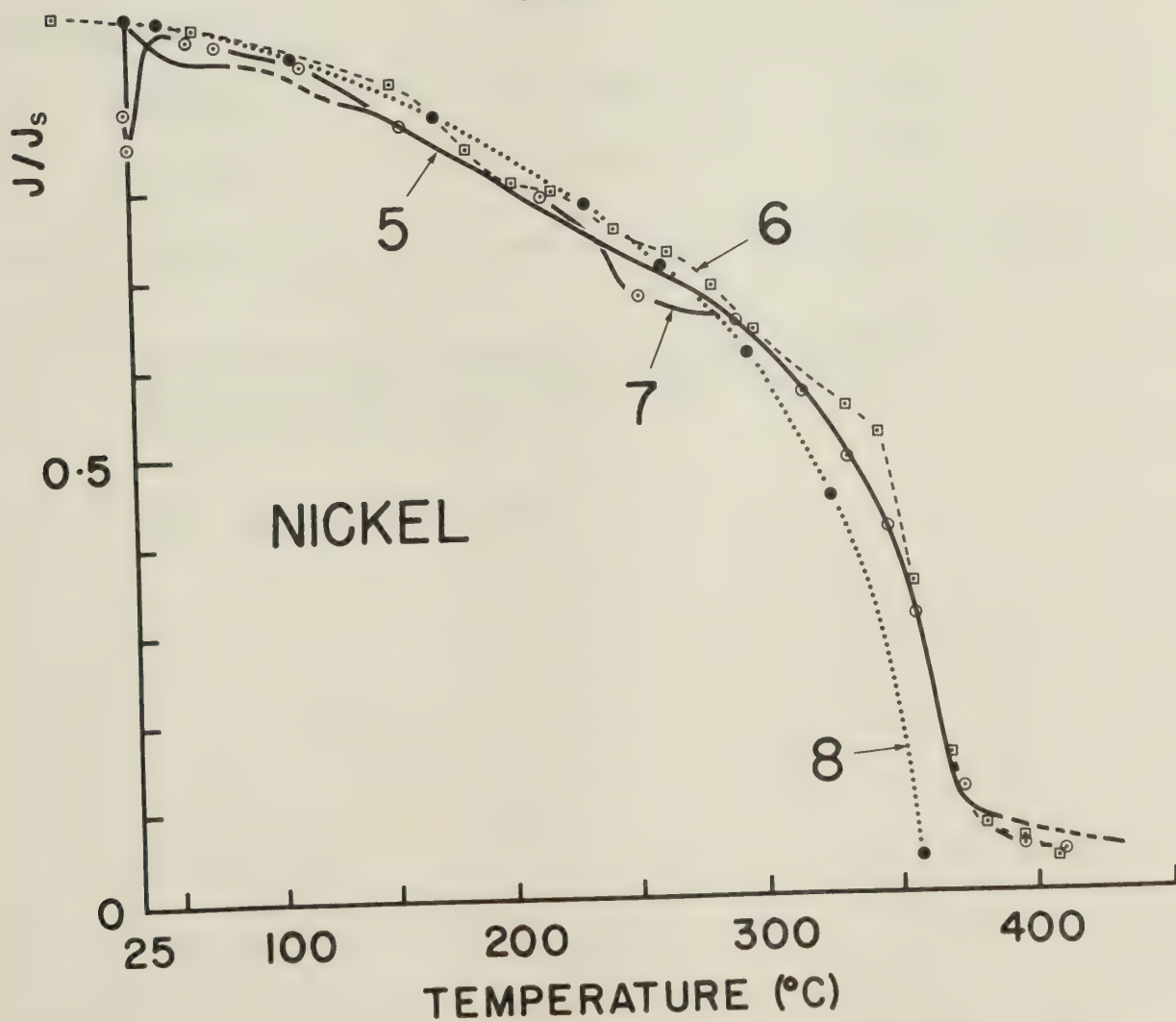
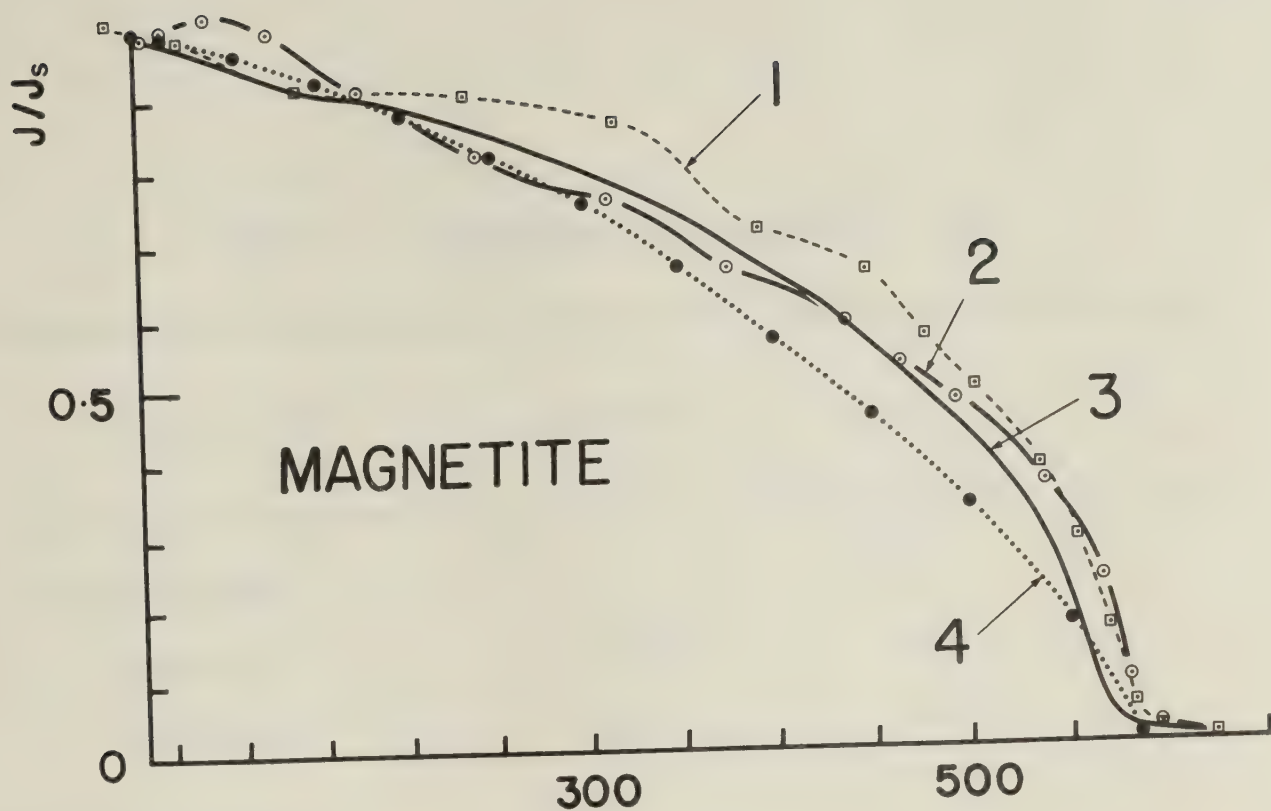




TABLE 4. MEASURED CURIE POINTS<sup>1</sup> (°C)

$J_s$ -T Curve <sup>2</sup>	Nickel	Magnetite
Discontinuous		
heating	376	589
cooling	376	589
Continuous		
heating	359	573.5
cooling	374	589.5

<sup>1</sup> determined by inflection point method.  
R.m.s. errors for nickel are  $\pm 4^\circ\text{C}$  and  
for magnetite  $\pm 5^\circ\text{C}$ .

<sup>2</sup> see Figs. 21 and 22.





thermomagnetic curve -- or defined more precisely, by using the Weiss theory (see Bozorth 1951).

All determined magnetite  $\theta$ 's are higher than the theoretical values (the continuous heating curves of magnetite and nickel were not used for  $\theta$  determination), and agree to within  $1^\circ\text{C}$  (Table 4). The maximum error ( $5^\circ\text{C}$ , see Table 3) brings the experimental value within range of the ideal Curie point for magnetite ( $585^\circ\text{C}$ ) quoted by Smit and Wijn (1959). Other authors quote  $575^\circ\text{C}$  (Bozorth 1951, Akimoto 1962),  $578^\circ\text{C}$  (McElhinny 1973), and  $580^\circ\text{C}$  (Irving 1964, Stacey and Banerjee 1974). One reason for the higher  $\theta$  may be the fact that because of the temperature gradient the lowest part of the sample will be 2 to  $3^\circ\text{C}$  cooler than the centre part and will therefore not be demagnetized until its central temperature is greater than  $\theta$ . In addition, the sample was measured at  $0.14 \pm 0.16$  cm below the oven centre (Table 1) which may account for another 1 to  $2^\circ\text{C}$  difference.

Like the experimental magnetite values all the nickel  $\theta$ 's determined using the empirical method are higher than the theoretical value ( $375 \pm 4^\circ\text{C}$  vs.  $358^\circ\text{C}$ ). Bozorth (1951) notes that determinations of the Curie temperature vary from  $358$  to  $382^\circ\text{C}$ , but that the true value probably lies between  $358$  and  $363^\circ\text{C}$ . This variation is probably due to the facts that the change from the ferromagnetic to the paramagnetic state is not sharp and that the shape of the curve changes -- especially in the critical  $\theta$  region -- when a high field



is applied ( Ibid., p. 717). The Weiss equation that essentially relates spontaneous magnetization <sup>2</sup> ( $J_S$ ) to absolute temperature ( $T$ ) is

$$\frac{J_S}{J_O} = \tanh \frac{J_S/J_O + H/LJ_O}{T/\theta} \quad (4)$$

where  $J_O$  is the spontaneous magnetization at 0°K,  $H$ , the applied field, and  $L$ , the molecular field constant. For weak fields, the term  $H/LJ_O$  is negligible, but for high fields, the thermomagnetic curve is distorted in the critical region such that the apparent  $\theta$ , given by the inflection point, increases for increasing  $H$ . From curves given in Bozorth the point of inflection for a curve modified by the  $H$  of the present experiments (4757 Oe) was estimated to be 372°C, in good agreement with the inflection points of the experimental curves (Table 4). By an inverse process one should be able to arrive at the true  $\theta$  by using the above equation; however values from the equation diverge from experimental data in the region of  $\theta$ .

### Measurements of Magnetic Domain State

It has been shown that "a random distribution of non-interacting single-domain grains having uniaxial

---

<sup>2</sup> $J_S$  = magnetization within magnetic domain,  $J$  = true magnetization in sample;  $J_S=J$  when the magnetic domains are completely aligned, therefore the value  $J$  should strictly be used in the above equation. However, the two quantities are almost indistinguishable except in high fields and at temperatures near the Curie point.



anisotropy will have a  $J_r/J_s$  ratio of 0.5 (Stoner and Wohlfarth 1948)". Davis and Evans (1976) suggest that ratios less than 0.5 are largely due to grain interactions rather than to the presence of multidomain grains as has been assumed by other workers. The lowering of this value is thought to be caused by the presence of a demagnetizing field associated with the surface distribution of poles on interacting grains. In this case, the relation between the external applied field,  $H_e$ , and the demagnetizing field,  $H_d$ , is as follows:

$$H_i = H_e - H_d = H_e - NJ \quad (5)$$

where  $H_i$  is the internal field and  $N$ , the demagnetization factor. For the magnetite powders dealt with here,  $H_d$  is not due to a solid mass, and therefore  $NJ$  is modified to  $NPJ$ , where  $P$  is the packing factor. In other words  $H$  must be proportional to the concentration of magnetite. The determination of  $J_r/J_s$  can thus be used with hysteresis loops generally to indicate the presence of single-domain grains and to gauge their degree of interaction.

This has been done for the three magnetite samples (Fig. 17) from a synthetic single-domain commercial powder (0.5  $\mu\text{m}$  lengths, axial ratio 6:1). M3 is a sample diluted to about 5% (28 mg) by KBr to make it comparable to the composition of basic igneous rocks. The  $J_s$  value is determined by the method of Bean and Jacobs (1960) by first plotting  $J$  against  $1/H$  for values of  $H$  between 3 and 6 kOe (Dunlop 1973), and then extrapolating to  $1/H = 0$  (see Fig.





43, Appendix 3). From these values the vertical scale for each hysteresis loop has been determined. The  $J_r$  value required is not the remanent magnetism when  $H = 0$  as shown in Fig. 17, but rather the value when  $H_i = 0$ , since  $J_r/J_s$  in the present context is concerned solely with the internal or intrinsic properties of the assemblage of magnetite particles. To find the intrinsic hysteresis loops one merely draws new axes which satisfy the condition  $H = 0$ . At this particular point  $H_e = NPJ$ , the slope of the new vertical axis is  $1/NP$ , and  $J = J_r$ . Calculations of  $N$  and  $P$  are given in Appendix 3.

The determined  $J_r/J_s$  values for M1, M2, and M3 are respectively  $0.46 \pm 0.01$ ,  $0.47 \pm 0.01$ , and  $0.26 \pm 0.00$ . The values for the most concentrated samples, M1 and M2, are quite close to the theoretical value of 0.5. The extremely low value for M3, the most dilute sample, is problematical.

## Calibration

There are two widely used methods for calibrating a VSM: the comparison method and the slope method (Case and Harrington 1966). The former uses a material of known magnetization -- usually a sphere of pure nickel; but the prime disadvantage of this method is the uncertainty in the absolute magnetization of the calibrating sample. In the case of nickel the magnetization depends on such parameters as purity, density, magnetic field, temperature, strains,





and annealing. The slope method was developed primarily to avoid the foregoing pitfall inherent in the comparison method (Ibid.), and is the method used here. This method uses the low-field linear portion of the hysteresis curve of a high-permeability ferrite or ultrapure iron for calibration. In the present experiments iron of 99.57 wt. % purity is used (analysis in Appendix 4). The calibration procedure involves the derivation of a calibration constant ( $K_1$ ).

The relevant formula for determining the magnetization ( $J_O$ , in gauss) is as follows:

$$J_O = \frac{1}{K_1} \frac{E_O}{D_O^3} \quad (6)$$

where

$$K_1 = \frac{[(\mu-1)^{-1} + N] \Delta E_C}{D_C^3 \Delta H_C} \quad (7)$$

and where  $D_C$ =diameter of calibrating sphere,  
 $D_O$ =diameter of unknown sample sphere,  
 $N$ =demagnetization factor of calibrating  
sample,



$\mu$  =relative permeability of calibrating sphere  
 $\Delta H_C$  =change in dc magnetic field applied to  
 calibrating sample in linear portion of  
 curve,  
 $E_O$  =coil voltage from unknown sample, and  
 $\Delta E_C$  =change in coil voltage from calibrating  
 sample corresponding to  $H$  ,

Derivation of this equation is given in Appendix 5. Using the iron calibrating spheres values of  $K_1$  were calculated and averaged (Table 5) and used to calculate the magnetization of the ultrapure nickel samples using equation (6) above (analysis in Appendix 5, relevant nickel parameters in Appendix 6). The average value ( $481 \pm 14$  gauss) compares favourably with that found in the literature ( $484.1$  gauss ( $15^\circ\text{C}$ ), Bozorth 1951). A similar attempt was made to calculate the magnetization of the magnetite samples using the calibration constant, but the result -- widely divergent from the true value -- indicates that true determinations will not be possible using large non-spherical samples.

The hysteresis curves of the nickel and iron calibration samples provide a reasonable test of instrument repeatability. The best test would be provided by repeat measurements on a single sample reinserted prior to each measurement. The iron calibration spheres are almost identical, as are the nickel spheres; so that in these cases the single-sample assumption is reasonable. Table 6 gives several examples testing repeatability, which involve raw



TABLE 5. VSM CALIBRATION CONSTANT ( $K_1$ )

Sample	$K_1 \pm \sigma$ (mV/Oe/cm <sup>3</sup> )
FE 1	$(3.612 \pm 0.131) \times 10^{-3}$
FE 2	$(3.455 \pm 0.195) \times 10^{-3}$
FE 3	$(3.474 \pm 0.102) \times 10^{-3}$
mean <sup>1</sup>	$(3.52 \pm 0.07) \times 10^{-3}$

<sup>1</sup> Weighted mean.





TABLE 6.  
TESTS OF MEASUREMENT REPEATABILITY

Calibration material	N	Magnetization (mV) (mean ±a%)	Calibration constant (mV/Oe/cm <sup>3</sup> ) (mean ±100E(%))
iron	3	1.831±0.68	3.52 × 10 <sup>-3</sup> ±2.11
			<u>Magnetization (gauss)</u>
nickel	2	0.651±1.92	475±2.90

N is the number of samples,  
a, the absolute error, and  
E, the relative error.



and processed data. As a first approximation to repeatability the raw voltage of the three iron samples at maximum applied field are found to repeat with <1% absolute error. For the two nickel samples the error is <2%. Since this error also involves any sample differences, the error in repeating measurements in general will be even lower. For the processed data, which takes sample differences and any error in basic measurements into consideration, the relative error associated with the calculation of the calibration constant ( $K_1$ ) using iron is only about 2% and with the calculation of the magnetization of nickel, <3%. The successively larger errors of the processed data are due to the combining of errors associated with the various parameters used in equations (7) and (6) above for the calculation of the calibration constant and then the magnetization of nickel respectively.



## Chapter 4: Remanence In Oxidized Olivines

### Introduction

Olivine is an important constituent of basic igneous rocks, which are generally a prime target for paleomagnetic studies. The other primary constituents of these rocks -- pyroxene and plagioclase -- have been shown in some cases to contain small magnetic particles carrying a stable remanence. Several studies have also shown that olivine too may contain magnetic minerals as products of high temperature oxidation, but relatively little work has been done on the actual magnetic properties of these minerals. In this chapter a summary of earlier work is presented followed by a description and discussion of the present work and of its relation to the earlier studies. First a brief summary of the types of remanent magnetizations (RM's) is given.

A number of different RM's are found in natural rocks constituting what is called the natural remanent magnetization (NRM). The useful stable RM's of igneous rocks are thermoremanent magnetization (TRM) and chemical remanent magnetization (CRM).

TRM is produced when a magnetic grain cools through its critical blocking temperature (BT) in the presence of a field ( $h$ ). On the other hand CRM is produced at constant  $T$  as a magnetic grain grows through its critical blocking volume (BV) in  $h$  due to chemical changes. Both



magnetizations are described by the same equation, and their relaxation times can be described in terms of the ratio  $v/T$  where either the volume,  $v$ , or  $T$  is constant.

A description of magnetic stability is much simplified by considering only single-domain (sd) grains. In this case the stability increases as the quantity  $v/T$  becomes larger. Other parameters which determine the stability are largely concerned with the elastic and magnetic properties associated with a particular magnetic mineral. These include the shape of the grain, the spontaneous magnetization, and the coercive force,  $H_C$ . Those parameters which tend to disrupt the stable magnetization are the thermal energy ( $k_1 T$ ) and the magnetic field ( $h$ ), where  $k_1$  is the Boltzmann constant. Below a critical  $v$  a grain at the ambient  $T$  will be superparamagnetic (sp); that is, having a very small relaxation time, its magnetic moment will freely rotates in response to thermal fluctuations. At increased ambient  $T$ 's more grains will be sp. In fact, virtually every sd grain will be sp at some  $T$ , and all become paramagnetic at the Curie  $T$  when they lose their spontaneous magnetization. If a sp grain increases in size at the ambient  $T$ , it will eventually grow through its BV and become stable. Continued growth will bring it to the point where it is energetically more favourable for the sd to break up into several domains. It then exhibits pseudo-single-domain (psd) behaviour; that is, it still behaves like sd's in many ways, but has a lower  $H$ . With increasing growth it becomes multidomain (md) and





increasingly less stable.

Just as  $T$  can overcome the effects of  $v$ , so too can  $h$  overcome the effects of  $H_C$ . In nature, magnetic fields associated with lightning produce an often very intense magnetization called isothermal remanent magnetization (IRM). It is essentially formed instantaneously and affects all grains having  $H_C$ 's less than  $h$ . It is a useful magnetization, since it can easily be produced in the laboratory, and it allows one to investigate all or a portion of the  $H_C$  spectrum. Another useful laboratory magnetization is anhysteretic remanent magnetization (ARM) which is produced by superimposing a small constant field on a large alternating field (AF) that is gradually reduced to zero. It has similar characteristics to TRM and is sometimes used as a non-destructive analogue, but is not used in the present work. All these magnetizations can be removed by sufficiently high  $T$ 's or  $h$ 's. Through the use of a stepwise progressive increase in either  $T$  or  $h$ , one can determine the  $BT$  and  $H_C$  spectrum of a sample. The usual field demagnetization method involves AF's. At a given AF, all domains with  $H_C$ 's less than the field move in unison with it, and as the field is decreased to zero become progressively randomized.

### Early Mineralogical Work

Haggerty and Baker (1967) studied the alteration



products of olivines from basalts and reheated gabbroic and ultrabasic xenoliths, and compared them to products obtained during various heating experiments on powdered and single crystal olivine samples of composition FA20 (for explanation of nomenclature see p.5). They determined that at temperatures between 600 and 820°C hematite exsolves from the olivine leaving a forsterite-enriched matrix. Commonly the hematite develops along hairline cracks and at grain boundaries where a poorly developed rim forms. They showed that the hematite rim was not related to iron-rich zones in the olivines, but instead resulted from the solid diffusion of iron.

Above 820°C magnetite and enstatite rather than hematite are the first products to appear; but these gradually invert to hematite and forsterite as oxidation proceeds. Magnetite first appears throughout each crystal as symplectic intergrowths (symplectites) due to nucleation processes. Oxidation is greatest at grain boundaries where the growth of the symplectite results first in lamellae and then irregular plates. As oxidation proceeds this magnetite transforms to hematite. Eventually a thick, usually discontinuous rim of hematite results, having a sharp inner boundary against a zone deficient in opaque oxides. These rims are especially well-developed at higher temperatures. Observation of the centres of these highly oxidized olivines revealed that the symplectic magnetite was well preserved. Haggerty and Baker explain this as being either due to the





hematite rim which acts as a semi-permeable barrier permitting only limited oxidation; or to the possible presence of small amounts of MgO in the magnetite which tends to stabilize it (Tsvetkov et al. 1966). The presence of both hematite and magnetite was confirmed during the course of their work by microsampling and X-ray powder photography and they were able to calculate the composition of the olivine after each heating run. However, they were not able to detect magnesioferrite ( $\text{MgFe}_2\text{O}_4$ ) -- a possible alteration product; and this apparent absence is supported by the mineralogical evidence in polished sections.

Champness and Gay (1968) and Champness (1968, 1970) extended the oxidation experiments of Haggerty and Baker (1967) to other olivine compositions (FA52 and FA100) and to a wider temperature range (200-1200°C) in order to clarify the mechanism of olivine alteration. They found that in early stages of the reaction a magnetite-like phase was precipitated. This was followed by a hematite-like phase, which was the main precipitate between 200 and 800°C. Both phases apparently grow as needles below 900°C, controlled by dislocations in the olivine lattice. During this process oxidation occurs at these dislocations or interfaces -- as Champness suggests -- by the solid diffusion of  $\text{Fe}^{2+}$  ions through the oxygen lattice to become  $\text{Fe}^{3+}$  at the interface. Simultaneously  $\text{Mg}^{2+}$  ions migrate in the opposite direction to maintain the charge balance, and thus make the interior parts of the grain more forsteritic. At higher temperatures





large-scale diffusion makes possible the formation of enstatite by the reaction of silica with forsterite. X-ray reflections of the oxide phases precipitated below 900°C are very diffuse and are indicative of imperfect or disordered precipitates. These coarsen above 1000°C and the corresponding reflections sharpen. Champness notes that above 900°C the magnetite-like phase is probably close to magnetite in composition, with perhaps some magnesium in solid solution.

### The Work of Hoyer

Later work on the opaque minerals of oxidized olivines was carried out by Hoyer (Hoyer and O'Reilly 1973, Hoyer and Evans 1975) using synthetic olivines: first, primarily to study the oxidation of olivines at lower temperatures (500°C) than did Haggerty and Baker (1967) (Hoyer and O'Reilly 1973), and second, to investigate the properties of the remanent magnetizations produced in the resultant oxidized and oxidizing olivines at the lower temperatures (Hoyer and Evans 1975). The lower temperature range was chosen, not only because earlier workers had primarily concerned themselves with alterations in the higher temperature range (500-1100°C), but also because low temperature alterations of the ferrimagnetic minerals could produce a paleomagnetically useful CRM comparable in intensity to TRM.



The first paper (Hoye and O'Reilly 1973) involves heating olivine of composition FA50 at temperatures between about 270 and 700°C, and monitoring the magnetic phases produced using thermogravimetric and thermomagnetic techniques.

As described in the first part of the paper three magnetic mineral phases were identified. Phase A, produced between 250 and 450°C, was identified as magnetite. In large olivine grains it was found to be stable up to 700°C, but in finely divided olivine it became chemically altered. Phase B with a Curie temperature between 350 and 370°C appeared when the ambient temperature was above 550°C, and was tentatively identified as magnesioferrite. The third phase, C, with a Curie temperature of 680°C, increased in quantity with prolonged thermomagnetic cycling and was identified as hematite. They observed that the oxidation of phase A did not produce phase B, but rather phase C. And they correlated phases B and C respectively with the magnetite-like and hematite-like products observed by Champness (1970) and Riding (1969).

A second part of the paper describes the growth of chemical remanent magnetization (CRM) in finely divided olivine. The sample was heated at a constant temperature of 345°C for a total of about 21 hours in an oxygen atmosphere and an 11 Oe field. After an initial 30 minute period during which there was no oxygen present, oxygen was introduced,



and the induced and remanent magnetizations measured at intervals with a VSM. The curve of remanent magnetizations is shown in Fig 24. According to Hoyer and O'Reilly the initial dramatic growth of remanence is due to the introduction of oxygen, and occurs as the magnetic grains grow through their blocking volumes, changing from sp to sd size. As they continue to grow they become md; hence the later decline of the remanence. They therefore concluded that magnetite originating at low temperatures in nature could acquire a CRM following long exposure to moderate temperatures under oxidizing conditions. From their higher temperature experiments, they concluded that the magnesioferrite and hematite produced under oxidizing conditions in nature could acquire a TRM which would constitute a significant portion of the NRM.

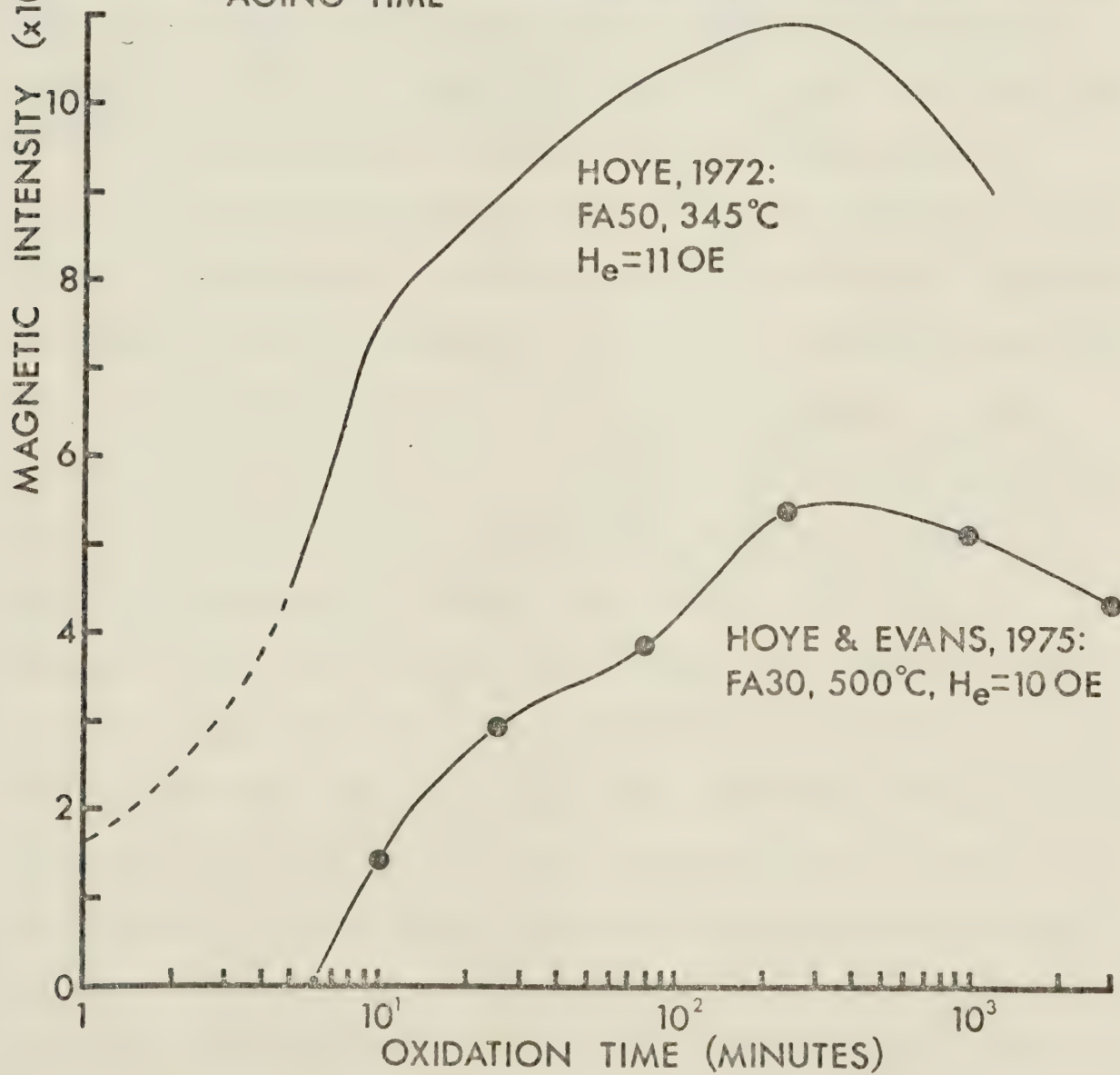
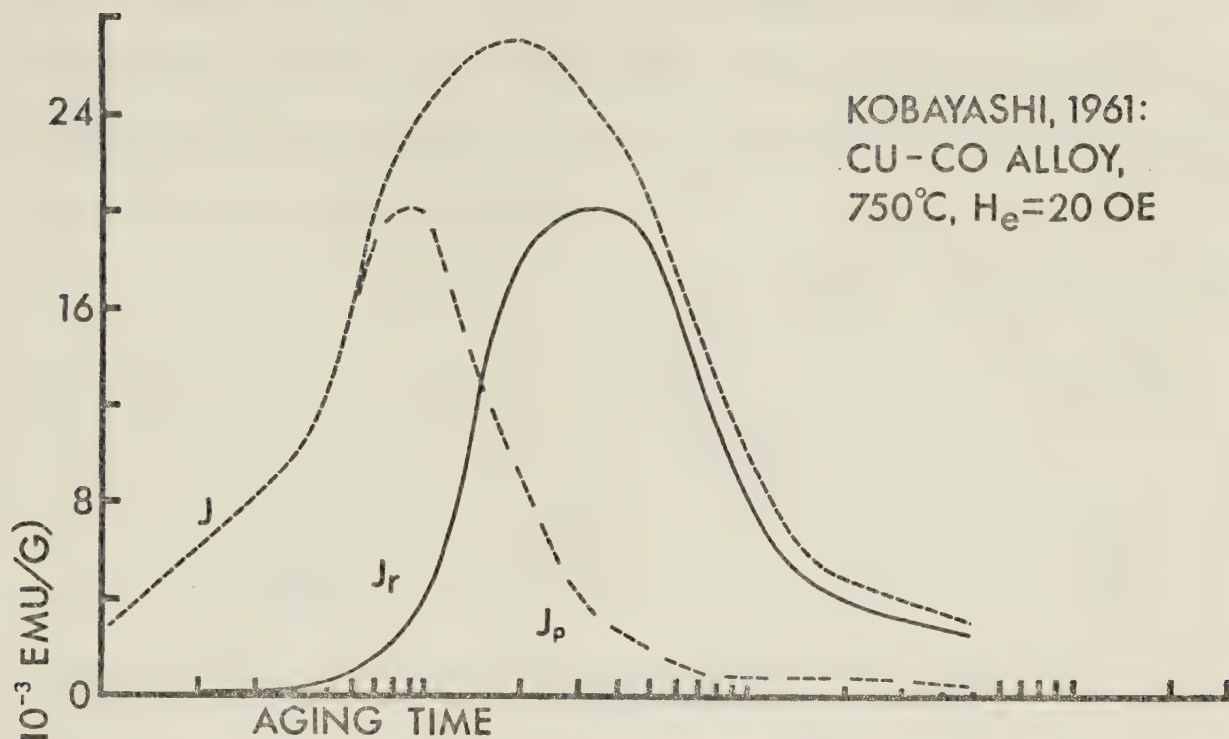
The second paper (Hoyer and Evans 1975) investigates the properties of remanent magnetizations produced in oxidized olivines, with the aim of determining the possible magnetic strength and stability of the correlative oxidation products found in nature. Initially, seven finely-divided synthetic olivine samples of composition FA30 were oxidized at 500°C for varying lengths of time in an oxygen atmosphere and a 10 Oe field. Each sample was then subjected to the following procedure: AF demagnetization in fields up to 1.8 kOe, imposition of an ARM in a 10 Oe dc field and 1.8 kOe AF, imposition of an IRM in increasing steady fields up to 10 kOe, and stepwise AF demagnetization to 1.8 kOe. A further







Fig. 24. CRM ( $J_r$ , solid curves) as a function of aging time (top) or oxidation time (bottom). The curves are adapted from the papers referenced. In the curves of Kobayashi the total quantity of magnetic material is constant with time, but essentially increases with time in the lower curves. The other curves in the top figure are the reversible magnetization ( $J_p$ ) and the total magnetization ( $J = J_r + J_p$ ). The dashed portion of Hoyer (1972) (also in Hoyer and O'Reilly (1973)) is not well-defined.





set of experiments on four of the samples concerned the acquisition of TRM and its study using the same procedure. The detailed techniques involved are described below when discussing the present work.

The growth of CRM in the FA30 olivine of Hoyer and Evans was observed to be similar to that occurring in the FA50 olivine of Hoyer and O'Reilly. Comparing the curves of total CRM (Fig. 24), both reached a maximum after about 400 minutes of oxidation and decreased slightly thereafter. The latter authors also had information on the increase of magnetic material with time obtained from the curve of growth of saturation magnetization with time, and were thus able to correct their total CRM curve to determine the growth of specific remanence with time. The corrected curve reveals a maximum at 10 minutes after a consistent build-up, and then a slight decrease. This type of behaviour was first observed by Kobayashi (1961) in his experiments on the growth of CRM in a Cu-Co alloy aged at 750°C in a constant field, where the amount of magnetic material present remained effectively constant with time (Fig. 24). He concluded that the increase to maximum CRM resulted from accreting magnetic particles exsolving from the matrix, passing from sp dimensions to stable sd size. The large drop in intensity after the maximum was attributed to the development of md grains. Hoyer and O'Reilly explain their results on FA50 in much the same way. Hoyer and Evans come to the same conclusion by a comparison of their total CRM curve



with that of Hoyer and O'Reilly. However, contrary to Kobayashi's result, neither of the curves decrease much after the maximum is reached (Fig. 24). This, Hoyer and Evans suggest, is due to the development of psd grains rather than md grains, since the mean grain size as constrained by the size of the olivine grains is about  $0.5\text{ }\mu\text{m}$ , -- much less than the critical size of  $20\text{ }\mu\text{m}$  calculated for equidimensional grains exhibiting true md behavior (Stacey 1963, Dickson et al. 1966). From the CRM work and studies of other magnetizations imposed on the oxidized olivines they inferred that a strong stable remanence associated with sd or psd magnetic inclusions could be acquired in nature by the high temperature oxidation of olivine.

## Present Work

### Introduction

The present work is in part an extension of the work of Hoyer and Evans (1975) to olivines of other compositions, but with emphasis on identifying the magnetic minerals present and their mode of occurrence.

In this section the experimental work is presented, together with the results and their analysis. First, the basic experiments to oxidize finely divided synthetic olivines and thus produce a CRM are described. Then a model of these oxidized or oxidizing olivines is proposed based on the earlier work discussed above. Experiments to test the





model are then described which seek to (1) identify the magnetic minerals present, (2) identify their mode of occurrence, and (3) reveal how the magnetic minerals and their mode of occurrence change with oxidation time. Lastly, the experimental conclusions resulting from these tests are compared to the model.

### Procedures Apparatus, and Experimental Details

The methods and procedure for preparing and oxidizing the olivine grains, and for producing a chemical remanence, closely follow those described by Hoyer and Evans (1975), and are detailed below. A resume of the experimental work is given in Appendix 7.

GRINDING OF OLIVINE SAMPLES. Three compositions of olivine were used: FA30, FA50, and FA90. These synthetic olivine compositions were prepared by Hoyer several years before the present experiments began and were subsequently stored in plastic containers. They were grown by means of a self-buffering process (Hoyer and O'Reilly 1972), which produces polycrystalline material with an impurity content of less than 0.01%. Immediately prior to the experimental work the samples FA50 and FA90 were mechanically ground for about eight hours in a coolant of dry acetone using a mullite mortar and pestle. Sample FA30 had been ground two years before by Hoyer using the same method. Final grain sizes of the FA50 and FA90 samples were not measured; but since the same technique and time interval used by Hoyer and



Evans (1975) were employed, the same grain size ranges were expected: namely, about 0.07 to 2  $\mu\text{m}$  with a mean of about 0.47  $\mu\text{m}$ . They found the distribution to be highly asymmetric, being dominated by small particles. Microscopic comparison of a polished thin section of sample FA30 with those of samples FA50 and FA90 (see Figs. 27 - 29) (the former ground by Hoyer and the latter by the author) reveals that the largest grain sizes are similar and of the order of 10  $\mu\text{m}$ ; thus tending to affirm the similarity of the grain size ranges. This microscopic examination also revealed that all unoxidized material was slightly contaminated by some opaque -- possibly magnetic -- grains (see Figs. 27-29). The possible effect of this contamination is discussed below.

OXIDATION AND THE GROWTH OF CRM. Samples were packed in special cylindrical silica holders consisting of thin-walled silica tubing (8 mm long) and ends (8 mm in diameter) of porous silica, -- one fixed and the other removable. The porous silica served to allow free access of oxygen into the sample. After packing, the removable top was fixed in place with a platinum wire. One sample of FA30 (FA30A) and FA90, and three samples of FA50 (A, B, and C) were packed for the CRM experiments. Sample FA50B was packed more tightly.

Samples were oxidized in a small non-inductively wound oven at a constant temperature of  $500 \pm 5^\circ\text{C}$ . It had earlier been surmized that at this temperature the rate of generation of oxide was likely to be a maximum (Hoyer 1972).



Also, the results could be directly compared to high temperature deuteric alteration occurring in natural olivine-bearing rocks. The furnace was located within three pairs of orthogonal coils which in turn were enclosed in a magnetically shielded room. Together, the coils and shielding reduced the ambient field to less than 50 gammas for the entire set of CRM experiments.

CRM's were imposed in the following manner. First, the oven was preheated to 500°C in a retracted position away from the sample, and then slid centrally over the sample. Following an initial period of about 7 minutes, during which the sample reached temperature, a bias field of 10 Oe together with a supply of oxygen were switched on. The field, directed along the axis of the oven and of the sample, was produced by a pair of Helmholtz coils coaxially surrounding the oven. The introduction of oxygen, as well as the finely divided nature of the olivine, helped to increase the reaction rate, thus bringing what would normally be the work of geological ages into the laboratory time scale. Oxygen (99.95% pure at atmospheric pressure) was continually passed over the sample from a pressurized cylinder. After a given oxidation time the oven, bias field, and oxygen supply were turned off; the oven slid from the sample; and the sample allowed to cool for 15 to 30 minutes in a helium atmosphere (99.995%).





MEASUREMENT AND STANDARD MAGNETIC PROCEDURES. Following the cooling period samples were immediately measured with a Schonstedt SSM-1 slow spinner magnetometer. After this step the order of procedure varied according to the experiment performed, and is detailed below when discussing these experiments. Standard procedures used during the experiments were AF demagnetization, production of IRM, and backfield demagnetization of IRM. AF demagnetization was carried out on an apparatus described by Murthy (1969) in peak fields up to 1.8 kOe. IRM's were produced by two different electromagnets: one described in Appendix 1 and the other a small 4 inch electromagnet available from an undergraduate laboratory.

### Contamination of Samples and their Holders

Measurements of samples made prior to oxidation revealed the presence of a slight remanence, which could be wholly or partly due to the sample holders (Table 7). Prior to the CRM experiment the holder of FA50C was given an IRM in a 10 kOe field. It gained a substantial remanence (Table 7), but was demagnetized to a low value ( $0.5 \times 10^{-6}$  e.m.u.) in an AF of 1.8 kOe. Only the FA50 samples were given an IRM build-up to 10 kOe in their unoxidized state, but each was demagnetized immediately prior to oxidation -- and FA50C as a last step following each oxidation interval. The contribution of the sample holder of this latter sample to the IRM build-up curves at maximum field amounts to less





TABLE 7.

## MAGNETIZATION OF OLIVINE PRIOR TO OXIDATION

Sample	Magnetization (e.m.u. $\times 10^{-6}$ )				
	Sample holder		Sample + Sample holder		
	0 Oe	10 kOe	0 Oe	10 kOe, 10 kOe+1.8 kOe AF	
FA30	0.5	--	1.9	--	--
FA50A	--	--	0.8	3030	37.0
FA50B	--	--	1.1	3820	46.8
FA50C	0.4	36.4	7.3	3520	38.5
FA90	1.6	--	0.5	--	--

## NOTES:

The remanent magnetization was measured either prior to the application of a field (0 Oe), after the application of a field (10 kOe), or after the AF demagnetization (1.8 kOe) of the remanence obtained in the applied field (10 kOe). The sample holder includes the actual sample container and its component parts as well as the cubic holder for orienting the sample in the magnetometer. The cubic holder has a remanence typically 1/3 to 1/2 that of the sample container.



than 0.4%. Only this one sample holder was measured for remanence after application of a high field, and it is therefore not certain whether all holders would behave similarly. In the low field (10 Oe) of the CRM experiment the FA50C holder has an estimated value -- interpolated from its IRM build-up curve -- of  $<1 \times 10^{-6}$  e.m.u. This value if present in the holder of the weakest sample (FA90) would introduce an error of <5% in the CRM curve. It is concluded that the magnetization of the holders will not affect results to any appreciable extent.

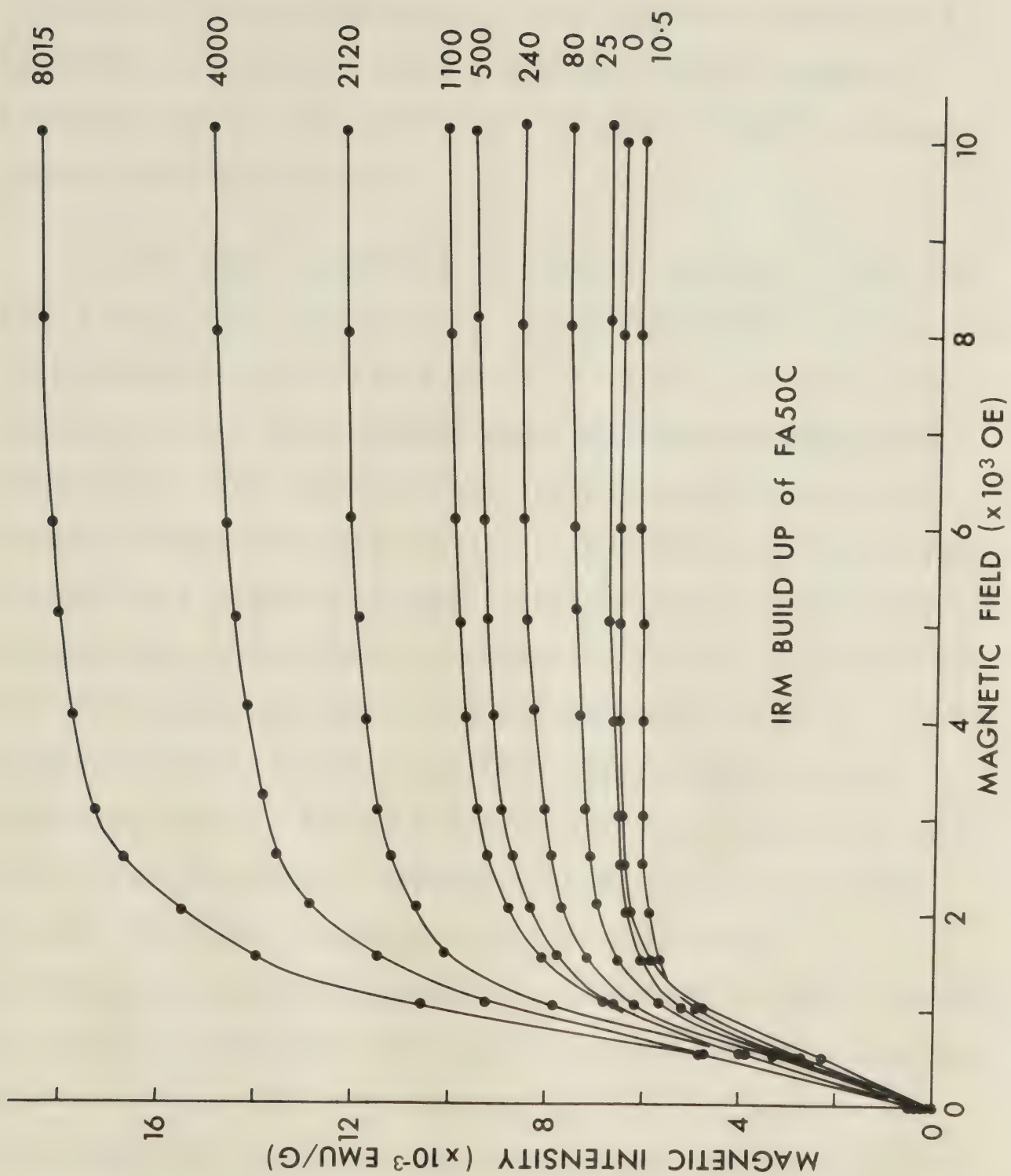
Hoye and O'Reilly (1972) mention that the impurity content of the synthetic olivines is less than 0.01%. Microscopic examination of the present unoxidized samples of all three compositions has revealed the presence of opaque grains which are not inclusions in the olivine. Some of these are undoubtedly magnetic as indicated by the IRM build-up curves of all three FA50 samples which are closely similar (see 0 curve, Fig. 25). Examination of the FA50C curve (Fig. 25) reveals that the contaminant has a substantial magnetization which is probably due to magnetite; the latter fact being verified by the isotropy of large contaminant grains viewed in polished thin sections under crossed nicols (see Figs. 27-29). Its remanence after AF demagnetization in 1.8 kOe ( $38.5 \times 10^{-6}$  e.m.u., Table 7) would constitute 17% or less of the CRM suggested by the curves of the similar samples FA50A and B. No IRM was given to samples FA30A and FA90 before oxidation, so that a





Fig. 25. - IRM build-up curves of sample FA50C for each successive oxidation interval (minutes). Oxidation was carried out at 500°C. Note that in the unoxidized state the sample reveals the presence of a magnetic contaminant.







similar IRM will not affect their CRM results. However, there will be an additional remanence in all cases; the high temperature IRM acquired by the impurity in the CRM bias field of 10 Oe. In the case of FA50C this may amount to a remanence of  $<15 \times 10^{-6}$  e.m.u., giving a total possible remanence due to the contaminant of about  $54 \times 10^{-6}$  e.m.u. (25% or less of the CRM).

In all cases oxidation to hematite during the CRM runs will reduce the proportion of contaminant magnetization. The hard remanence will likely be due to small sd grains. And inasmuch as the large grains observed microscopically as a contaminant were separate from the olivine grains, it is thought likely that the smaller unresolvable sd contaminant grains are likewise free and therefore easily accessible and susceptible to oxidation to hematite. This is suggested by the AF demagnetization of the CRM of sample FA50C in 1.8 kOe following the 10.5 min. oxidation step, which reveals a remanence that is 17% ( $6.4 \times 10^{-6}$  e.m.u.) of the hard IRM left after the similar demagnetization of the unoxidized sample. The total contaminating remanence after demagnetization should constitute a maximum of from 5 to 10% of the FA50 CRM curves, but much less of the curves for FA30 and FA90 which were not given an initial IRM prior to oxidation. The effect on the other experimental curves for FA50C may grow less with oxidation time but this is not known. Values derived from these experimental curves will only be approximately correct, but will be suitable for



comparative purposes.

### Growth of CRM

The resultant oxidation curves of the FA30 and FA90 samples (Fig. 26) are very similar to those of Hoyer and O'Reilly (1973) and Hoyer and Evans (1975) (Fig. 24). Like the curve of the latter they have not been corrected for the increase of magnetic material with time (to produce curves of specific remanence), yet they show a similar marked decrease in intensity after reaching a maximum.

The curves of FA50 show a sharp increase in intensity at the 80 minute oxidation step, which is probably related to an inadvertent increase in temperature during that step to at least 550°C for several minutes. The increase would then in large part be due to the acquisition of a partial TRM (PTRM) on cooling to 500°C, and in lesser degree to the acquisition of some 'extra' CRM. A similar temperature increase occurred during the FA30A run during the 240 minute oxidation step, but it seems to have had little if any effect on the curve. The whole matter of the PTRM in FA50 samples and how it relates to their properties as deduced from various magnetic curves is discussed below in a separate section.

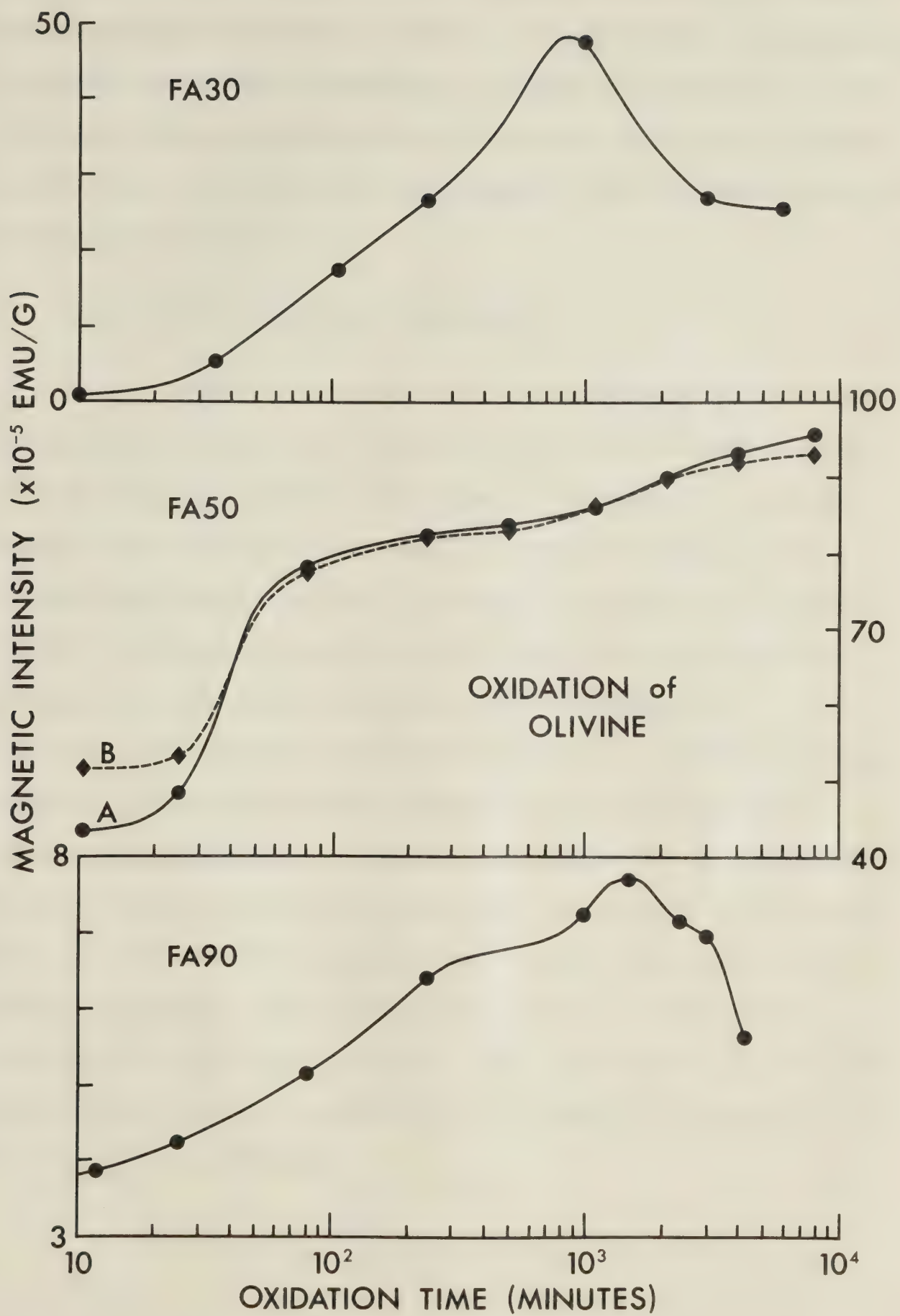
The decrease in the FA30A and FA90 curves possibly results from the phenomenon suggested by Hoyer and O'Reilly (1973) and Hoyer and Evans (1975); that is, the growth of







Fig. 26. Increase of CRM with oxidation time for three olivine compositions. Two samples of FA50 were run concurrently: one packed 'normally' (A), and one tightly (B). The effective oxidation time of FA30A is somewhere between 4920 and 6020 min.

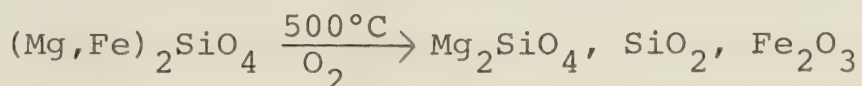




magnetite to psd sizes. There is another possibility which could explain the effect; namely, the oxidation of magnetite to weakly magnetized hematite. The lack of decrease in the FA50 case may either be due to the curve not having reached maximum or to the increase of magnetic material with time as suggested by Fig. 25.

### Model of the Oxidized Olivine

On the basis of results from the previous work on the oxidation of natural and synthetic olivines a model of an olivine grain oxidizing with time is proposed. This model assumes the oxidation temperature of 500°C used in the present experiments. First a magnetite symplectite begins forming from the matrix. As oxidation proceeds magnetite occurring on the outer rim and along fractures is preferentially further oxidized to hematite. Oxidation also occurs in the increasingly Mg-enriched cores away from convenient interfaces, changing the magnetite to hematite -- but at a much reduced rate from that occurring at the rim. This rate is reduced even further as the rim grows to its limit; becoming a semi-permeable barrier to the oxygen. Given sufficient time, however, the end product will be the stable assemblage of forsterite and hematite according to the following relation:





However, in the model of the oxidizing olivine proposed for the present work hematite will occur at the rim with a mixture of hematite and magnetite in the core; and the hematite will increase with time. This model can be tested: first, by identifying the magnetic minerals present; second, by identifying their place and mode of occurrence; and third, by determining how both minerals and their mode of occurrence change with oxidation time. Various tests of the model are discussed below under these headings.

### Identifying the Magnetic Minerals

Previous work on the oxidation of the olivines suggests that there are only three magnetic minerals likely to be produced: magnetite, hematite, and magnesioferrite. Since the CRM experiments were conducted at a constant temperature of 500°C (with the momentary exception of the FA50 samples), it is unlikely that magnesioferrite will be present as a measurable quantity, for Hoyer and O'Reilly (1973) only found evidence of its production when the ambient temperature was above 550°C.

There are many methods available for identifying minerals. These include optical microscopy, transmission electron microscopy, X-ray diffraction, and electron microprobing. Since the minerals are magnetic, methods involving thermomagnetic techniques, differential thermogravimetric analysis, hysteresis, and susceptibility can be used to advantage. Of the non-magnetic methods





optical microscopy, X-ray diffraction, and electron microscopy were used. The opaque grains within the olivines were much too small ( $<1\ \mu\text{m}$ ) for the beam of an electron microprobe, and so that technique was not attempted. Hoyer and O'Reilly (1973) used the four magnetic techniques listed, but these were not conveniently available to the author. Instead, other magnetic techniques, most of which were used by Hoyer and Evans (1975), were employed. These included IRM build-up, AF demagnetization of CRM, and AF and backfield demagnetization of IRM.

OPTICAL MICROSCOPY. Polished thin sections of both unoxidized and oxidized samples of FA30 and FA90 composition, and an unoxidized sample of FA50 were microscopically examined with both reflected and transmitted light. The latter method proved useless, since sections remained almost opaque; and so all results detailed below were obtained using reflected light. With and without the microscope the unoxidized samples appeared grayish-green (Figs. 27-29). A few bright opaque grains were present, which proved to be isotropic under crossed nicols. This contaminant is therefore probably magnetite.

Oxidation produced a marked color change in all three olivine compositions, ranging from yellowish-brown in FA30 to reddish-brown in FA90. The same general colours are apparent under the microscope (Figs. 27 and 29). On closer inspection the rare FA30 grain shows a bright or reddish





Fig. 27. Photomicrographs of unoxidized (top) and oxidized (bottom) olivine grains of sample FA30A taken in plane polarized light (top and bottom left) and under crossed nicols (bottom right).

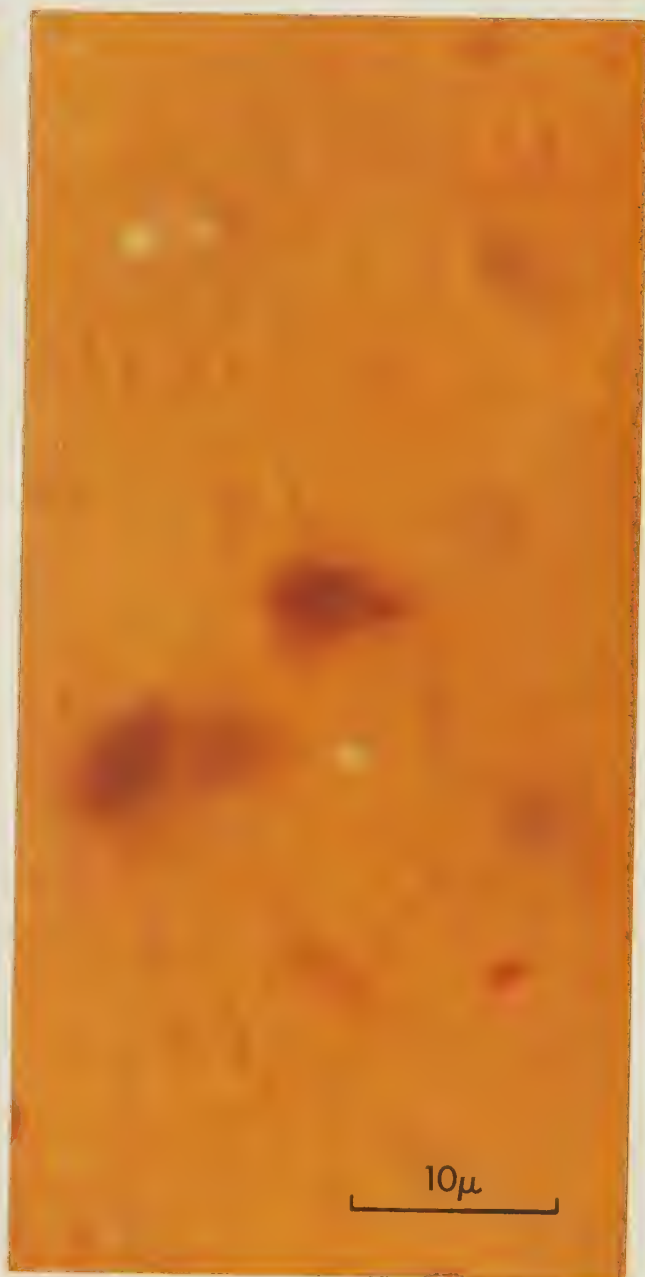








Fig. 28. Photomicrographs of unoxidized olivine grains of composition FA50 taken in plane polarized light (top) and under crossed nicols (bottom).

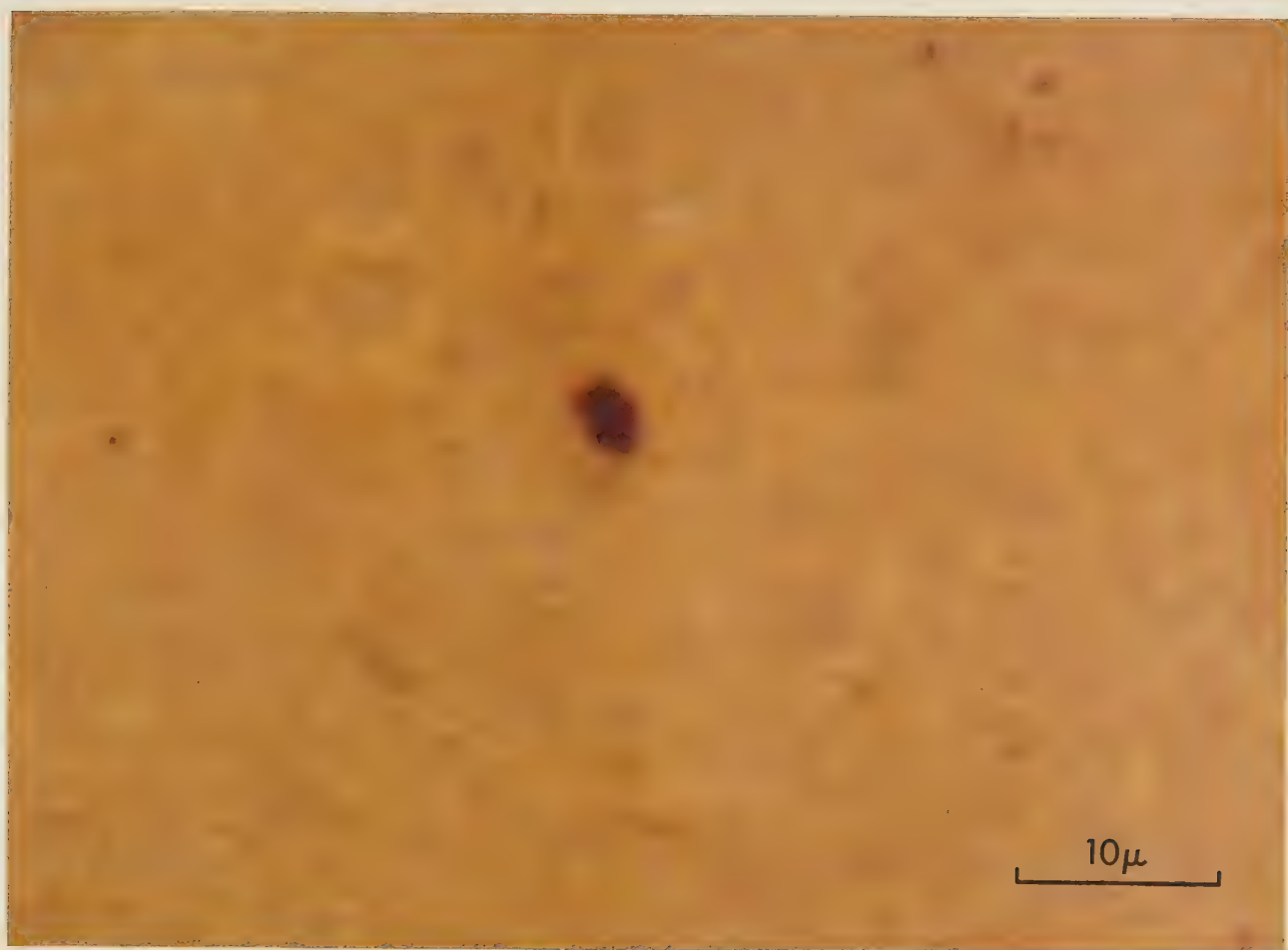






Fig. 29.- Photomicrographs of unoxidized (top) and oxidized (bottom) olivine of composition FA90 taken in plane polarized light (left) and under crossed nicols (right).







opaque-like rim. This is in strong contrast to the FA90 samples where many of the larger grains display bright discontinuous rims (Fig. 29). Under crossed nicols these rims become dark or reddish, and display anisotropy and red internal reflections (Figs. 29 and 38). Many of the other resolvable FA90 grains show reddish borders both in plane polarized light and under crossed nicols. Away from the edges most of these grains are dark in color, and very dark under crossed nicols.

The bright and reddish rims of the oxidized grains with their associated anisotropy and red internal reflections, indicate hematite. With the increase in iron content from composition FA30 to FA90, there appears to be a general increase in the hematite as evidenced by the general increase in redness and in the appearance of large numbers of bright opaque rims in FA90. The darkness of many of the oxidized grains under crossed nicols suggests that they are full of minute opaque particles which cannot be optically resolved and identified. Haggerty and Baker (1967) suggested that the anomalous nature of some of the magnetite they observed within some olivine cores was partly due to extremely fine grain sizes. Whether or not the cores in the present case contain magnetite cannot be determined with the optical microscope.

X-RAY DIFFRACTION. X-ray diffraction work was carried out on samples of all three compositions (FA30, 50, 90), but



only in the most iron-rich sample was hematite identified (Fig. 30). This technique can only identify a mineral positively if it constitutes more than about 5% of the sample. Magnetite was not identified; however, the olivine composition could be determined both before and after oxidation (Table 8).

BUILD-UP OF IRM. Samples were given an IRM by placing them between the poles of an electromagnet in a fixed position and orientation, gradually increasing the applied field from zero to some predetermined value, holding it at maximum for about ten seconds, and decreasing the field to nearly zero. Measurements were made almost immediately. It was necessary to maintain a fairly constant time lag between magnetization and measurement as well as a consistent measurement routine in order to minimize distortions of the IRM curves due to the logarithmic decay of sample intensity. The curves are fairly regular, but there are some small irregularities which can be readily accounted for by this effect (see Figs. 25 and 31).

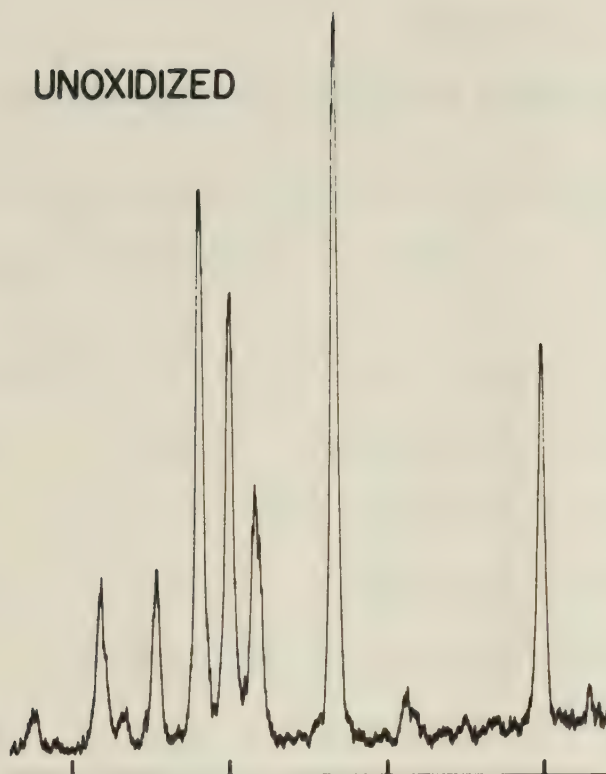
IRM build-up experiments were performed on samples of each composition at some stage following the last oxidation step (Fig. 31). Sample FA50C was selected for IRM build-up to be performed after each successive oxidation step following the AF demagnetization of CRM (Fig. 25). All curves show the same general features (Figs. 25 and 31): namely, a steep initial rise in fields under about 1.5 kOe



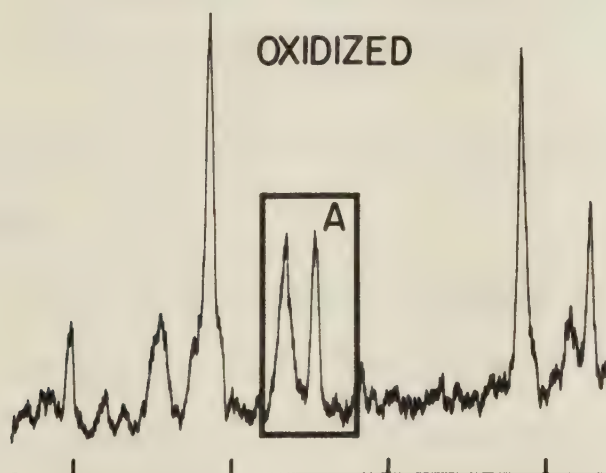


Fig. 30. Partial X-ray diffractograms of FA90 olivine: unoxidized (top left), oxidized (middle left), and treated for 29 hours in diammonium citrate following oxidation (bottom left). At the right critical lines of hematite (at left,  $2.69 \text{ \AA}$ , most intensive line) and olivine (at right,  $d_{130}$ ) are compared for the oxidized olivine before (top) and after (bottom) treatment in diammonium citrate.

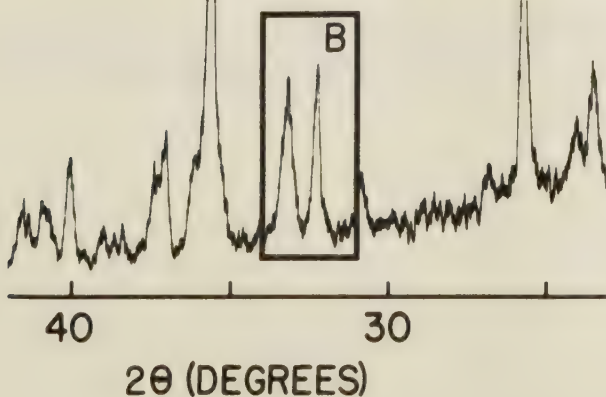
UNOXIDIZED



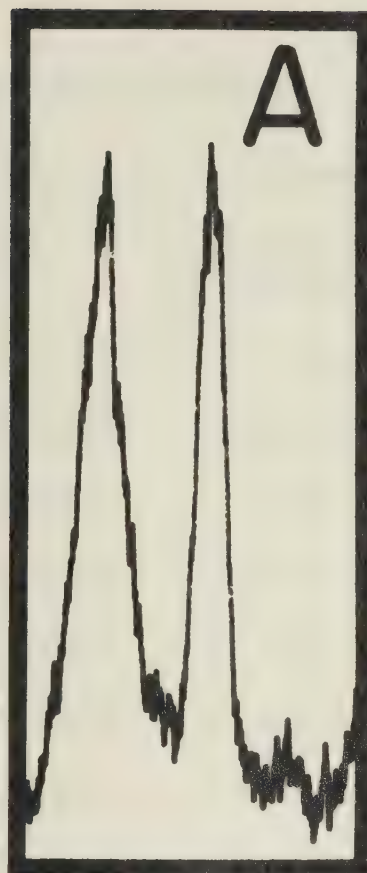
OXIDIZED



OXIDIZED,  
+ 29 HRS IN  
DIAM. CITR.



A



B







Handwritten text in a cursive script, likely a signature or a short note. The ink is light and the characters are somewhat blurred.



Handwritten text in a cursive script, continuing from the top section. The ink is light and the characters are somewhat blurred.

TABLE 8.

## COMPOSITION OF OLIVINE BEFORE AND AFTER OXIDATION

Sample	Treatment	$2\theta^0$	$d_{130}^{\circ}(\text{\AA})$	fayalite (molar %)
FA30	none	$32.13 \pm 0.01$	$2.7858 \pm 0.0008$	$29.7 \pm 1.3$
	oxidation <sup>1</sup>	$32.36 \pm 0.01$	$2.7665 \pm 0.0008$	$0.7 \pm 1.2$
FA50	none	$31.96 \pm 0.01$	$2.8003 \pm 0.0008$	$51.6 \pm 1.3$
	oxidation <sup>1</sup>	$32.25 \pm 0.02$	$2.7756 \pm 0.0017$	$14.4 \pm 2.6$
FA90	none	$31.65 \pm 0.01$	$2.8268 \pm 0.0008$	$91.4 \pm 1.4$
	oxidation <sup>1</sup>	$32.28 \pm 0.02$	$2.7732 \pm 0.0017$	$10.8 \pm 2.6$
	OX. + DC <sup>2</sup>	$32.23 \pm 0.01$	$2.7772 \pm 0.0008$	$16.8 \pm 1.4$

## NOTES:

$2\theta^0$  is the angle between the primary X-ray beam and the reflected beam for the olivine atomic lattice spacing  $d_{130}$ . Absolute errors are given.

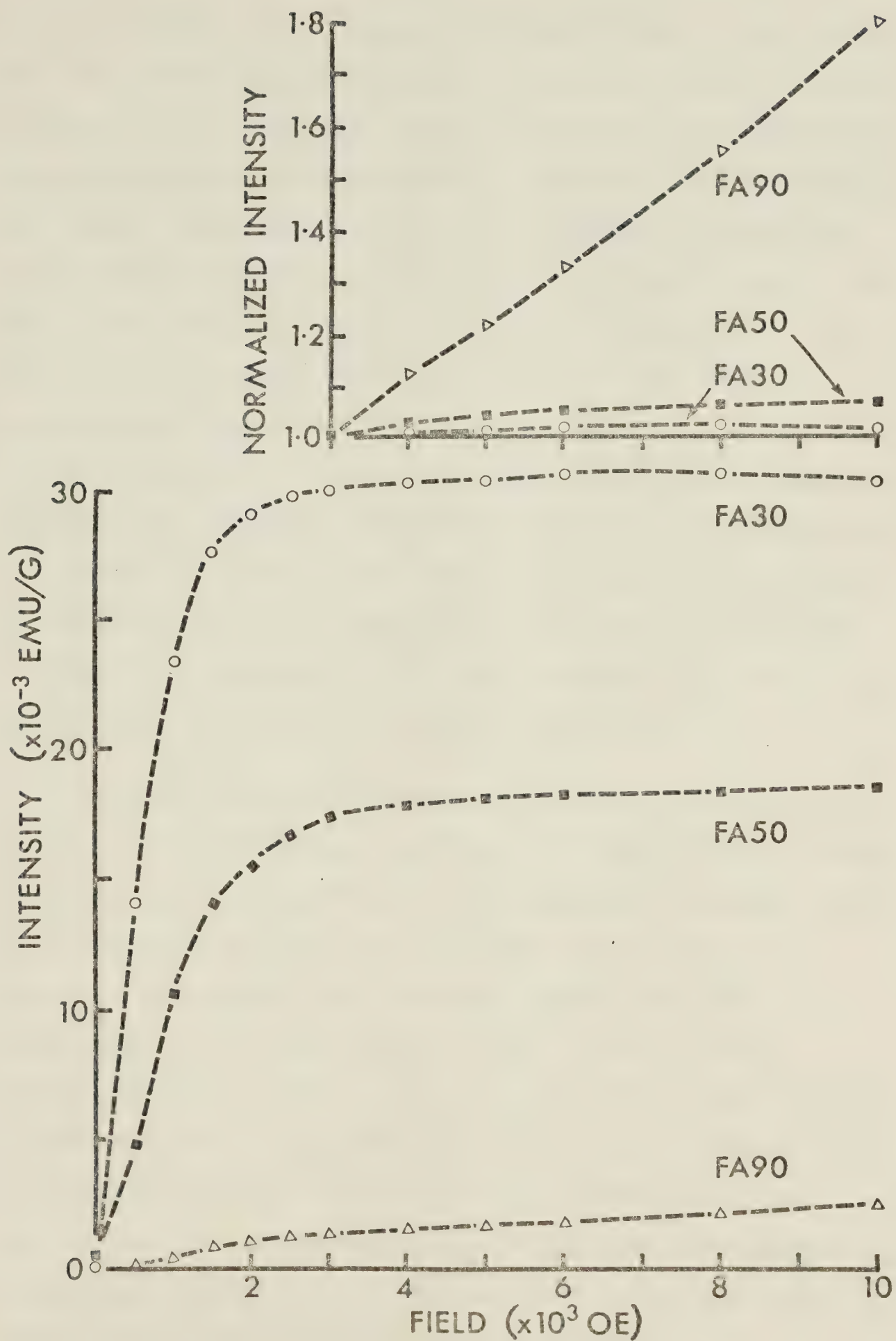
<sup>1</sup> Oxidation times of 6020 min. (FA30A), 8015 min. (FA50), and 8008 min. (FA90).

<sup>2</sup> Treatment in diammonium citrate (DC) for 28.8 hours following oxidation (OX.).





Fig. 31. IRM build-up curves obtained following the last oxidation step on olivines of different compositions. The three curves were normalized to the value at 3 kOe, and a portion of the resulting curves (3 to 10 kOe) plotted in the top figure. Sample of FA50 composition is FA50C.







and a usually steady increase to about 10 kOe, -- the limit of the applied field. These features are indicative of the presence of at least two magnetic minerals: magnetite and/or magnesioferrite, and hematite. The initial sharp increase in the curves is probably mainly due to magnetite, since the experimental conditions preclude the creation of much -- if any -- magnesioferrite. But its possible presence in FA50 samples is discussed later. The effect of the initial contaminant, represented by curve 0 in Fig. 25, is thought to be negligible as far as the later curves of the oxidized material is concerned. The steady increase in magnetization -- especially above 3 kOe, the highest theoretical coercive force for magnetite -- must be due to hematite. Thus the oxidized correlatives of all three compositions reveal the presence of hematite and probably magnetite.

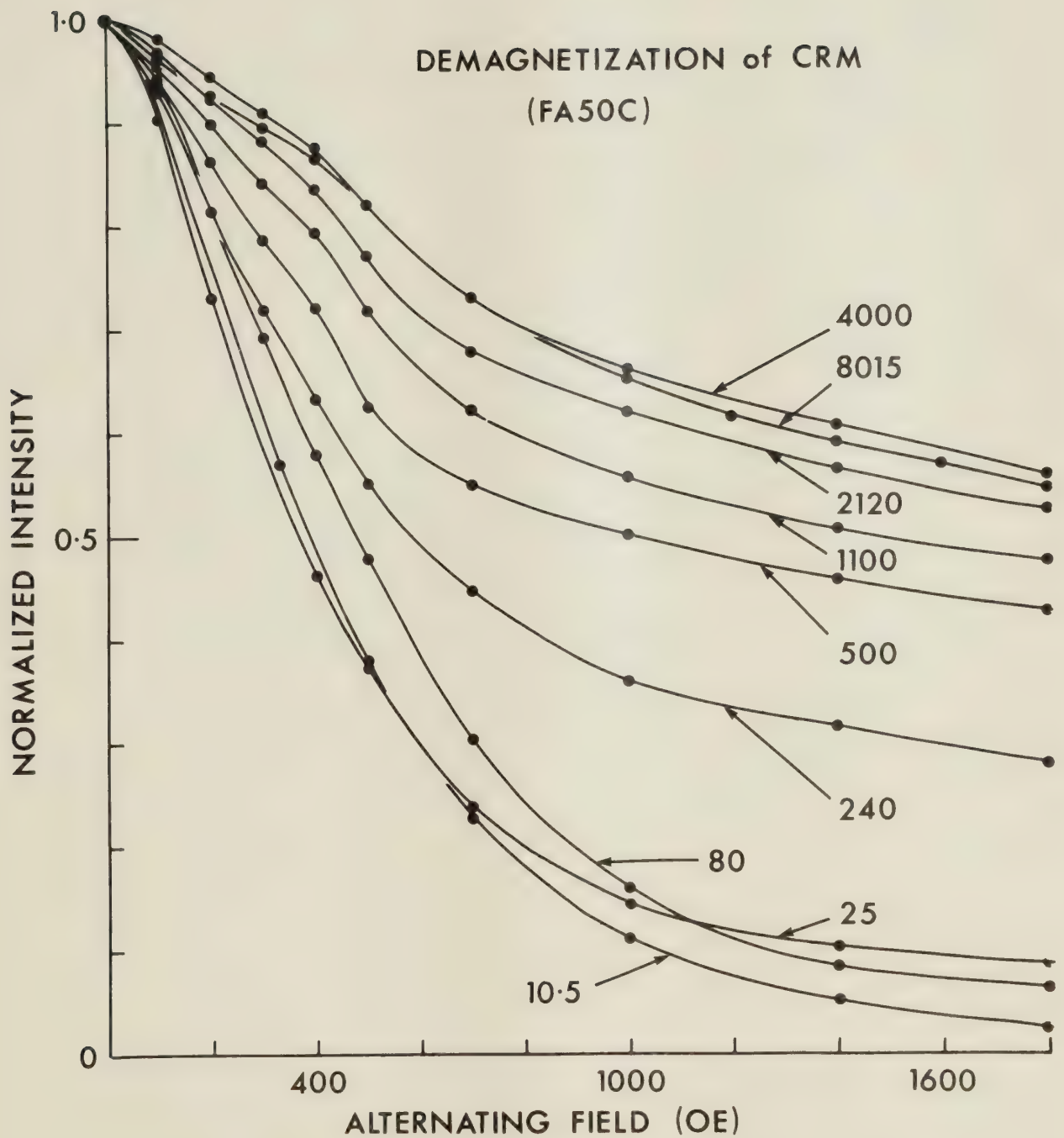
AF DEMAGNETIZATION OF CRM. AF demagnetization of CRM in fields up to 1.8 kOe was performed on sample FA50C following each oxidation step (Fig. 32). The increased remanence after this treatment at each step indicates the growth of a magnetic phase with high coercive forces. When the magnitudes of the last three or four values of each demagnetization curve are plotted versus the logarithm of field (Fig. 33), they tend to lie on straight lines whose intercepts with the field-axis range up to 50 kOe. All curves but that representing the least oxidized material apparently reveal coercive forces above 3 kOe, and again definitely point to the presence of hematite.





Fig. 32. AF demagnetization of the CRM of sample FA50C at various stages of oxidation. Curves are labelled by oxidation time in minutes. In Fig. 33 portions of the same curves are plotted, but the field is on a logarithmic scale.

DEMAGNETIZATION of CRM  
(FA50C)

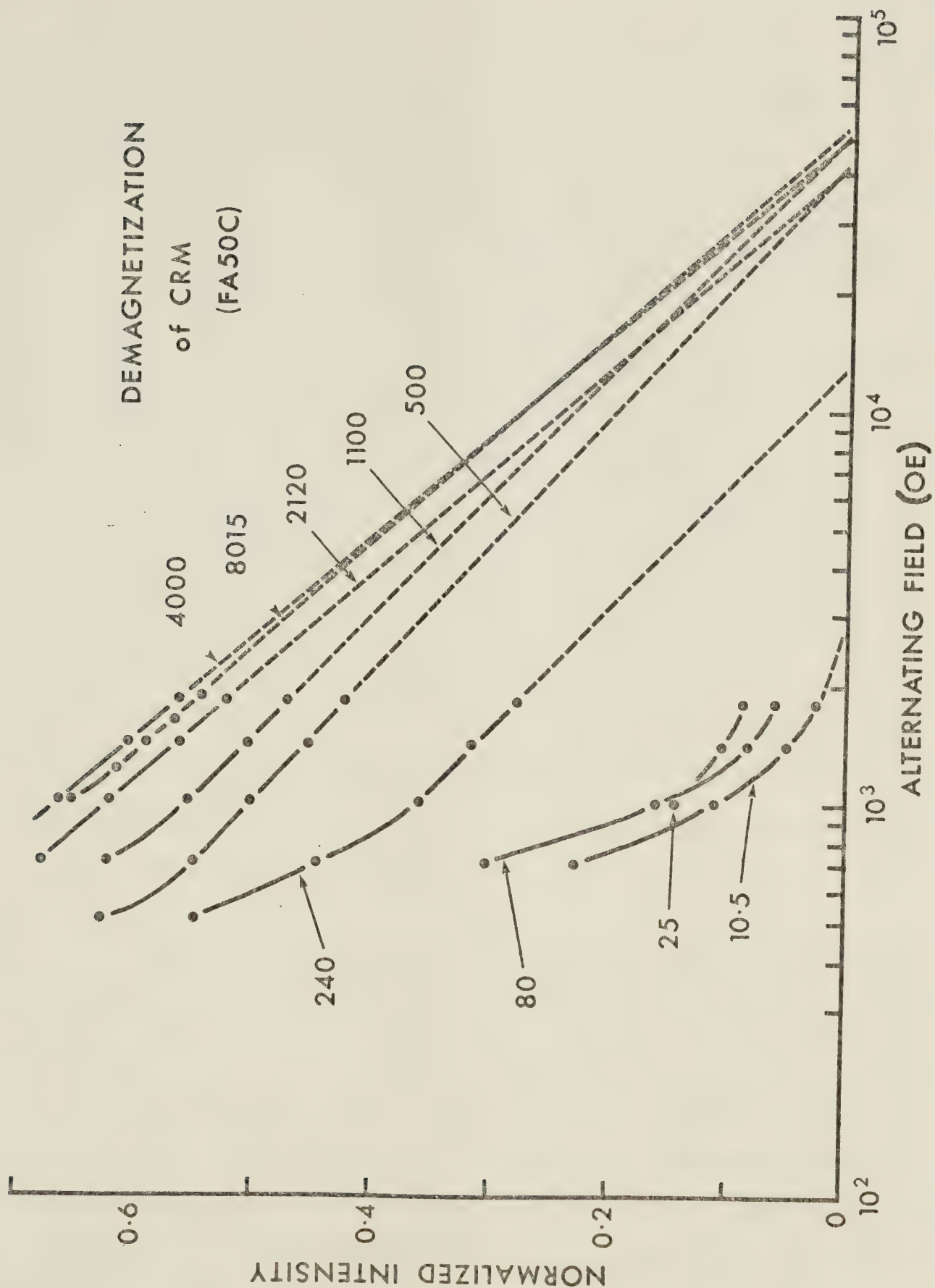


*[Faint, illegible text, likely bleed-through from the reverse side of the page]*





Fig. 33. Portions of the curves of AF demagnetization of CRM of sample FA50C (Fig. 32) plotted versus the logarithm of field. These have been extrapolated (dashed lines) to zero magnetization.





## Identifying the Mode of Occurrence of the Magnetic Minerals

METHOD OF APPROACH. Hematite has been optically identified at grain boundaries in FA90 as forming discontinuous rims (Fig. 29). The darkening of the core material of many grains under crossed nicols suggests the presence of another opaque, but this has not been identified. The presence of magnetite is strongly suggested by the IRM build-up curves, but whether it occurs in the rim, the core, or both is not clear. Likewise, though hematite has been formed in the rim, it is possible that it also occurs in the core. An attempt was made to clarify these relationships by means of two chemical techniques. The presence of a distinct rim for FA90 and the obvious outside oxidation of FA30 suggested this method of approach. It was felt that this rim could be removed by a suitable solvent, and experiments conducted on the remaining core material to identify its magnetic phases.

The effect of removing hematite and/or magnetite from the rim can be illustrated by the effect this has on the IRM build-up curves produced after each chemical treatment. If all the hematite is at the surface, with prolonged treatment time the curve will gradually increase in intensity, and the portion above 3 kOe will decrease in positive slope until it is horizontal -- indicating that all the hematite has been removed. If only magnetite is being removed, the intensity



will gradually decrease: but the portion of curve above 3 kOe will maintain the same slope (Fig. 34) . And, if both hematite and magnetite are being removed, then mixed behaviour will be observed. By plotting a ratio of the initial curve (A) in each case to any of the other curves, one should be able to determine which magnetic mineral -- hematite or magnetite -- is being preferentially removed. With increasing field the ratio will increase if hematite is preferentially removed (Fig. 34), decrease if magnetite is preferentially removed, and remain the same if both are removed in proportion to their occurrence in the sample (i.e. mass of hematite/ mass of magnetite remains is a constant). Two chemical treatments are described below: one using diammonium citrate and the other the dithionite-citrate-bicarbonate (D-C-B) method.

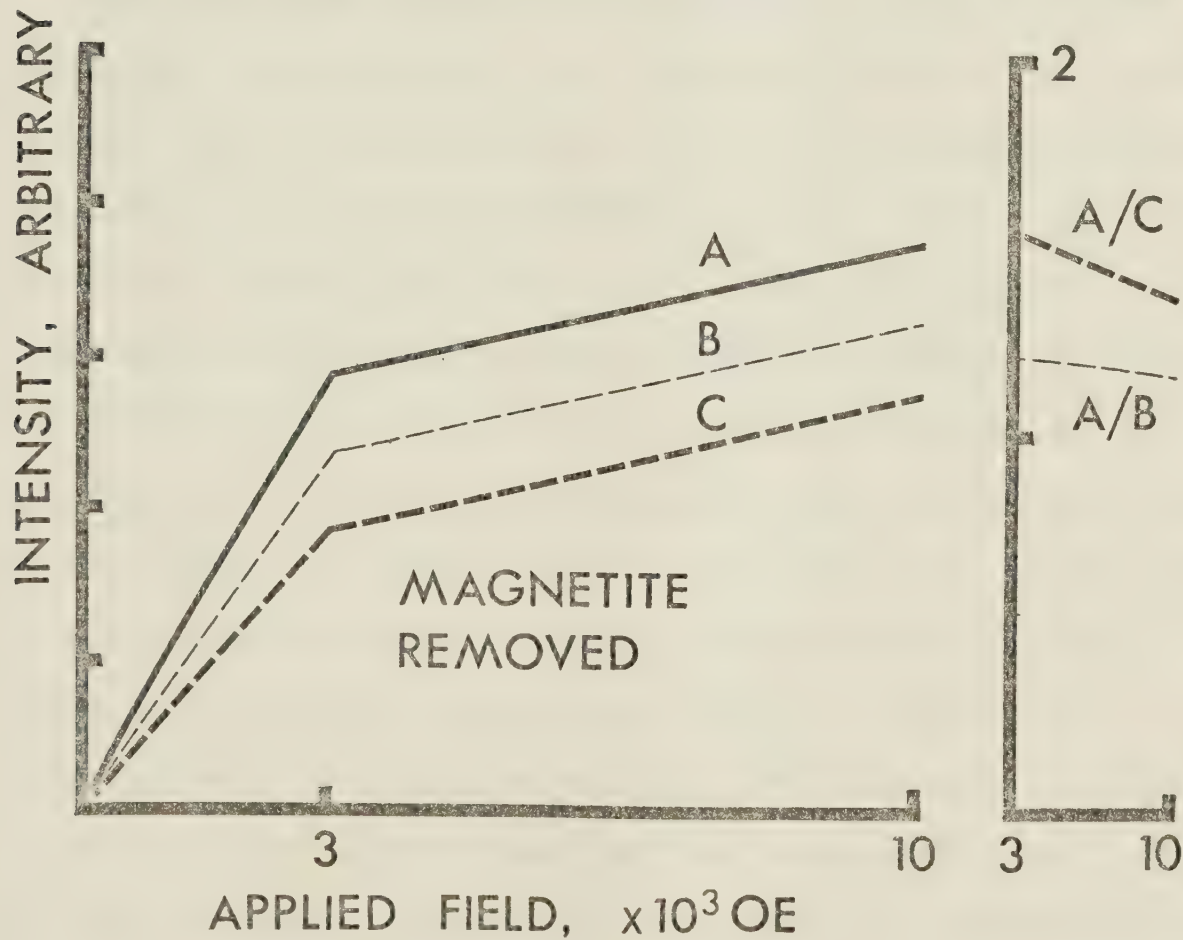
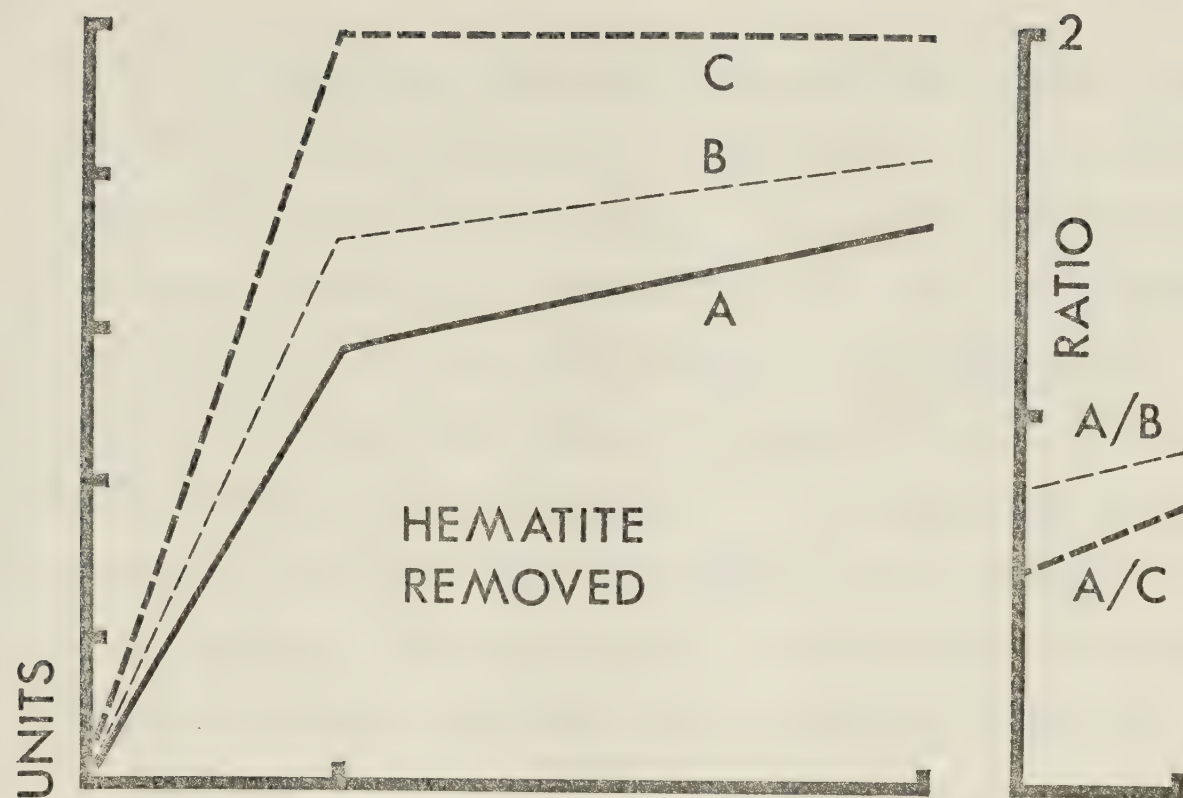
CHEMICAL TREATMENT USING DIAMMONIUM CITRATE. Diammonium citrate  $((\text{NH}_4)_2\text{HC}_6\text{H}_5\text{O}_7)$  was a natural choice of chemicals to use for the removal of hematite, since it is used by the iron and steel industry for removing rust coatings. The present procedure was to place a powdered sample in a 1 molar solution of this chemical for a set time; to filter, wash, dry, and reconstitute the sample; and to give it an IRM build-up. Unfortunately, with this procedure some sample mass is lost during each run. Experiments were initially performed on composition FA30 as a trial, and then on FA90. The FA30 sample used (FA30B) was a sample of Hoyer and Evans (1975) oxidized two years previously (see Appendix 7 for







Fig. 34. A model for the chemical leaching of oxidized olivine showing the theoretical effects on the IRM build-up curves of leaching either hematite or magnetite. The magnetic contribution of hematite to the total intensity is assumed to increase linearly with increasing field from 0 to 10 kOe, and that of magnetite to increase linearly from 0 to 3 kOe and to remain constant thereafter.





details).

No IRM build-up curves were produced for sample FA30B after each chemical treatment, but instead a single IRM from an applied field of 10 kOe. These values are listed in Table 9. There is a steady increase in the IRM with the exception of the last value, which was obtained for a very small amount of material. The increase suggests that hematite is being preferentially removed. This is corroborated by the decrease in the coercivity of remanence ( $H_{cr}$ ) between the last two values, which can be attributed to the elimination of a high coercive force component--namely, hematite.

Initial experiments on FA90 were conducted so that each treatment was performed on a different piece of the same sample, but on each additional piece for a longer period of time. This was subsequently found to be a rather falacious procedure, when it was discovered that the magnetic properties of the FA90 sample varied from place to place within the original oxidized sample. This variation is demonstrated in Fig. 35, which shows how the IRM build-up curves differ in pieces selected from the top, middle, and bottom of the sample. In view of these results it was decided to treat one piece from the FA90 sample for progressively longer time periods. Unfortunately no IRM build-up curve was obtained for the untreated piece of FA90 chosen, but this lack should not affect any conclusions arising from the result. IRM build-up curves were obtained



TABLE 9.  
EFFECT OF DIAMMONIUM CITRATE ON THE  
OXIDIZED OLIVINE FA30B

Total treatment time (hours)	IRM ( $\times 10^{-2}$ e.m.u./g)	H <sub>cr</sub> (Oe)	Mass (mg)
0	2.48 $\pm$ 0.02	--	524 $\pm$ 4
16.8	2.70 $\pm$ 0.07	--	179 $\pm$ 4
35.8	3.02 $\pm$ 0.09	695	130 $\pm$ 4
83.3	2.73 $\pm$ 0.14	677	78 $\pm$ 4

NOTES:

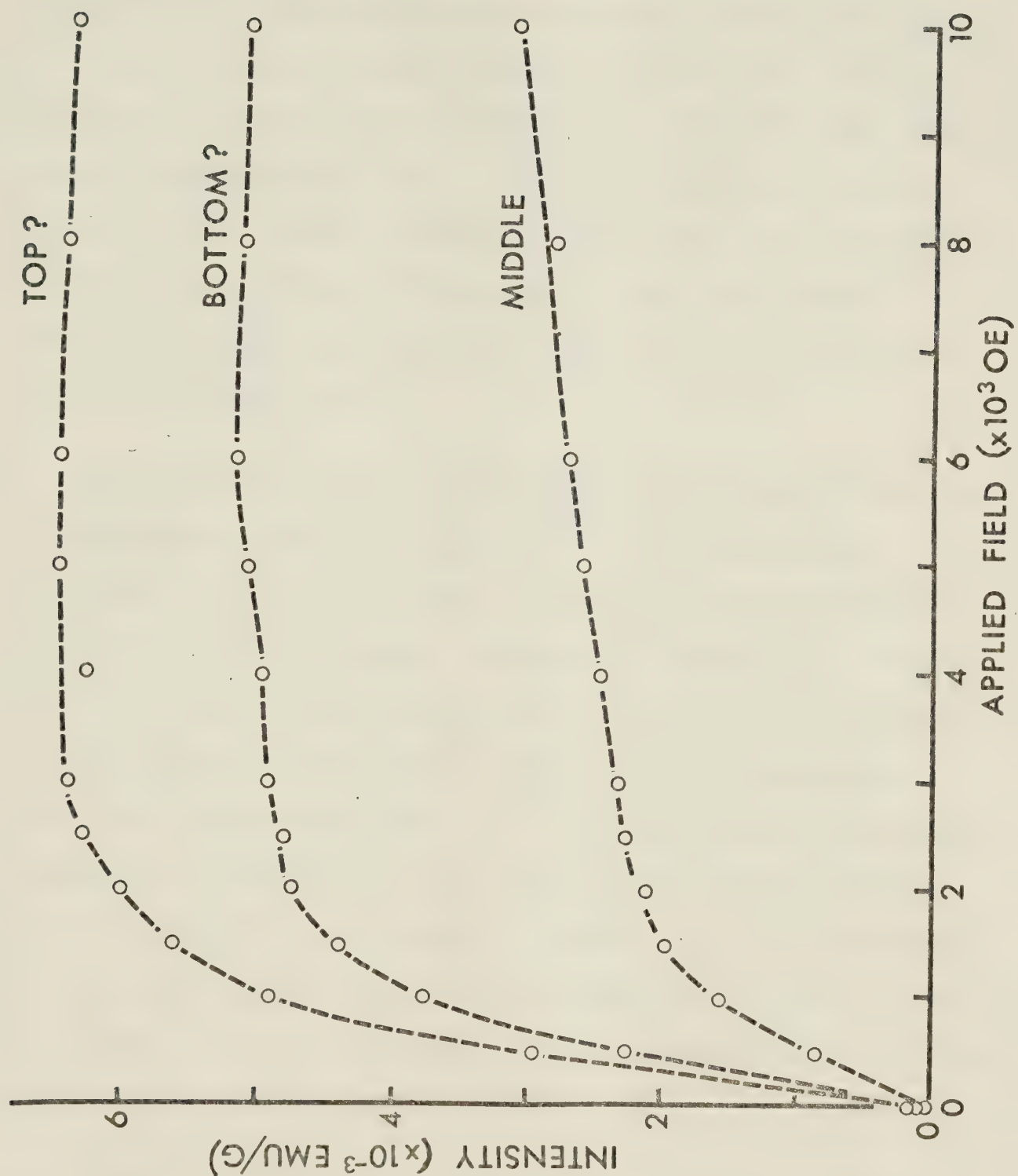
An IRM was imposed in 10 kOe following treatment in diammonium citrate (1 molar solution). H<sub>cr</sub>, the coercivity of remanence, was measured from the curve of backfield demagnetization of IRM. Absolute errors are given.







Fig. 35. IRM build-up experiment conducted on various parts of the olivine sample, FA90. The top two curves may be reversed.





for cumulative treatment times of 11.8 hrs. (Fig. 36, A), 15.2 hrs. (B), and 28.8 hrs. (C). The curves show an increase in intensity after the first leaching period, which suggests that hematite is being removed. Indeed, the ratio of A to B and C both show a positive slope. The lack of difference between curves B and C may mean that there was an error in determining mass -- possibly due to incomplete drying of the sample. Errors of this nature will not affect the sign of the slope of the ratio-curves for either hematite or magnetite being removed, and hence will not affect the conclusion.

An auxiliary test was conducted to determine the effect of diammonium citrate on essentially pure samples of magnetite and hematite. Equal amounts of each substance were separately placed in equal portions of diammonium citrate and of distilled water. Following an arbitrary duration of 34 hrs. there was no visible change in the quantities of hematite or magnetite, but the diammonium citrate solution containing magnetite was yellowish. This result suggests that magnetite is more prone to react with the diammonium citrate than is the hematite, and so reinforces the argument that there is little if any magnetite at the borders of the FA90 grains, but instead a reasonably pure rim of hematite.

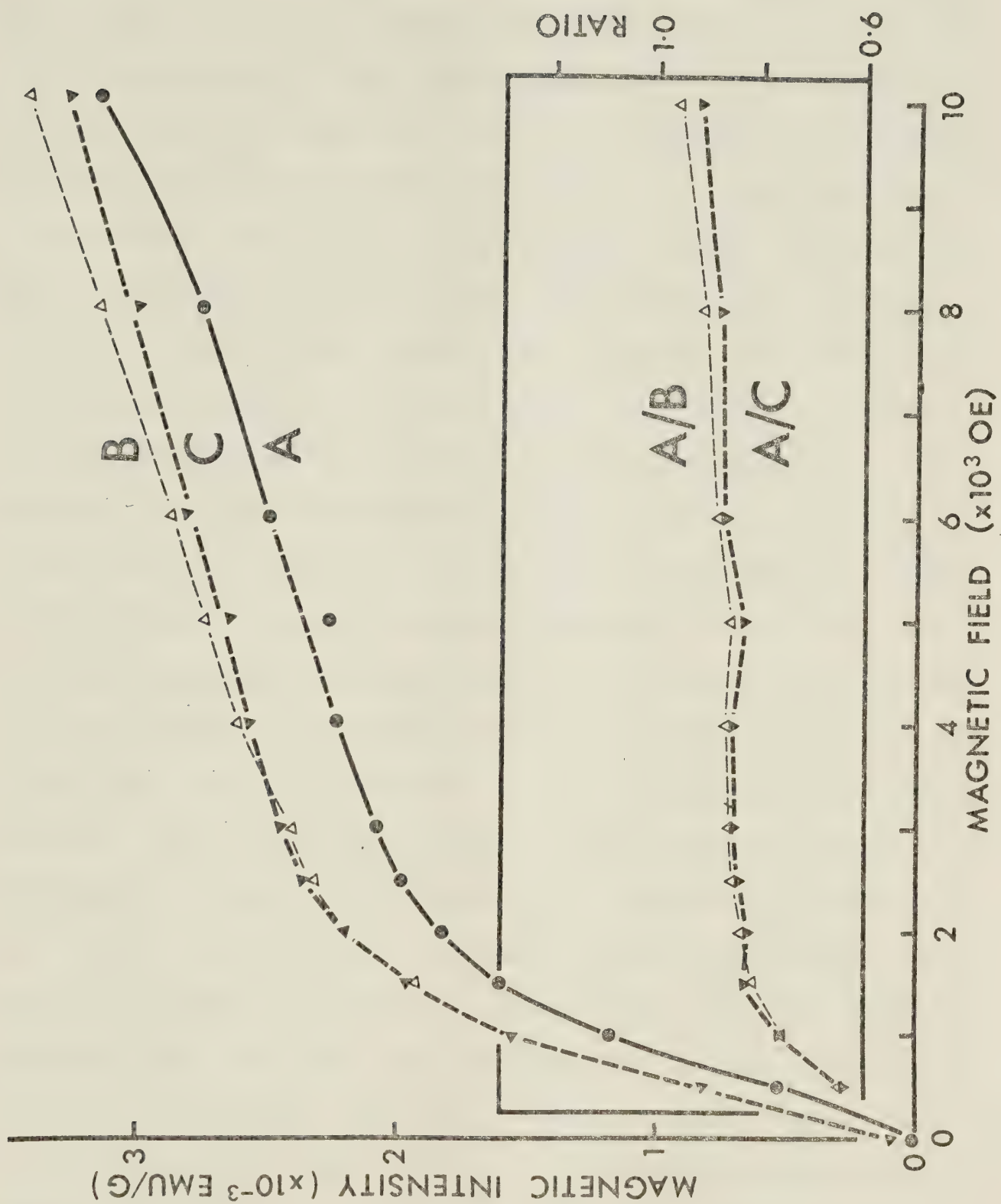
Portions of the chemically treated samples FA30B and FA90 were made into polished thin sections and also used for X-ray diffraction work. A polished thin section of FA30B







Fig. 36. IRM build-up curves of the oxidized olivine sample FA90A obtained following successive leaching periods in diammonium citrate solution. Cumulative time periods are: A: 11.8 hours; B: 15.2 hours; and C: 28.8 hours. The ratios of A to B and A to C (inset) can be compared to the curves of the theoretical model (Fig. 34). The differences in the upper three curves are explained as probably due to errors incurred during the experimental procedure.





revealed no apparent changes following treatment in diammonium citrate (Fig. 37), but one of the FA90 samples does suggest possible changes (Fig. 38). The top set of photomicrographs of the FA90 sample shows the oxidized olivine prior to treatment; and the middle and lower sets, the olivine following treatment times of 6.1 and 28.8 hrs. respectively. One gets the impression that the lower set of photos is slightly less red than the middle one, and that there are less, bright opaque rims present. Both effects may be interpreted otherwise: the former to a lighting effect and the latter to the choice of grains photographed. However, the X-ray diffraction data obtained before and after treatment tends to support the microscopic data. X-ray diffractograms reveal a definite decrease in the ratio of the most prominent hematite peak to an adjacent olivine peak and thus suggest a relative decrease in the hematite present (Fig. 30). But this evidence too could be misleading. The apparent but perhaps not actual loss of hematite may be explained by possible differences in the hematite content of the various samples used, because (1) such differences have been documented for different parts of the oxidized FA90 samples (Fig. 35), (2) the photomicrographs are of different parts of the sample, and (3) the X-ray diffractograms also were made on different parts of the originally-constituted sample. X-ray data for two oxidized FA90 samples -- one treated in diammonium citrate -- reveal a difference in the fayalite component; a 60% increase after treatment (Table







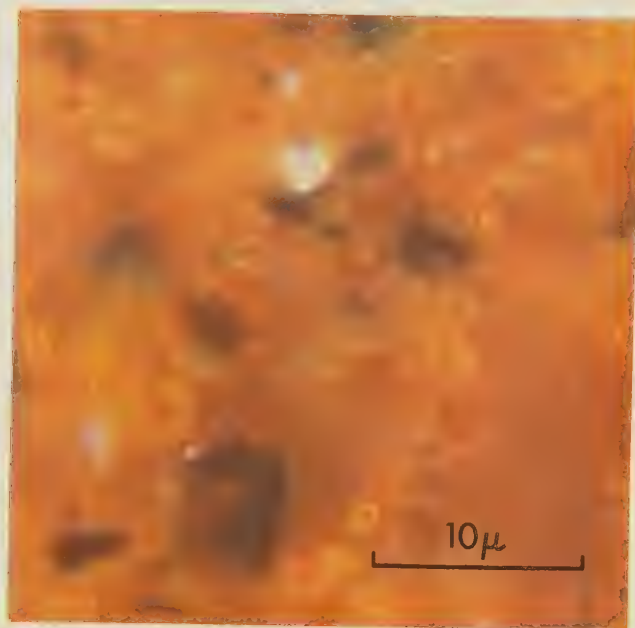
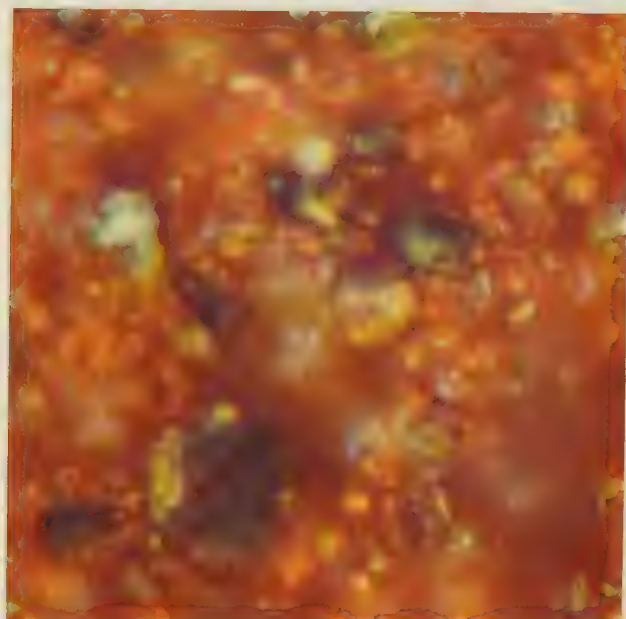
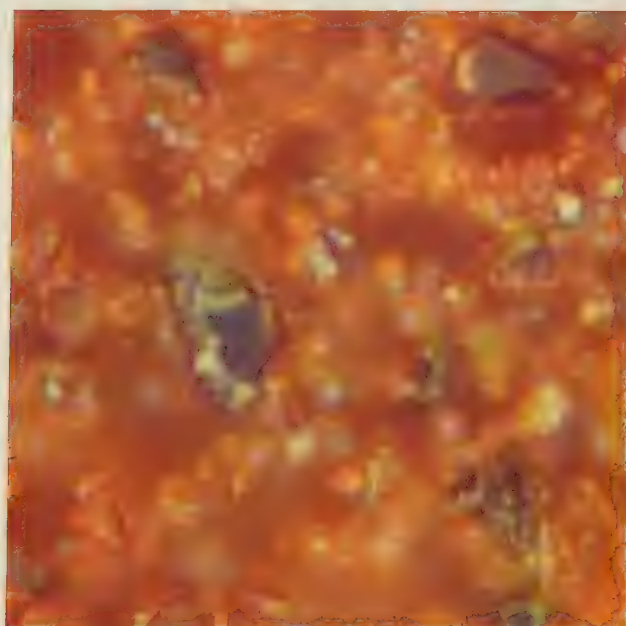
Fig. 37. Photomicrographs of the oxidized olivine sample FA30B before (top) and after (bottom) treatment in a diammonium citrate solution for a total of 83.3 hours, taken in plane polarized light (left) and under crossed nicols (right). This particular sample was ground and oxidized by Hoyer and Evans (1975).







Fig. 38. Photomicrographs of separate portions of the oxidized olivine sample FA90 before (top) and after treatment in a diammonium citrate solution for 6.1 (middle) and 28.8 hours (FA90A, bottom ). Photographs were taken in plane polarized light (left) and under crossed nicols light (right).







8). This difference could be accounted for by sample variability (see Fig. 35); the fayalite component in the oxidized sample being more largely converted to hematite. Therefore the visual and X-ray evidence that the diammonium citrate has leached some of the hematite is equivocal, but the magnetic evidence (Fig. 36) quite clearly indicated the removal of hematite

The scanning electron-microscope was also used in an attempt to document changes after treatment in diammonium citrate. However, no apparent changes in the olivine grains are evident (Fig. 39).

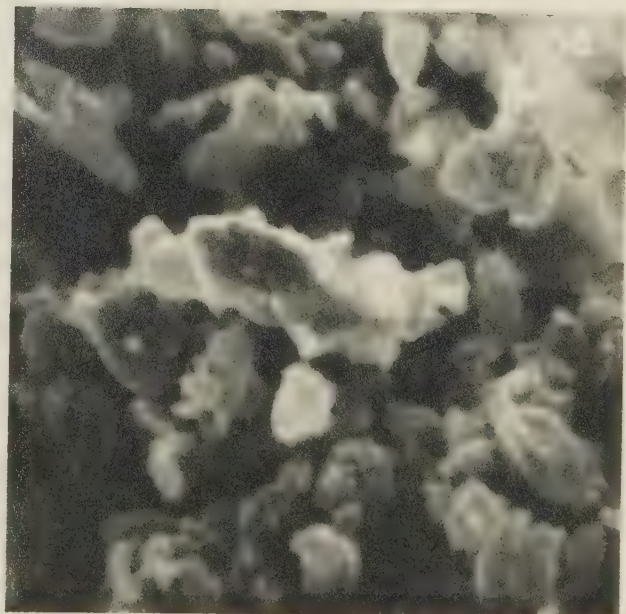
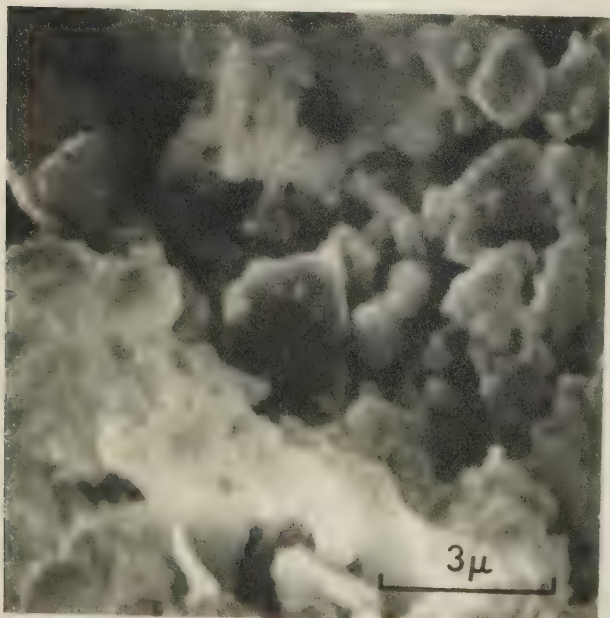
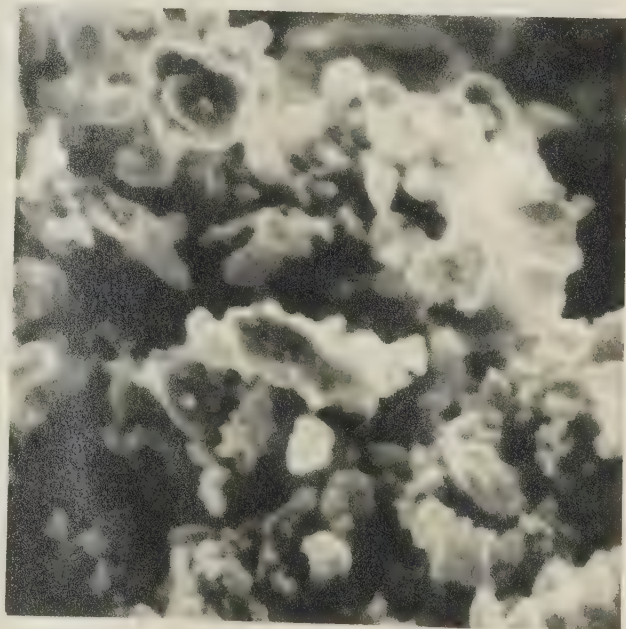
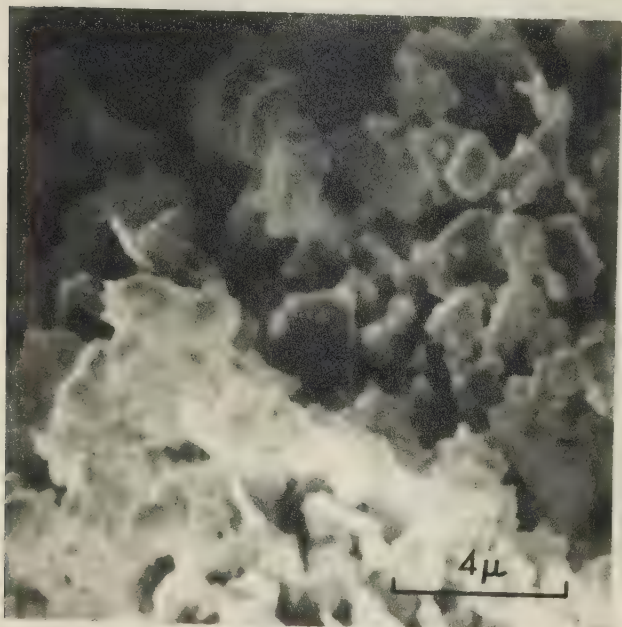
CHEMICAL TREATMENT BY THE D-C-B METHOD. A second method for removing the apparent hematite skin involved use of a chemical solution of the sodium salts of dithionite, citrate, and bicarbonate. This method has been successfully used by soil scientists to remove from soils free crystals and amorphous coatings of the oxides and oxyhydroxides of iron, -- especially hematite and goethite. The relative effect of the chemical solution on magnetite compared to hematite is not known. The method described in Mehra and Jackson (1960) involves(1) adding in turn a sodium citrate-sodium bicarbonate solution and sodium dithionite to the powdered sample in a tube, (2) placing the tube for 15 minutes in a water bath heated to 80°C, (3) extracting the iron oxide by the addition of a saturated solution of sodium chloride after the tube has been removed from the bath, and





Fig. 39. Scanning electron photomicrographs of separate portions of oxidized FA90 olivine grains before (right) and after (left) treatment in a diammonium citrate solution.









(4) centrifuging. In the prescribed method steps (1) to (4) are repeated before drying the sample, but in the present case the procedure was modified to include 7 and 15 minute extraction periods. Following each treatment period the sample was repacked in a holder and given an IRM build-up. In addition, some AF and backfield demagnetization was carried out on the IRM's produced after each treatment.

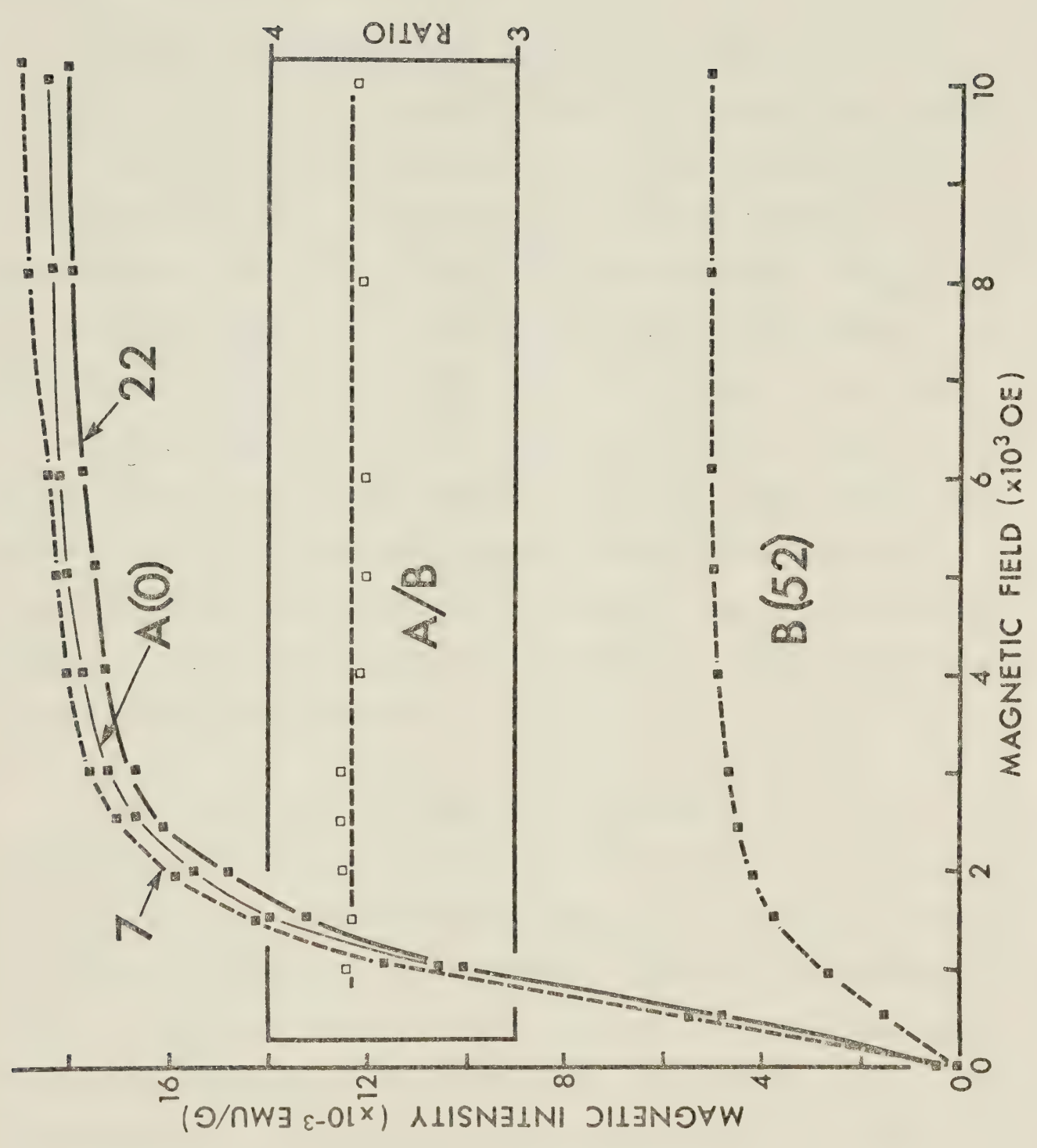
The chemical treatment was conducted on sample FA50C, -- the sample on which other detailed work had been carried out during the oxidation run. The IRM build-up results after each treatment are displayed in Fig. 40. There is not much, if any, change from the initial IRM build-up curve (A) following extraction periods of 7 and 15 min. (22 min. cumulative), but there is a dramatic decrease in the intensity following the recommended 30 min. extraction period (52 min. cumulative). The curve of the ratio A/B is slightly irregular -- perhaps due to experimental error, -- and can be construed to be either horizontal or slightly decreasing with increasing field. The fact that it is nearly horizontal for such a large decrease in the amount of magnetite suggests that nearly equal percentages of both hematite and magnetite have been leached, though perhaps with a slight preference for magnetite. Such a large decrease in the magnetite intensity suggests that the chemical solution has penetrated the cores of the olivine grains to some degree, perhaps even breaking up the smaller grains. The latter effect would more readily explain the







Fig. 40. IRM build-up curves obtained on sample FA50C following successive leaching periods using the dithionite-citrate-bicarbonate method. The sample was leached for cumulative time periods of 0, 7, 22 and 52 minutes. A ratio of A (prior to leaching) to B is shown in the middle inset, and may be compared to the theoretical curves given in Fig. 34.





apparently equal percentages of both hematite and magnetite removed and suggest that the D-C-B chemical solution attacks both minerals almost equally.

A polished thin section was made of the sample following the last treatment. Prior to treatment the sample was a yellowish-brown color, but after, it appeared gray; thus revealing the effectiveness of the D-C-B solution in leaching the outer rim. Under the microscope the sample was a yellowish-green color. Due to the fineness of grains polishing was difficult, and only a few areas of the slide reveal the inner portions of the olivine grains. Most of these grains have bright opaque patches at their edges, but some appear to be entirely opaque. Since the grains were quite small it was difficult to identify the opaque material present; but some at least is hematite, as evidenced by the anisotropy under crossed nicols.

There is better evidence that magnetite has been preferentially leached. This evidence derives from results of the Backfield and AF demagnetization of IRM after each treatment. Table 10 shows that with increasing treatment time the  $H_{Cr}$  and the MDF of IRM increase. In addition, the percentage of remanent magnetization after AF demagnetization in 1.8 kOe is about twice as large after the 52 min. treatment as after the 22 min. treatment. These results could mean that a greater proportion of the lower coercive force inclusions -- namely, magnetite -- have been





TABLE 10.

IRM PROPERTIES OF SAMPLE FA50C AFTER EACH STEP  
OF TREATMENT (trt) BY THE DITHIONITE-CITRATE-  
BICARBONATE METHOD

Total trt time (min.)	$H_{cr}$ (Oe)	AF demagnetization	
		$MDF^1$ (Oe)	RM(%)
0	$631 \pm 2^2$	--	$6.3^2$
7	--	$425 \pm 2$	5.5
22	$676 \pm 2$	$430 \pm 2$	5.6
52	$800 \pm 2$	$525 \pm 5$	11.2

## NOTES:

Treatments and IRM work were carried out on sample after the last oxidation step. The coercivity of remanence,  $H_{cr}$ , and  $MDF^1$  (median destructive field) of IRM were obtained from backfield and AF demagnetization respectively of IRM's acquired in 10 kOe. RM is the remanent magnetization after AF demagnetization in 1.8 kOe. Absolute errors are given.

<sup>1</sup> Usual definition of MDF of IRM (see Note 1, Table 13).

<sup>2</sup> Values obtained prior to pulverizing sample; therefore affected by a slight CRM.



removed, thus shifting the median coercive force higher. The apparent elimination of a hematite rim combined with the evident presence of hematite in the IRM build-up curve after treatment reinforces the evidence for hematite in the cores of the FA50 grains.

SUMMARY OF CHEMICAL WORK. The two methods of chemical treatment differ in their effectiveness and thus in their abilities to reveal the modes of occurrence of the magnetic minerals. Diammonium citrate with a lower reaction rate appears to be effective in removing hematite from the rim of the oxidized FA90 olivines, as verified by the IRM build-up results. The microscopic and X-ray evidence also suggests this result, but is equivocal. Besides verifying the presence of hematite in the rim, these results indicate that there is little if any magnetite intermixed with it. Results also suggest that diammonium citrate removes a hematite rim from the FA30 olivine.

Chemical treatment using the D-C-B method appears to be the more effective of the two methods for removing the outer rim of the oxidized olivines. However, this is by no means certain, because the visual evidence consists only of the color change visible to the naked eye, and such evidence could be refuted if the rims of the FA50 olivines are found to be much thinner than those of the FA90 olivines. Other evidence suggests, though, that the method is much more destructive to fine olivine grains. IRM data seem to



indicate that magnetite and hematite have been leached almost proportionately to their occurrence; this may be an effect due to the complete destruction of the abundant fine grains. This would explain the large drop in the magnetite intensity without invoking the presence of magnetite in the rims. The increase in stability of the magnetic material with treatment time (Table 10) may be a side effect of this destruction and indicate a slight preference for the leaching of magnetite from the exposed cores. What is certain though from the microscopic evidence is the greater abundance of opaque material in the cores of the FA50 olivines compared to the FA90 olivines. The microscopic combined with the chemical evidence suggests that much of this opaque material is hematite.

#### Identifying Changes in the Magnetic Minerals with Oxidation Time

The present experimental work documents relative rather than absolute changes in the quantity and stability of the magnetic minerals with oxidation time. Since more information is available on the changes in sample FA50C, the results on this sample will be particularly emphasized in this section. The possible effects of the PTRM on the magnetic properties of the FA50 samples is discussed at the end.





ESTIMATES OF QUANTITATIVE CHANGES. Observations with the naked eye and microscope have revealed changes in color, which evidence the increase of hematite with oxidation time. These changes vary with initial olivine composition; the more iron-rich olivines generally having a greater quantity of hematite. The absolute quantities of hematite produced cannot be presently calculated, because much of it is probably in the sp range and so escapes detection by the magnetic methods used which rely on remanence. One can however estimate the quantity of hematite occurring in the stable sd range as a proportion of the total possible sd hematite that could be produced. The method involves calculating the hematite remanence in the sample, and comparing it to the remanence of the total possible sd hematite. For non-interacting sd grains, as in the case of hematite, the remanence will be 0.5 of the saturated value; and so in finding the above proportion this factor cancels out and one needs only to consider the estimated remanences from the appropriate curves. The hematite remanence in the sample can be approximately determined from the slope of the IRM build-up curves between 3 and 10 kOe. The maximum possible remanence can be calculated from the maximum possible mass of hematite, using reference data for a sd hematite powder (0.1  $\mu$ m grain size) determined by Roquet (1954). Appendix 8 explains the calculations involved. Values for hematite after each oxidation step are given for sample FA50C in Table 11, and for FA30A and FA90 in Table





TABLE 11.  
SINGLE-DOMAIN HEMATITE IN SAMPLE FA50C

Oxidation time (min.)	Remanent magnetization (e.m.u. $\times 10^{-3}$ )	Wt. % of total hematite	Mass (mg)	Wt % of total sample
10.5	0.20	0.6	2	--
25	0.53	1.2	4	--
80	0.85	1.9	7	--
240	1.14	2.6	9	--
500	1.41	3.1	12	--
1100	1.53	3.4	13	--
2120	1.57	3.5	13	--
4000	2.37	5.3	20	--
8015	2.31	5.2	19	3.5

NOTES:

See Appendix 8 for details of the calculation. The IRM build-up curves of Fig. 25 are used for calculating the actual remanence due to hematite. The wt % of total hematite is determined from the remanence and from the theoretical amount of hematite that could be produced from complete oxidation. Total mass of sample is 538 mg.



TABLE 12

SINGLE-DOMAIN HEMATITE IN THE OXIDIZED  
OLIVINE SAMPLES OF EACH COMPOSITION

Sample	Theoretical maximum		sd hematite present			Wt.% of total sample
	Mass (mg)	$RM_1$ ( $\times 10^{-3}$ e.m.u.)	$RM_2$ ( $\times 10^{-3}$ e.m.u.)	% ( $RM_2/RM_1$ )	Mass (mg)	
FA30A	261	31	0.59	1.9	5	1.2
FA50C	370	44	2.31	5.2	19	3.5
FA90	454	54	2.36	4.4	20	3.2

## NOTES:

An explanation of the above calculations is given in Appendix 8.  $RM_2$  is the actual estimated remanent magnetization of hematite determined by measuring the increase in moment in the IRM build-up curves between 3 and 10 kOe (Fig. 25), and extrapolating this value by means of the slope to 0 and 30 kOe.  $RM_1$  is the theoretical maximum remanence determined from the IRM curve for hematite powder at 30 kOe (Roquet 1954, found in Irving 1964).



12. Sd hematite appears to constitute 1.2, 3.5, and 3.2% of samples FA30A, FA50C, and FA90 respectively. Sd magnetite also increases with oxidation time in sample FA50C as evidenced by the general increase of the IRM with time (Fig. 25), but appears to constitute much less of the samples compared to hematite judging by the same IRM curves (at 8015 minute oxidation step there is about 20 times more sd hematite than sd magnetite).

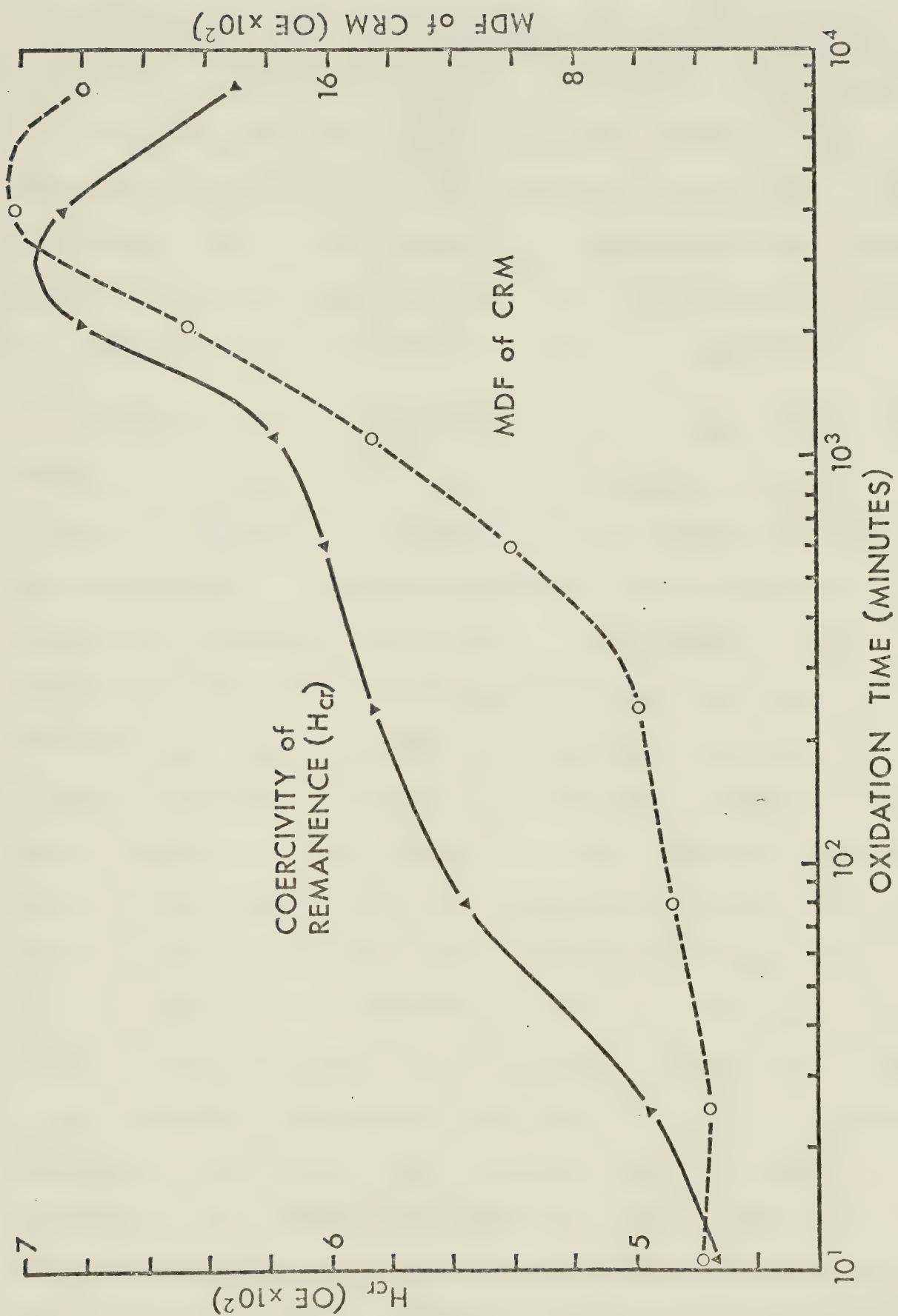
CHANGES IN STABILITY. Documentation for the change in stability of the magnetic minerals with oxidation time is lacking for all samples except FA50C. Curves of the AF demagnetization of CRM of this sample reveal an increase in magnetic hardness after each successive oxidation step (Fig. 32). This can be attributed to either or both of two concurrent effects: a decrease in the amount of magnetite present through oxidation to hematite and a growth of hematite into the stable sd range. Magnetite too will grow into the sd range, and this will nullify somewhat the former effect. Because the growth of magnetite and hematite are so intimately intermixed, it is difficult to document their individual changes in stability. However, overall changes can be gauged. And this has been done by plotting curves of the MDF (median destructive field) of CRM and of  $H_{Cr}$  (Fig. 41) as derived from the AF demagnetization of CRM (Figs. 32 and 33) and the backfield demagnetization of IRM respectively. Both curves show an increase of stability with oxidation time and a decrease after reaching a maximum







Fig. 41. Coercivity of remanence ( $H_{cr}$ ) and median destructive field (MDF) of CRM versus oxidation time for the oxidizing olivine sample FA50C.  $H_{cr}$  = MDF of IRM (from AF demagnetization of IRM curves) when all components are aligned (Park and Irving 1970). This is not true in the present case, because the CRM was not completely eliminated prior to the sample being given an IRM.





between 3000 and 5000 minutes. The decrease is possibly attributable to a relative increase in the rate at which magnetite as opposed to hematite is entering the sd region; an increasing proportion of sd magnetite shifting the stability indexes (MDF and  $H_{cr}$ ) to lower values. This could be an effect due to the build-up of the hematite rim, which would increasingly limit the oxidation of magnetite within the core and permit more of it to reach sd proportions.

CHANGES ACCORDING TO INITIAL OLIVINE COMPOSITION. The differences in the amounts of hematite present in the different compositions following the last oxidation steps have been noted. It should be possible to draw certain conclusions regarding variations in the amounts of hematite and possible magnetite with composition by studying variations in various parameters. Comparisons among the different compositions should not be unduly affected by the varying oxidation times, since the major oxidation changes appear to have taken place and any further changes will be very slow. Are there any trends in the various parameters? One such trend is the increase in hematite with iron content of the original olivine as already noted (Table 12). Another is the attendant decrease in IRM (Figs. 31 and 42). However, the CRM's do not follow such a simple trend, the FA50 samples being anomalously strong. The FA50C sample also exhibits anomalously low 'hardness' parameters (Table 13,  $H_{cr}$  and MDF of IRM). These anomalous values may be due to the PTRM acquired early in the oxidation run by the FA50







Fig. 42. IRM (after magnetization in 10 kOe) of oxidized olivine samples versus initial olivine composition. The CRM of all samples had been demagnetized in 1.8 kOe AF prior to being given an IRM. There will be a very slight error ( $<2\%$ ) due to the presence of a hard, undemagnetized component of CRM.

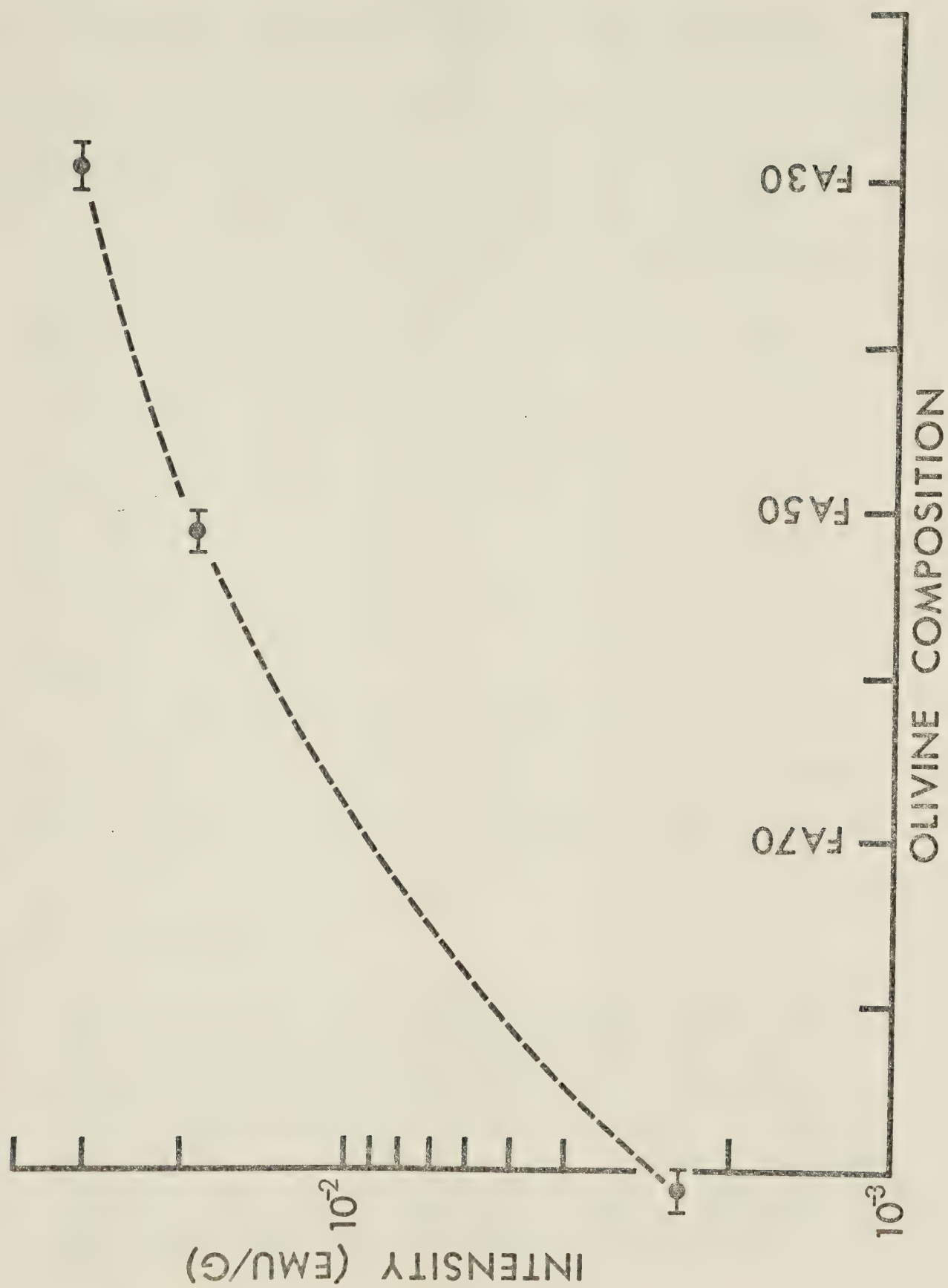




TABLE 13.

## MAGNETIC STABILITY VERSUS OLIVINE COMPOSITION

Sample	Oxidation time (minutes)	H <sub>cr</sub> (Oe)	MDF of IRM <sup>1</sup> (Oe)
FA90	8008	2175	790
FA50C	8015	630	425 <sup>2</sup>
	2190	(684) <sup>3</sup>	--
FA30B <sup>4</sup>	2190	695	--
FA30HE <sup>5</sup>	2190	--	(568) <sup>1</sup>

## NOTES:

H<sub>cr</sub> (coercivity of remanence) and MDF (median destructive field) of IRM values are derived from the curves of the backfield and AF demagnetization of IRM respectively. IRM's were produced in 10 kOe. Estimates in parentheses.

<sup>1</sup> Hoyer and Evans (1975) define the MDF of IRM or CRM differently than in the present work. Their MDF's are the AF's required to destroy one half the remanence that can be destroyed by an AF of 1.8 kOe, whereas in the present case the MDF's are defined in the usual manner as the AF's required to destroy one half of the total remanence. In comparing values from the two works the values will be stated according to one or the other definition. Values according to the usual definition are quoted in this Table.



- <sup>2</sup> Treated for 7 min. by D-C-B chemical method.
- <sup>3</sup> Estimated from Fig. 41.
- <sup>4</sup> Treated for 35.8 hours in diammonium citrate solution.
- <sup>5</sup> FA30 sample of Ibid. The MDF of IRM value is an interpolation using the curves obtained for their 1000 and 3040 min. oxidation samples.





samples. And this possible effect is fully discussed in the next section.

THE EFFECT OF PTRM ON THE FA50 SAMPLES. The effect of the PTRM on the magnetic properties of the FA50 samples can be pieced together from the various magnetization curves. The first obvious effect is the dramatic increase in the intensity of the CRM curves of samples FA50A and B after the 80 min. oxidation step which produced the PTRM (Fig. 26). This increase is predictable from theory. For a particular sd grain the TRM acquired will always be greater than the CRM; a typical TRM/CRM ratio being about 2.5 (Stacey and Banerjee 1974).

Contrary to samples A and B, sample FA50C was given detailed magnetic treatments between oxidation steps. The critical question is whether the temperature increase affects the subsequent values derived from its associated magnetic curves. In particular can it explain the anomalously low  $H_{Cr}$  value for FA50 (Table 13). The temperature increase could affect magnetic properties in at least two ways: first by the imposition of a PTRM, and second by increasing the amounts of magnetite and hematite above what would be normally produced at 500°C. The PTRM will clearly have an effect unless it can be removed by the AF demagnetization used after each successive oxidation step. The effectiveness of AF demagnetization in removing the PTRM is illustrated in Table 14 which documents the CRM



TABLE 14.

REMANENT MAGNETIZATIONS OF SAMPLE FA50C PRODUCED  
BY SYSTEMATIC MAGNETIC TREATMENTS FOLLOWING THE  
ACQUISITION OF CRM AT EACH OXIDATION STEP

Oxida- time (min.)	CRM in 10 Oe ( $\times 10^{-5}$ )	AF demag. in 1.8kOe ( $\times 10^{-5}$ )	IRM in 3kOe ( $\times 10^{-3}$ )	IRM in 10kOe ( $\times 10^{-3}$ )	AF demag. in 1.8kOe ( $\times 10^{-5}$ )
0	--	--	6.49	6.54	7.2
10.5	46.3	1.2	6.06	6.16	10.6
25	24.4	2.1	6.56	6.84	24.1
80	80.8	4.9	7.24	7.67	42.1
240	32.3	9.0	8.09	8.64	58.1
500	36.5	15.5	8.94	9.66	73.2
1100	47.6	22.5	9.42	10.23	79.5
2120 <sup>1</sup>	58.7	30.7	11.49	12.31	95.1
4000	70.5	39.7	13.81	15.05	104.1
8015	80.4	44.9	17.28	18.48	115.9

## NOTES:

The magnetizations (e.m.u./g) were acquired  
consecutively from left to right.

<sup>1</sup> Bias field for CRM was 10.8 Oe.



acquired during each oxidation step. Apart from the 10.5 and anomalous 80 min. values the increase in CRM is monotonic from 25 min. on and the PTRM appears to have been eliminated following AF treatment in 1.8 kOe. This means that the bulk of the PTRM must be carried by sd magnetite rather than hematite. It cannot be carried by magnesioferrite, since this mineral is paramagnetic at 500°C.

That the PTRM has been eliminated is also verified by the various indices of stability derived from the various curves mentioned. When Hoyer and Evans (1975) gave a total TRM to several of their CRM samples, they found that the remanences were magnetically softer to AF demagnetization. This does not appear to be the present case as indicated in Table 15. Here, values of MDF of CRM for FA50C -- except for the 80 min. value -- duplicate the trend of the FA30 sample of Hoyer and Evans (FA30HE), showing reasonable values before and after the anomalous step. The MCF of IRM values for the former change fairly regularly with time, but there is no anomaly at the 80 min. step. This apparent lack of any permanent change in the magnetic properties is probably due both to the brevity of duration of the higher temperature and to the limited temperature range.

The second possible effect of the temperature increase is the production of greater amounts of hematite and magnetite. However, the reasonable values of the stability parameters just discussed argue against the proposition. In





TABLE 15

COMPARISON BETWEEN MAGNETIC STABILITIES OF  
OLIVINES FA30 (HOYE AND EVANS) AND FA50  
(PRESENT WORK) WITH OXIDATION TIME

Oxida- tion time (min.)	MDF OF CRM <sup>1</sup> (Oe)		MCF OF IRM (Oe)	
	FA30 <sup>4</sup>	FA50	FA30	FA50
6	570	--	830	--
10.5 <sup>2</sup>	550	380	800	580
25	490	332	800	600
80	560	450	840	650
240	570	393	840	690
500	(580)	410	--	680
1100 <sup>3</sup>	590	475	830	760
2120	(600)	514	--	820
3040	610	(550)	820	(850)
4000	--	576	--	880
8015	--	590	--	920

## NOTES:

MDF<sup>1</sup> is the median destructive (AF) field and MCF is the median constructive, -- that is, the field required to produce 50% of the saturated remanence. Parentheses indicate interpolated values. For the FA50 values errors are about  $\pm 5$  Oe for the MDF's and





$\pm 20$  Oe for the MCF's.

<sup>1</sup> Definition of Hoyer and Evans (1975) used here; see note<sup>1</sup>, Table 13.

<sup>2</sup> Oxidation time of Ibid. is 10 min.

<sup>3</sup> Oxidation time of Ibid. is 1000 min.

<sup>4</sup> The FA30 sample is labeled FA30HE in the text and the FA50 sample, FA50C.



addition, the remanence after the AF treatment of CRM increases regularly for successive oxidation intervals, thus indicating that there has not been any appreciable change in the growth rate of hematite (Table 14). Likewise, in the IRM curves (values listed in Table 14), there is no deviation from the regular increase in intensity at the 80 min. step for plots of the 3 kOe and 10 kOe values with time. This indicates that no additional amount of magnetite has been created, nor any observable amount of magnesioferrite.

Hence, in conclusion, the PTRM affects the magnetite intensity only briefly. It is eliminated by AF demagnetization and produces no further effects on the parameters of intensity and stability. Nor is there any additional hematite or magnetite created by the temperature excursion. Therefore, the apparently low value of  $H$  for FA50C must be approximately correct.

### Verification of Model?

The model of the oxidized olivine proposed earlier consists of a rim of hematite and a core of hematite and magnetite, with the hematite increasing with oxidation time.

Hematite was positively identified to be present by X-ray diffractograms of the oxidized FA90 sample, and verified by microscopic and chemical work as occurring in the form of discontinuous rims. IRM build-up curves indicate hematite to be present in all three compositions. Various



indices of stability indicate that hematite generally increases with time in the FA50 sample.

Magnetite was not identified by any of the usual tests, but can be construed to be present by the nature of the IRM build-up curves and by the fact that hematite must in large part be its alteration product. The chemical work suggests that if it exists it occurs almost entirely within the cores of the olivine grains. Chemical work too suggests that hematite resides at least in the core of the FA50 grains. This is verified by the microscopic work.

Experiments on different compositions thus tend to verify different aspects of the model.

### Comparison with Work of Hoyer and Evans

As discussed previously Hoyer and Evans (1975) conducted magnetic experiments on oxidized olivines of FA30 composition (the FA30 sample(s) used in their paper are identified as FA50HE). The present experiments have extended this work to other compositions (FA50, FA90) using essentially the same techniques and facilities. Two samples of FA30 composition were used for limited experiments, but provide the main link for a comparison of the two studies. This relationship will be explored first, and then the properties of the FA30HE samples will be compared to FA50C.

The CRM curves for both studies of FA30 (FA30A of this





study) are found in Figs. 24 and 26. Both curves rise to a maximum and then decrease; but there the similarity ends. The curve of Hoyer and Evans has a different shape, reaches maximum much sooner (400 as opposed to 800 min.), and -- what is most surprising -- has an intensity about ten times greater. Perhaps the first two features can be explained by the fact that the points on their curve each represent a different sample, and hence minor differences such as packing could be responsible for the difference (eg. see the curves for the differently packed FA50A and FA50B samples, Fig. 26). However, the intensity difference is problematical. One possibility is that the field used by Hoyer and Evans was unintentionally ten times greater -- namely, 100 Oe. The difference is apparently not due to a ten-fold increase in magnetic material, because an IRM build-up on another of their samples (FA30B), used in conjunction with the present work, shows a similar intensity after magnetization in a field of 10 kOe, as other samples given a CRM by them at the same time, and as the present samples (FA30A; Table 16).

The similarity in IRM values among the FA30 samples also probably indicates that there is no large discrepancy among each of their magnetic properties. This means that the magnetic properties of the FA30HE samples can be compared in a relative manner with those of FA50C.

Again, as in Table 13, the apparent anomaly of lower



TABLE 16.

COMPARISON BETWEEN SOME MAGNETIC PROPERTIES OF  
THE OXIDIZED FA30 OLIVINE OF HOYE AND EVANS  
AND THAT OF THE PRESENT WORK

Sample	Oxidation time (min.)	CRM ( $\times 10^{-3}$ e.m.u./g)	IRM ( $\times 10^{-2}$ e.m.u./g)
FA30A	6020 <sup>1</sup>	0.25	3.03
	(2190)	(0.31)	--
FA30B	2190	(4.7)	2.48
FA30HE	2190	(4.7)	(2.0)

## NOTES:

FA30B is a sample of Hoyer and Evans (1975) used in the present work but not used by them in their paper. FA30HE is a hypothetical sample of Ibid. whose values are interpolations using the CRM and IRM curves of their paper. Values in parentheses are estimates. Values of FA30HE are measured in a single direction only -- the direction along which the magnetizations were imposed. Other values are complete measurements of all components.

<sup>1</sup> Oxygen supply ran out during run. The true oxidation time lies between 4920 and 6020 min., but is probably closer to the former.



stabilities in the FA50 sample is evident. For both compositions MDF's increase smoothly versus oxidation time, except in the lower range (<80 min.). Both show a dip at 25 minutes, which could be due to the elimination of most of the contaminant magnetite by oxidation and the simultaneous growth into the sd range of a much larger quantity of magnetite. The value at 80 minutes for FA50C is due to the PTRM which is eliminated before the next oxidation step. The MCF values likewise emphasize the lower stability of the oxidized FA50C sample, but also indicates a marked increase in stability with time as contrasted to the FA30HE values which are relatively constant. The FA30HE MDF values suggest the growth of a small hematite component with oxidation time, but at a much slower rate than in FA50C as indicated by the increase in its MDF values with time. Hematite is also suggested to be present in the FA30HE samples by the slight increase in the IRM build-up curves of the two most-highly oxidized samples between 3 and 10 kOe and by the residual values after AF demagnetization of the CRM in 1.8 kOe. Study of the relative stabilities of the two oxidized olivines thus reaffirms the lower magnetic stability of the FA50 composition compared to the FA30, as well as the increased rate of growth with oxidation time of hematite relative to magnetite.





## Chapter 5: Summary and Conclusions

### Vibrating Sample Magnetometer

#### Introduction

The present VSM was designed to operate with fields up to 10 kOe and variable temperatures up to 750°C, while maintaining a reasonable sensitivity. How well the VSM fulfilled these objectives is discussed below. At the same time possible improvements in its operation are suggested. Conclusions with regard to the general operation of the instrument for hysteresis and thermomagnetic studies are given last.

#### Signal and Sensitivity

With many parameters set by the VSM construction the signal only depends on sample magnetization and positioning, vibration frequency and amplitude, and applied field. The signal can also be optimized somewhat by alterations to the peripheral equipment. These factors combine to determine the signal strength. And this, together with the noise, determines the signal to noise ratio, and with amplification considerations, the instrument sensitivity. The sensitivity is first discussed, and then in general how it can be improved by optimizing the above factors. Then sample positioning is discussed.





A qualitative measure of the present sensitivity is the lowest amount of hematite necessary to record a hysteresis curve. With the present values of vibration frequency (35 Hz), vibration amplitude ( $<1$  mm), and field (5.7 kOe) used in the experiments, the hysteresis of a magnetite sample, which has a composition corresponding to a typical natural basic rock with 5% magnetite, can be easily measured. But judging by the hysteresis curve for a 100% hematite sample, with a magnetization some 100 times weaker, the typical red sediment with 1 to 3% hematite could not be easily measured. Therefore the VSM is not as sensitive as desired.

However, the sensitivity can be improved. The frequency chosen was a convenient one below the mains frequency which was high enough -- for most part -- to avoid sticking problems associated with the vibrating rod, and low enough to avoid appreciable energy loss to the VSM. The geophone drive is quite capable of operating at frequencies from 5 Hz to 50 kHz or more, with a maximum signal output from the sample occurring at 12 kHz. With proper shielding and vibration isolation one could increase the 35 Hz signal by about 600 times. However, barring this ideal, a useful operating range after some noise reduction might be 10 to 100 Hz. At 100 Hz the signal is four times greater than at 35 Hz.

The next possibility is to increase the vibration amplitude. This is not physically possible at 35 Hz, as it



is already adjusted to maximum, but could be increasingly done at higher frequencies since vibration amplitude decreases with frequency for constant oscillator output. However, even though it might be increased somewhat, when combined with the higher frequency, it could result in damage to the system. The thermocouple is more resistant than most to vibration, but it could wear out faster. Also, the cone and socket method of sample attachment and the powder sample would be susceptible to disruption.

The third way of increasing the signal is by increasing the field to 10 kOe. This would increase the magnetization of hematite threefold. The electromagnet is quite capable of producing 10 kOe within the present pole gap, but was unable to during the time of the experiments due to unforeseen problems involving the original power supply.

Other things that could be done to improve the sensitivity include reducing the noise level and using impedance matching. The importance of the latter was not apparent at the time. With impedance matching the signal will increase and the preamplifiers will be much more effective than at present.

With some of the foregoing improvements, such as increase in vibration frequency and of field, it should at least be possible to increase the signal tenfold. A further improvement by impedance matching and the use of suitable preamplifiers to the lock-in amplifier should bring the



hematite signal of the typical red sediment into a range where hysteresis can be recorded.

All of the above factors for improving the sensitivity assume that the sample has been correctly positioned. It turns out in fact that sample positioning is not as critical as expected, for the signal remains constant to within 0.5 or 1% for sample displacements within  $\pm 0.2$  or  $\pm 0.6$  cm of the centre of the detection coil array respectively.

### Hysteresis Tests

The hysteresis curves obtained appear at face value to represent the substances tested (Ni, Fe, magnetite, hematite). Pure spherical iron and nickel samples were used to derive and test the calibration constant, and magnetite powder samples for the calculation of  $J_r/J_s$  for sd grains.

The nickel curves reveal a slight negative slope after sample saturation has been reached, which is possibly caused by increased friction between rod and guide tube with increasing field. However, the effect has little influence on the calculation of the magnetization of nickel using the derived calibration constant. The magnetization found agrees within error ( $481 \pm 14$  gauss) with that found in the literature ( $484.1$  gauss) thus tending to validate the hysteresis curves and the slope method of calibration. The derived calibration constant is only valid for the present instrumental set-up and will change for different







amplification factors. Use of this constant to find the magnetization of the magnetite powders showed that the method breaks down when using large non-spherical samples.

Another test of the hysteresis curves involved calculation of the quantity  $J_r/J_s$  for comparison with theoretical values. For non-interacting sd particles this value is 0.5. Calculations involving the two largest sd magnetite samples resulted in values of  $0.46 \pm 0.01$ , and  $0.47 \pm 0.01$ , quite close to the theoretical value. Though these calculations tend to verify the curves, the extremely low value (0.26) for the smallest magnetite sample (28 mg) -- derived from what appears to be a reasonable curve -- is presently unexplained.

Measurements involving the hysteresis curves of three iron and two nickel samples were used to test measurement repeatability. It was thought that the near identical nature of the two sets of samples would provide a good simulation of the best test which consists of repeatedly reinserting the same sample. Raw voltage measurements of the iron and the nickel samples compare within 1 and 2% respectively. Taking into account the minor inconsistencies among the samples, the repeatability should be even better.



## Thermomagnetic Tests

The oven was tested and found to have a temperature range varying between 0 and at least 750°C. Heating to 600°C could be accomplished in as little as 15 min. and subsequent cooling to room temperature in as little as 40 min. The absolute error in sample temperature determination ranged from 5 to 12°C between 300 and 700°C, and the corresponding r.m.s. error from 3 to 6°C. The temperature gradient in the oven meant a temperature error of 1°C or less for each  $\pm 0.2$  cm displacement of the sample from the oven centre out to about  $\pm 0.6$  cm for temperatures up to at least 600°C. Outside the oven the temperature was maintained below 40°C for internal temperatures up to 600°C through the use of Fiberfrax insulation and cooling by forced air or evaporating liquid nitrogen.

Two thermomagnetic runs were made on each of two samples: nickel and magnetite; both continuous and discontinuous heating and cooling curves being obtained. Curie points for each substance, derived using the inflection point method, agreed to within 1 or 2°C, except for those from the respective continuous heating curves; and all Curie points except for the latter were higher than the listed values. In the case of magnetite the experimental error ( $\pm 5^\circ\text{C}$ ) brings the values ( 589°C) within range of the highest literature value. The fact that the lowest part of the sample is about 2 or 3°C cooler than the sample centre,



and that the sample centre is possibly 0.3 cm below the oven centre -- a further 1 or 2°C difference -- may account for the high measured value. For nickel the determined Curie point of about  $375 \pm 4^\circ\text{C}$  was much higher than the usually quoted value of  $358^\circ\text{C}$ ; however, determinations in the literature have ranged from 358 to  $382^\circ\text{C}$ . The nickel thermomagnetic curve is apparently dependent in the critical Curie point region on the applied field. When the present field (4760 Oe) is taken into account using standard Weiss theory, the  $358^\circ\text{C}$  value increases to  $372^\circ\text{C}$  in conformity with the measured value.

For careful experimental work the discontinuous or point curves are considered best, since at each desired temperature, sample and thermocouple are allowed to reach thermal equilibrium before a reading is taken. Samples used suffered from several effects that made comparison between repeated curves difficult. The magnetite sample was subject to slight oxidation which served to decrease the intensity; and the nickel to a probable annealing effect which apparently increased its intensity in the initial heating run but not in the second heating run. In addition, runs were also subject to noise problems due variously to the movement of coil leads and to sticking of the vibrating rod. The former effect was caused by the forced air cooling and by the cooling contractions associated with the liquid nitrogen; the latter by a possible slight rotation of the rod from its initial optimum orientation. These two problems





became most serious in the thermomagnetic runs where temperatures and a comparatively long time period were involved.

## Remanence in Oxidized Olivines

### Introduction

The purpose of the present work was to extend the work of Hoyer and Evans (1975) to olivines of other compositions; in particular, to identify the magnetic phases present in oxidized olivines and to describe their nature, occurrence, and properties. To facilitate the oxidation process and reduce the number of chemical variables present finely-ground synthetic olivine samples were used. Below are summarized the major findings of the experiments performed on olivines of composition FA30, FA50, and FA90. First, the identity and mode of occurrence of their magnetic phases are described, and then changes occurring in these phases with respect to oxidation time. The findings are then compared to those of Hoyer and Evans. Finally, a note is given on the application of these results to paleomagnetic studies.

### Identity and Occurrence of Magnetic Phases

Initial examination of olivines by microscope and IRM work prior to oxidation revealed the presence of a magnetic contaminant which was tentatively identified as magnetite. It acquired a hard remanence in high fields which was not





eliminated in AF's of 1.8 kOe. During the early oxidation the hard remanence was reduced considerably, suggesting that it was predominantly carried by free sd grains of magnetite that easily oxidized to hematite. However, a possible contaminating remanence of from 5 to 10% of the FA50 CRM curves, and less for the FA30 and 90 curves, may be present. It is thought that, barring the elimination of this component upon further oxidation, the experimental curves (CRM and others) are suitable for comparative purposes.

With oxidation at 500°C in a 10 Oe bias field a CRM is gradually acquired by all three olivine compositions. Below, the identity and occurrence of the magnetic phases present in each oxidized sample are discussed.

Results show that all three compositions contain hematite and magnetite. The presence of magnesioferrite was not verified, but if present probably occurs in very minor amounts compared to magnetite. Hematite definitely occurs as rims in FA90, with apparently little if any magnetite intermixed. Rims are rare in FA30. They were not observed in FA50 due to the lack of a polished thin section, but can be inferred to be present from the chemical results. In addition, hematite was identified in cores of FA50 grains. Magnetite was not identified optically, but from the nature of the various magnetic curves (e.g. IRM curves) and their derived stability values, it can be inferred to be present. It would appear to be concentrated in the olivine cores;



certainly this is the case for FA90.

The magnetic properties of FA90 were found to change with position in the originally-oxidized sample, thus suggesting local variations in the proportions of hematite to magnetite and in the amount of magnetite present. The effect is probably governed by the availability of oxygen. The conclusions below largely concern results from whole samples and so are not influenced by local variations in the magnetic properties.

#### Changes in Magnetic Phases with Oxidation Time

The CRM's of FA30 and FA90 increased with oxidation time to a maximum value between 700 and 1500 minutes and decreased somewhat thereafter. There was no information on the growth of magnetic material with time and so these curves could not be corrected for this effect. But comparison of these curves with the similar uncorrected curve of Hoyer and O'Reilly (1973) suggests the same explanation for the behaviour that they proffered for their subsequently corrected curve; namely, that the initial increase is due to the growth of magnetite from sp to sd size, and the decrease to its growth into the psd range.

FA50 has an anomalously high CRM over most of its oxidation curve which can be explained by the acquisition of a PTRM during the 80 min. oxidation step when the temperature accidentally reached about 550°C. It is not



caused by any increased amount of magnetite or hematite produced at the higher temperature. And it is certainly not caused by magnesioferrite which if present would be paramagnetic at 500°C.

In sample FA50C, which was AF demagnetized after each CRM step, the PTRM is apparently eliminated within a field of 1.8 kOe following the step of its acquisition. It is therefore concluded that the magnetic properties measured subsequently have not been affected to any noticeable degree.

With increasing oxidation time there is an apparent increase in the amount of hematite present which is especially well-documented in sample FA50C. Although the actual growth in FA50C cannot be detailed, because hematite of sp dimensions cannot be detected by magnetic remanence studies, the growth of the stable sd fraction can be roughly estimated. At the highest oxidation attained FA50C contains about 3.5% by weight of sd hematite, compared to 1.2 and 3.2% for FA30 and FA90 respectively. X-ray diffractograms have verified that there is at least a minimum of 5% total hematite present in FA50C. Sd magnetite also appears to increase with each oxidation step for this sample except the last one. Comparing the three compositions there is an increase in hematite with iron content or increasing fayalite, and a concurrent decrease in magnetite.







Changes in stability -- especially in FA50C -- have also been documented. The overall stability of FA50C increases with time as shown by the increase in the MDF of CRM and the  $H_{Cr}$  values, and likely reflects the relative increase of sd hematite over sd magnetite -- perhaps due to oxidation of the latter. Compared to other compositions the various indices of stability of FA50C appear to be anomalously low. This seems to be a real effect which indicates a higher ratio of sd magnetite to sd hematite.

#### Comparison with Work of Hoye and Evans

The FA30 CRM curve of Hoye and Evans (1975) is directly comparable to the FA30 curve of the present work. Both experiments were run using essentially the same facilities and techniques. Both curves rise to a maximum and then decrease somewhat; however, the shapes are different, the maxima occur at different times (400 min., Ibid.; 800 min. present work), and perhaps most surprising, the intensity of Hoye and Evans' curve is ten times greater. The first two differences are possibly due to the fact that Hoye and Evans used a different sample for each oxidation step; the latter is problematical, but could be explained if their field was ten times greater. The higher intensity certainly cannot be explained by a tenfold increase in magnetic material, because the IRM's of the FA30 samples agree quite well. This likely means that the proportions and amounts of the magnetic phases present in the samples of both are similar.



If so, then the magnetic properties of the FA30 samples of Hoyer and Evans can be compared to those of the FA50 sample of the present work; that is, disregarding the CRM intensities.

First, the magnetic phases present will be compared and then the overall stabilities. Hoyer and Evans suggested that the remanent magnetizations of FA30 were carried by magnetite. The most oxidized samples showed evidence of a hard magnetic component which they attributed to the production of a small amount of hematite after prolonged heating. One of their samples treated with diammonium citrate in the present work was interpreted to have hematite on the outside. This sample oxidized by them for 2190 min. falls within the oxidation time range of those of their samples suggested to have hematite present. A polished thin section of this sample shows the odd thin rim of hematite. FA50 on the other hand has comparatively abundant hematite -- probably in the rim as well as in the core. FA30 samples are apparently more stable, despite the apparently lower hematite content; but do not increase in stability as rapidly with oxidation as does FA50. It is concluded that the FA50 sample has a greater quantity of hematite but a lower hematite - to - magnetite ratio than do the most oxidized FA30 samples.



## Application to Paleomagnetism

The maximum intensities indicated by the CRM curves for FA90 and FA30 ( $8-50 \times 10^{-5}$  e.m.u./g) convert to values in terms of regular paleomagnetic samples of  $2.4-15 \times 10^{-5}$  e.m.u./cm<sup>3</sup>. This assumes a sample with 100% olivine. When diluted to 10% or less for a regular basalt or gabbro, the intensity reduces to a maximum  $1.5 \times 10^{-5}$  e.m.u./cm<sup>3</sup> which would be almost solely due to magnetite in olivines of composition FA15 to FA60 (Deer et al. 1966). Such values would be ordinarily swamped by the magnetization possessed by other magnetite present, and by magnetite produced during low temperature alteration of olivines, but could be resistant to much higher AF's during magnetic cleaning. The hematite magnetization, though theoretically recoverable following the thermal demagnetization of the magnetite, would probably be lost in the noise level of the instrument and the noise presented by easily remagnetizable magnetite having low coercive forces. It is concluded that CRM in oxidized olivines whether due to magnetite or hematite is of little paleomagnetic significance in common basic igneous rocks using the paleomagnetic techniques and instrumentation presently available. Magnetizations associated with TRM, however, may be another matter.





## Bibliography

- AKIMOTO, S. 1962. Magnetic properties of  $\text{FeO-Fe}_2\text{O}_3\text{-TiO}_2$  system as a basis of rock magnetism. J. Phys. Soc. Japan, 17 (Suppl. B1), pp.706.
- BANERJEE, S. 1971. New grain size limits for palaeomagnetic stability in hematite. Nature Physical Science, 232, pp. 15-16.
- BEAN, C.P. and JACOBS, I.S. 1960. Magnetization of a dilute suspension of a multidomain ferromagnetic. J. Appl. Phys., 31, pp. 1228-1230.
- BOWDEN, G.J. 1972. Detection coil systems for vibrating sample magnetometers. J. Phys. E.: Sci. Instr., 5, pp. 1115-1119.
- BOZORTH, R.M. 1951. Ferromagnetism. D. Van Nostrand Co. Ltd., Princeton, N.J., 968 pp.
- CAREY, R. and ISAAC, E.D. 1966. Magnetic domains, English Universities Press, London.
- CASE, W.E. and HARRINGTON, R.D. 1966. Calibration of vibrating-sample magnetometers. J. Res. Natl. Bur. Std. (U.S.), 70c, pp. 255-262.
- CHAMPNESS, P.E. 1968. The nature of oxidation processes in certain mineral systems. Ph.D. thesis, U. Cambridge.
- CHAMPNESS, P.E. 1970. Nucleation and growth of iron oxides in olivines,  $(\text{Mg, Fe})_2\text{SiO}_4$ . Mineral. Mag., 37, pp. 790-800.
- CHAMPNESS, P.E. and GAY, P. 1968. Oxidation of olivines. Nature, 218, pp. 157-158.
- CURIE, P. 1895. Magnetic properties of bodies at various temperatures. Ann. Chim. Phys., 5, pp. 289-405.
- DAVIS, P.M. and EVANS, M.E. Interacting single-domain properties of magnetite intergrowths. J. Geophys. Res., 81, pp. 989-994.
- DEER, W.A., HOWIE, R.A., and ZUSSMAN, J. 1962. Rock-forming minerals (5 volumes), Longmans, London.
- DICKSON, G.O., EVERITT, C.W.F., PARRY, L.G., and STACEY, F.D. 1966. Origin of thermomagnetic magnetization. Earth





- Planet. Sci. Letters, 1, pp. 222-224.
- DUNLOP, D.J. 1971. Magnetic properties of fine-particle hematite. Ann Geophys., 27, pp. 269-293.
- DUNLOP, D.J. 1972. Magnetite: behavior near the single-domain threshold. Science, 176, pp. 41-43.
- DUNLOP, D.J. 1973. Superparamagnetic and single-domain threshold sizes in magnetite. J. Geophys. Res., 78, pp. 1780-1793.
- DWIGHT, K. 1967. Experimental techniques with general applicability for the study of magnetic phenomena. J. Appl. Phys., 38, pp. 1505-1509.
- DWIGHT, K., MENYUK, N., and SMITH, D. 1958. Further development of the vibrating-coil magnetometer. J. Appl. Phys., 29, pp. 491-492.
- EVANS, M.E. 1972. Single-domain particles and TRM in rocks. Comments Earth Sci., Geophys., 2, pp. 139-148.
- EVANS, M.E. and MCELHINNY, M.W. 1969. An investigation of the origin of stable remanence in magnetite-bearing igneous rocks. J. Geomagn. Geoelectr., Kyoto, 21, pp. 757-773.
- EVANS, M.E., MCELHINNY, M.W., and GIFFORD, A.C. 1968. Single domain magnetite and high coercivities in a gabbroic intrusion. Earth Planet. Sci. Lett., 4, pp. 142-146.
- EVANS, M.E. and WAYMAN, M.L. 1970. An investigation of small magnetic particles by means of electron microscopy. Earth Planet. Sci. Lett., 9, pp. 365-370.
- EVANS, M.E. and WAYMAN, M.L. 1974. An investigation of the role of ultra-fine titanomagnetite intergrowths in palaeomagnetism. Geophys. J.R. Astr. Soc., 36, pp. 1-10.
- FONER, S. 1956. Vibrating-sample magnetometer. Rev. Sci. Instr., 27, 548 pp.
- FONER, S. 1959. Versatile and sensitive vibrating-sample magnetometer. Rev. Sci. Instr., 30, pp. 548-557.
- FONER, S. 1967. Special magnetic measurement techniques. J. Appl. Phys., 38, pp. 1510-1519.
- FONER, S. 1974 Sensitivity of vibrating-sample magnetometers -- and how to increase sensitivity if needed. Rev. Sci. Instr. 45, pp. 1181-1183.
- HAGGERTY, S.E. and BAKER, I. 1967. The alteration of olivine



in basaltic and associated lavas. Part I: High temperature alteration. *Contr. Mineral. Petr.*, 16, pp. 233-257.

HARGRAVES, R.B. and YOUNG, W.M. 1969. Source of stable remanent magnetism in Lambertville diabase. *Amer. J. Sci.*, 267, pp. 1161-1177.

HOYE, G.S. 1972. A study of the magnetic properties of synthetic ferromagnesian olivines and their oxidation products, Ph.D. thesis, U. Newcastle upon Tyne, England.

HOYE, G.S. and EVANS, M.E. 1975. Remanent magnetizations in oxidized olivines. *Geophys. J. R. Astr. Soc.*, 41, pp. 139-151.

HOYE, G.S. and O'REILLY, W. 1972. A magnetic study of ferromagnesian olivines  $(\text{Fe}_x\text{Mg}_{1-x})_2\text{SiO}_4$ ,  $0 < x < 1$ , *J. Phys. Chem. Solids*, 33, pp. 1827-1834.

HOYE, G.S. and O'REILLY, W. 1973. Low temperature oxidation of ferro-magnesian olivines -- a gravimetric and magnetic study. *Geophys. J.R. Astr. Soc.*, 33, pp. 81-92.

IRVING, E. 1964. Paleomagnetism and its application to geological and geophysical problems. Wiley-Interscience, New York, N.Y., 399 pp.

KINZIE, P.A. 1973. Thermocouple temperature measurement, Wiley-Interscience, New York, N.Y., 61 p.

KITTEL, C. 1949. Physical theory of ferromagnetic domains. *Rev. Mod. Phys.*, 21, pp. 541-583.

KOBAYASHI, K. 1959. Chemical remanent magnetization of ferromagnetic minerals and its application to rock magnetism. *J. Geomagn. Geoelectr.*, Kyoto, 10, pp. 99-117.

KOBAYASHI, K. 1961. An experimental demonstration of the production of chemical magnetization with Cu-Co alloy. *J. Geomagn. Geoelectr.*, Kyoto, 12, pp. 148-163.

McELHINNY, M.W. 1973. Palaeomagnetism and plate tectonics, Cambridge University Press, Cambridge, England, 358 pp.

MEHRA, O.P. and JACKSON, M.L. 1960. Iron oxide removal from soils and clays by a dithionite-citrate system buffered with sodium bicarbonate. *Clays and Clay Minerals*, 7, pp. 317-327.

MURTHY, G.S. 1969., Paleomagnetic studies in the Canadian Shield, Ph.d. thesis, University of Alberta.





- MURTHY, G.S., EVANS, M.E., and GOUGH, D.I. 1971. Evidence of single-domain magnetite in the Michikamau anorthosite. *Can. J. Earth Sci.*, 3, pp. 361-370.
- NAGATA, T. 1961. Rock magnetism. Maruzen, Tokyo, 1 st ed. 1953. 225 pp.
- NAGATA, T. and AKIMOTOA, S. 1961 Outline of ferromagnetism, and magnetic properties of rock-forming ferromagnetic minerals, in Nagata (1961), pp. 1-39.
- OLSEN, L.O. and FREEZE, P.D. 1964. Reference tables for the platinel II thermocouple. *J. Res. Natl. Bus. Std. (U.S.)*, 68c, pp. 263-282.
- PARK, J.K. and IRVING, E. 1970. The Mid-Atlantic Ridge near 45°N. X11. Coercivity, secondary magnetization, polarity, and thermal stability of dredge samples. *Can. J. Earth Sci.*, 7, pp. 1499-1514.
- READMAN, P.W. and O'REILLY, W. 1970. The synthesis and inversion of nonstoichiometric titanomagnetites. *Phys. Earth Planet. Int.*, 4, pp. 121-128.
- RIDING, A. 1969. Magnetic materials in oxidized olivine and their contribution to the natural remanent magnetization of rocks. The natural remanent magnetization of some Triassic red sandstones. Ph.d. thesis, U. Liverpool.
- ROQUET, J. 1954. Sur les rémanences des oxydes de fer et leur intérêt en geomagnétisme (first and second parts). *Ann. Geophys.*, 10, pp. 226-247.
- SILL, L.R. and DRENSKY, S.M. 1975. Sample temperature measurement in the PAR vibrating sample magnetometer oven. *Rev. Sci. Instr.*, 46, pp. 221-222.
- SMIT, J. and WIJN, H.P.J. 1959. Ferrites. Wiley-Interscience, New York, N.Y., 369 pp.
- SMITH, D.O. 1956. Development of a vibrating-coil magnetometer. *Rev. Sci. Instr.*, 27, pp. 261-268.
- SOFFEL, H.C. 1971. Single domain-multidomain transition in natural intermediate titanomagnetites. *Z. Geophys.*, 37, pp. 451-470.
- STACEY, F.D. 1963. The physical theory of rock magnetism. *Adv. Phys.*, 12, pp. 45-133.
- STACEY, F.D. and BANERJEE, S.K. 1974. The physical principles of rock magnetism. American Elsevier Publishing Co., Inc., New York, n.Y., 195 pp.





- STONER, E.C. and WOHLFARTH, E.P. 1948. A mechanism of magnetic hysteresis in heterogeneous alloys. Phil. Trans. Roy. Soc. London, Ser. A, 240, pp. 599-642.
- STRANGWAY, D.W., LARSON, E.E., and GOLDSTEIN, M. 1968. A possible cause of high magnetic stability in volcanic rocks. J. Geophys. Res., 73, pp. 3787-3795.
- TSVETKOV, A.I., MYASNIKOV, V.S., SCHEPOCHKINA, N.I., and MATVEYEVA, N.A. 1966. Tabular formations in titanomagnetite. Int. Geol. Rev. 8, No. 6, pp. 676-688.
- VAN HOUTEN, F.B. 1973. Origin of red beds: A review -- 1961-1972. Annual review of earth and planetary science, 1, pp. 39-61.
- WU, Y.T., FULLER, M., and SCHMIDT, V.A. 1974. Microanalysis of n.r.m. in a granodiorite intrusion. Earth Planet. Sci. Lett., 23, pp. 275-285.



## Appendix 1

### Electromagnet

The VSM electromagnet is a model 4, ESM-1002 made by O.S. Walker Co., Inc. It was designed to incorporate a model 65, ESP-1002 power supply, with a maximum output of 65 amps at 33 D.C. volts, but problems with this unit prompted the substitution of another power supply which was less powerful.

The magnetic circuit consists of two energizing coils, two flat pole pieces, and two magnet iron backing plates. Energizing coils consist of 320 turns of tape-wound aluminum encapsulated in epoxy. Each layer is interleaved with epoxy-coated mylar tape. Cooling is accomplished by water flowing around cooling fins which are epoxy-bonded to the coil edges. The 10.16 cm diameter pole pieces were machined from soft iron containing a few percent lead. They are chrome plated to prevent corrosion. At the base of the pole pieces next to the backing plates are identical ferrous shims which establish a pole gap of  $3.810 \pm 0.003$  cm ( $1.5 \pm 0.001$  in.) centrally located with respect to the energizing coils.

The whole system rests on a 1.27 cm (0.5 in.) thick square aluminum plate.



## Appendix 2

### General User's Guide to VSM

#### Positioning of the Sample

Sample positioning is not critical in that one can allow a vertical centring error of about  $\pm 0.2$  cm and still obtain a signal amplitude within 0.5% of maximum. However, in order to ensure the freest movement of the vibrating rod, and to have confidence in the results, proper orientation and alignment of the VSM parts -- and therefore of the sample -- is essential. Positioning of the sample is the last manipulation of the positioning process. It is discussed below after a description of the orientation and positioning of various components of the VSM.

The detection coil(s) must be positioned first. This procedure consists of positioning each individual coil and then the whole array. The former action, in general, only needs to be performed once. Four coils are mounted on each sliding piece in an approximately square arrangement. Horizontal distances between coil centres are fixed, but vertical distances are adjustable by means of an adjustable plate and screws at each coil (M2, M1; Fig. 11). The configuration on each sliding piece mirrors the other. After the coils are mounted, the unit comprising the sliding





pieces is slid into the grooves in the teflon pole covers. The coils at this point are centred with respect to the pole pieces. Then the coil array is rotated by rotating the pole covers in unison until the coil axes are horizontal. When the interconnecting bolts (M6, Fig. 12) are tightened, orthogonal distances between coil centres within the cubic array will be ideally 2.86 cm.

The next positioning operation involves the oven. First, the slotted positioning rails (E) and cross pieces (F1) are positioned (Fig. 6). Then the square support plate (D) bearing the geophone holder (C) is moved with respect to the positioning rail until it is exactly centred above the pole pieces (or coils); that is, directly above the hole in the plate which carries the support stand (O) for the guide tube/oven (Figs. 1 and 10). The vertical height of the oven can be adjusted by screwing the geophone holder within the square plate while the furnace is detached. A brass section screwed into the base of the holder (Fig. 1) supports the guide tube/oven (G). When the correct vertical adjustment of the geophone holder has been made, the guide tube can be screwed into place. If the forced air cooling system (I) is required, it must be maneuvered into position at this point. Once the oven is in place, the support stand can be adjusted upwards to hold it rigid.

Now the sample can be positioned. First, the geophone (B, Fig. 1) is inserted into its holder (C). Then the





vibrating rod is inserted through the top of the geophone (A). Since the rod is constrained in the horizontal plane by the guide tube, only the vertical position needs to be adjusted. This can be done by screwing the rod (A3) within the top cap (A2, Fig. 8). To ensure that the thermocouple wires (A1) are not twisted during this operation, the cap is screwed about the rod to the desired position and then fastened to the aluminum tube (B1, Fig. 6) in the geophone. Another nut can be fastened above the cap as a locking nut (A2, Fig. 8). When vertical positioning is correct, a maximum signal is obtained from the sample. This signal can be enhanced somewhat by ensuring that the rod is vibrating freely. To do this, first the whole rod assembly with magnet is rotated, and then the three leveling screws (B9, Fig. 6) at the base of the geophone housing are adjusted; correct adjustment being indicated by the signal amplitude. An estimate of the best orientation and level adjustments can also be made by observing the vibration, sound, and 'feel' of the vibrating rod. There is no provision for preventing rotation of the sample during experiments.

### Hysteresis Loops

A specific experimental procedure to be followed in producing hysteresis loops or thermomagnetic curves is at present of no advantage to future users of the instrument, since the peripheral electronic instruments will be different and some manual functions will be automated.



However, the following general procedure should hold.

1. Turn on instruments at least ten minutes before use.
2. Turn on water for the electromagnet.
3. Set up the x-y plotter. Determine x-scale.
4. Weigh the sample.
5. Insert sample in appropriate holder. If the sample is a powder, pack it tightly, and determine its height, width, and volume, and its centre with respect to the base of the holder. A layer of KBr or other suitable material can be packed on top to prevent the sample from loosening during vibration.
6. Secure the holder on the end of the rod.
7. Insert the rod into the guide tube and adjust its vertical position so that the sample is centred in the coil array. Lock into position with the top nut.
8. Turn on the oscillator to vibrate the rod. To obtain the maximum signal the rod must first be rotated into a position of least resistance and then leveled (see 'Positioning of the Sample' above).
9. Begin hysteresis curve at zero applied field. Increase field smoothly, using an instrument time constant commensurate with the rate of increase, until the maximum desired field is attained. Reduce field. At zero current reverse the field and increase it in the opposite direction until a field of the same magnitude as that attained in the positive direction is produced. Decrease field. At zero current again reverse the field



and build to the previous maximum.

10. Several hysteresis loops may be made; but in order to start again from the demagnetized state the sample must either be completely remixed or else cycled through loops of even decreasing amplitude.
11. Either prior to or after the experiment a hysteresis loop should be obtained for the empty sample holder.

### Thermomagnetic Curves

1. Follow steps (1) to (7) under 'hysteresis loops'.
  2. Feed liquid nitrogen through the detection coils and cooling system.
  3. Record the temperature at the thermocouple cold junction and monitor throughout the run.
  4. Mark the baseline on the x-y plotter when no field is applied.
  5. Begin vibrating sample with field set at a constant value (usually maximum).
  6. Obtain a maximum signal as indicated by the procedure under 'positioning of the sample' above.
  7. Heat sample at such a rate that sample and thermocouple will have a known constant temperature difference.
- Discontinuous recording might be best, since it allows sample and thermocouple to come to thermal equilibrium before a reading is taken. In either case readings must be taken periodically in order to obtain a calibrated





temperature scale.

8. At the maximum desired temperature turn off the oven and record the cold junction temperature.
9. Continue to take readings while the sample cools.
10. At room temperature again record the baseline with the field turned off.
11. Record the thermocouple cold junction temperature.
12. A dry run with an empty sample holder is not critical, since one is usually just concerned with determining the Curie point(s) and the general shape of the curve.



### Appendix 3

#### Determination of $J_r/J_s$ for Magnetite Samples

##### Calculation of $J_s$

From the hysteresis curves values of  $J$  and  $H$  were tabulated at regular intervals between 3 and 5.4 kOe (Dunlop 1973) together with errors.  $J$  (in terms of the arbitrary units called divisions) was then plotted against  $1/H$  and extrapolated to zero by linear regression (Fig. 43). The regression of both  $J$  on  $1/H$  and  $1/H$  on  $J$  was obtained for both normal and reversed curves of the approach to saturation. Intercept values for the normal case were simply averaged; the error being the r.m.s. of the individual errors. The same was done for the reversed case. Then the weighted mean and error were calculated from the two determinations. These values are given below (Table 17).

##### Calculation of $J_r$

$H_i = H_e - NJ$ , where  $H_i$  is the internal field,  $H_e$ , the external applied field, and  $NJ$ , the demagnetizing field, --  $N$  being the demagnetization factor. We are interested in the value of  $J$  when  $H_i = 0$ . One merely constructs a new axis to satisfy this condition. Where this axis crosses the curve,  $H_e = NPJ_r$  with  $1/NP$  being the slope of the new axis.



Since we are only interested in determining the ratio  $J_r/J_s$ ,  $J_r$  need only be found in terms of the same arbitrary units as  $J$  (ie. divisions). To find  $J$  the following procedure was used:

1. The slope of the new axis was determined by calculating  $N$  and  $P$  (the packing factor, see Table 17).
2. The old axis was calibrated in terms of  $j$  gauss/div. by assuming the mean saturation divisions (determined above by the Bean and Jacobs (1960) extrapolation) to be equal to the theoretical magnetization value for magnetite ( $\approx 480$  gauss).
3. The slope was equated to  $J/H$ , -- that is

$$\frac{1}{NP} = \frac{J}{H} \quad (1)$$

--and the value at  $\pm H$  determined for  $\pm y$  vertical divisions (refer to Fig. 44). Since  $J = jy$  ,

$$H = (jy)NP \text{ Oe} \quad (2)$$

(Oe numerically equivalent to gauss in e.m.u. system)

4.  $H$  was converted to  $x$  divisions by means of the formula

$$x = \frac{H - h}{fg} , \quad (3)$$

where  $f, g, h$  are scale factors (Table 19, Appendix 5).



5. From  $x$  and  $y$  the new axis was plotted and the  $J_r$  divisions measured for both normal and reversed curves (see Fig. 44).

Values of  $J_r/J_s$  were calculated separately for normal and reversed curves and simply meaned together (Table 17).







Fig. 43. The approach to saturation of the normal (solid lines and dots) and reversed (dashed lines, open circles) portions of the hysteresis curves of the magnetite samples (see Fig. 17) as a function of  $1/H$ . This is the method of Bean and Jacobs (1960). Only the experimental points within the  $H$  range of 3 to 6 kOe (Dunlop 1973) have been considered in computing the lines of linear regression. For M3 only the last four points have been used.

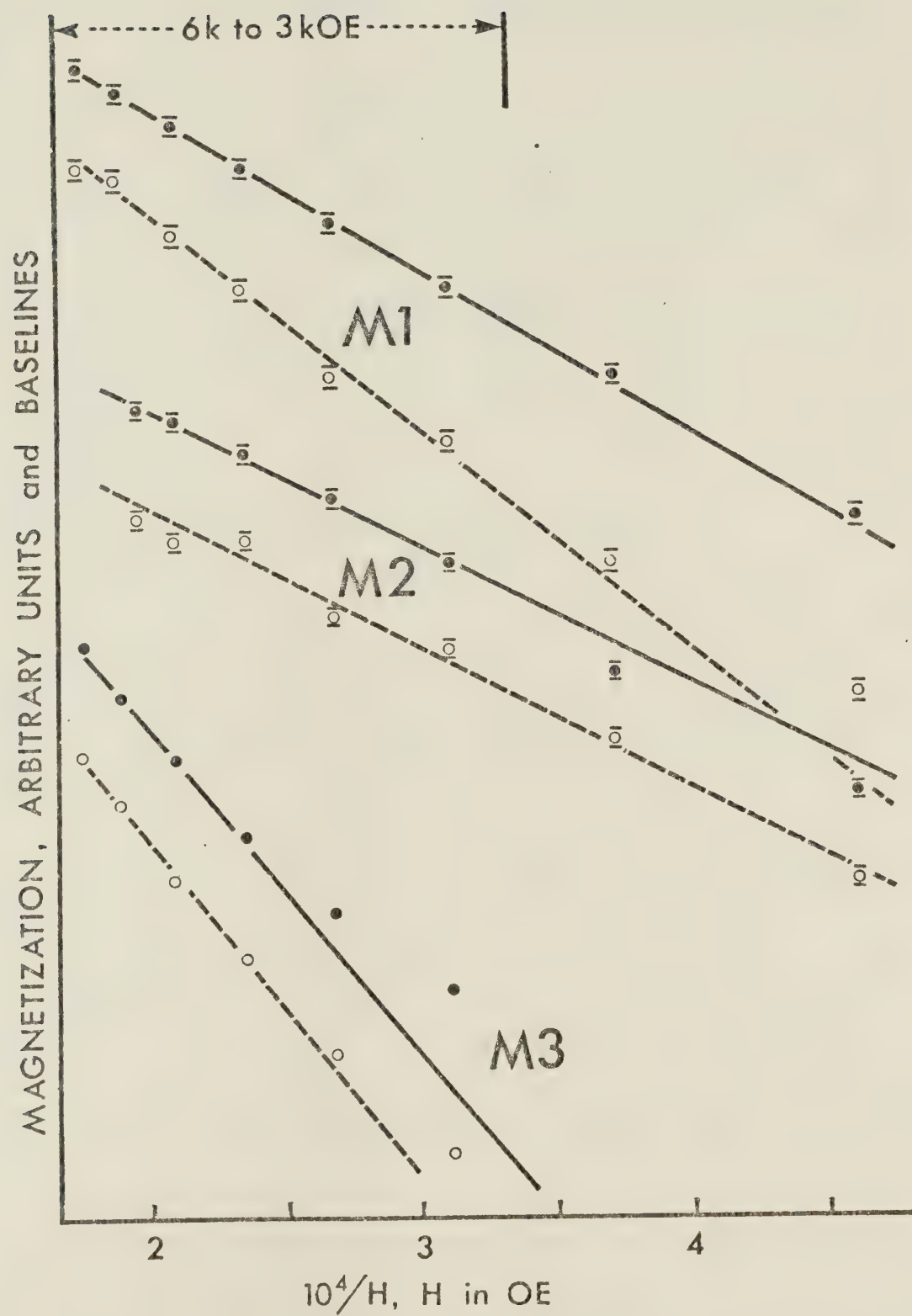




TABLE 17.

BASIC AND DERIVED DATA OF THE MAGNETITE SAMPLES  
AND HYSTERESIS CURVES USED IN THE CALCULATION OF  $J_r/J_s$

Parameter	M1	M2	M3
Data for derivation of demagnetization factor, $N_a$			
$a(\text{cm})^1$	$0.450 \pm 0.015(a)$	$0.450 \pm 0.015(a)$	$0.450 \pm 0.015(a)$
$c(\text{cm})^1$	$0.475 \pm 0.025(a)$	$0.400 \pm 0.020(a)$	$0.475 \pm 0.025(a)$
$N_a^2(1)$	$0.340 \pm 0.001(a)$	$0.318 \pm 0.003(a)$	$0.340 \pm 0.001(a)$
(2)	0.340	0.317	0.340
Data for derivation of packing factor, P			
$\rho(\text{g/cm}^3)^3$	$5.200 \pm 0.001$	$5.200 \pm 0.001$	$5.200 \pm 0.001$
volume ( $\text{cm}^3$ )	$0.551 \pm 0.034(a)$	$0.464 \pm 0.038(a)$	$0.551 \pm 0.034(a)$
mass <sub>a</sub> (g) <sup>4</sup>	$0.479 \pm 0.004(a)$	$0.306 \pm 0.004(a)$	$0.028 \pm 0.004(a)$
mass <sub>t</sub> (g) <sup>5</sup>	$2.87 \pm 0.18$	$2.41 \pm 0.08$	$2.87 \pm 0.18$
P	$0.167 \pm 0.012(a)$	$0.127 \pm 0.012(a)$	$0.0098 \pm 0.0020(a)$
Additional data for derivation of $J_r$ and $J_r/J_s$			
slope <sup>6</sup>	$1.40 \pm 0.10$	$1.98 \pm 0.21$	$23.92 \pm 4.98$
$J_s(\text{G})^7$	480	480	480
$J_s(\text{div.})^8$	$42.5 \pm 0.3$	$41.2 \pm 0.1$	$51.9 \pm 0.3$
$y(\text{div.})^9$	50	50	50
f,g,h	(see Table 19, Appendix 5)		
$j(\text{G/div.})^{10}$	$11.3 \pm 0.1$	$11.6 \pm 0.0$	$9.2 \pm 0.1$





$x(\text{div.})^{11}$	3.66 $\pm 0.29$ (a)	2.65 $\pm 0.30$ (a)	0.11 $\pm 0.04$ (a)
$J_r(\text{div.})$ norm. <sup>12</sup>	19.7 $\pm 0.3$	19.1 $\pm 0.4$	13.8 $\pm 0.1$
$J_r(\text{div.})$ rev. <sup>12</sup>	19.8 $\pm 0.3$	19.7 $\pm 0.3$	13.6 $\pm 0.1$
$J_r/J_{s13}$ norm. <sup>13</sup>	0.468 $\pm 0.008$	0.462 $\pm 0.010$	0.267 $\pm 0.003$
$J_r/J_{s13}$ rev. <sup>13</sup>	0.460 $\pm 0.007$	0.479 $\pm 0.007$	0.260 $\pm 0.003$
$J_r/J_{s13}$ mean	0.46 $\pm 0.01$	0.47 $\pm 0.01$	0.26 $\pm 0.00$

## NOTES:

Errors are standard deviations or absolute errors (a).

<sup>1</sup> 'a' and 'c' are the equatorial and polar semi-axes of the sample. M1 and M3 approximate prolate spheroids and M2 approximates an oblate spheroid.

<sup>2</sup>  $N_a$  along the equatorial axis, was calculated for comparison purposes by using the approximate formulas derived from a power series (1) and by using the exact formulas (2) given below:

prolate spheroid

$$N_c = 4\pi(r^2-1)^{-1} \left\{ r(r^2-1)^{-\frac{1}{2}} \ln[r+(r^2-1)^{\frac{1}{2}}] - 1 \right\}$$

$$N_a = 4\pi(1-N_c)/2, \text{ where } r = c/a$$

oblate spheroid

$$N_c = 4\pi r^2 (r^2-1)^{-1} \left\{ 1 - (r^2-1)^{-\frac{1}{2}} \sin^{-1}[r^{-1}(r^2-1)^{\frac{1}{2}}] \right\}$$

$$N_a = 4\pi(1-N_c)/2, \text{ where } r = a/c$$

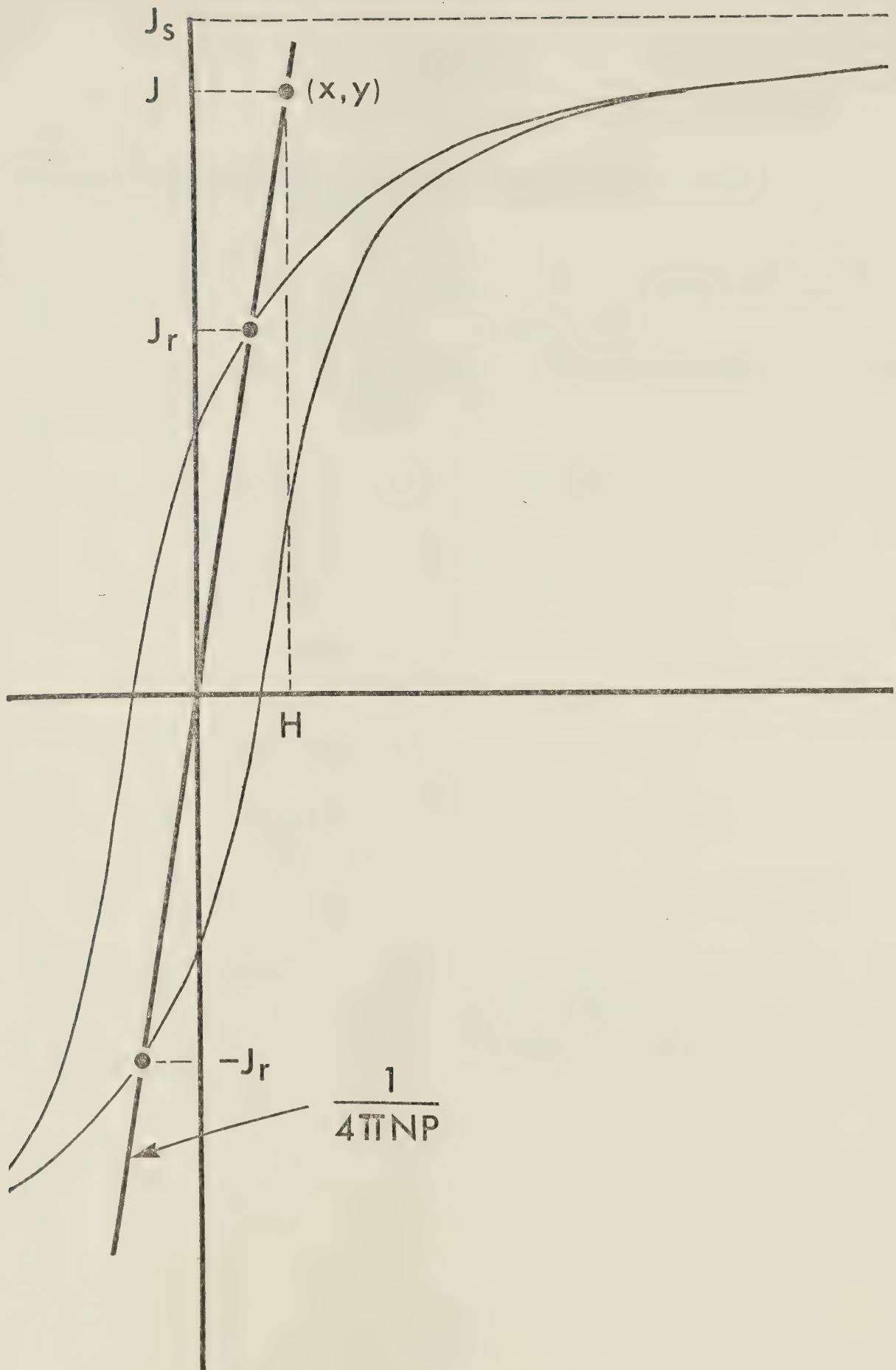


- 3 X-ray density data at 22°C.
- 4 The actual measured mass.
- 5 The theoretical mass of a solid magnetite sample calculated from the theoretical density and measured volume.
- 6 The slope of the new axis equivalent to  $1/NP$ .
- 7 Approximate theoretical saturation magnetization value for magnetite ( $\pm 0.2\%$ ).
- 8 Weighted mean of the values determined for the normal and reversed curves by the method of Bean and Jacobs (1960).
- 9  $y$  is arbitrary.
- 10 Calculated from  $J_s(G)/J_s(\text{div.})$ .
- 11 Calculated from equations (1), (2), and (3) of this Appendix.  $x$  and  $y$  are used to construct the slope of the new axis (see Fig. 44).
- 12 The vertical divisions at remanent saturation are determined from the intersection of the new axis with the normal and reversed portions of the hysteresis curve.
- 13 The normal and reversed  $J_r/J_s$  ratios are meaned.





Fig. 44. Some parameters used in the determination of  $J_r$  for the magnetite hysteresis curves. Equations are given in Appendix 3.







## Appendix 4

Table 18. Chemical analysis of calibration  
samples (wt. %)

Element	Iron <sup>1</sup>	Nickel <sup>2</sup>
Fe	99.567	0.002
Ni	0.078	>99.983
Cu	0.178	<0.001
W	0.143	--
Mn	0.014	0.001
Co	0.012	<0.001
Si	0.008	<0.001
C	---	0.01

<sup>1</sup> Iron was analyzed by atomic absorption and X-ray fluorescence. The latter method reveals only Fe, W, and Cu (M. Wayman, personnel communication).

<sup>2</sup> Nickel (270) analysis by Huntington Alloys, Inc., Huntington, West Virginia. Nickel also contains <0.001% of S, Cr, Ti, and Mg.



## Appendix 5

### Calculation of the Calibration Constant

#### Derivation of the Formula

The following, up to equation (9), is generally after Case and Harrington (1966).

The internal field ( $H_i$ ) of a finite sample can be defined in terms of the external field ( $H_e$ ) and the demagnetizing field ( $NJ$ ) thus

$$H_i = H_e - NJ \quad (1)$$

where  $N$  is the demagnetization factor and  $J$ , the magnetization. For a material in the demagnetized state the following relation holds

$$J = (\mu - 1)H_i \quad (2)$$

where  $\mu$  is the relative permeability. Substituting (1) into (2),



$$J = \frac{H_e}{(\mu-1)^{-1} + N} . \quad (3)$$

For the calibration sample, equation (3) can be written

$$J_C = \frac{H_C}{(\mu-1)^{-1} + N} , \quad (4)$$

or as

$$\Delta J_C = \frac{\Delta H_C}{(\mu-1)^{-1} + N} , \quad (5)$$

since we are concerned with the linear segment of a curve which essentially goes through the origin.

The voltage ( $E_C$ ) induced in the detection coils is proportional to the magnetization ( $J_C$ ) of the calibration sample. Hence

$$E_C = KV_C J_C$$

where  $V_C$  is the calibration sample volume and  $K$ , the proportionality constant. This equation too may be written after the manner of equation (5) as





$$\Delta E_c = KV_c \Delta J_c \quad (6)$$

substituting (5) into (6) and rearranging terms

$$K = \frac{[(\mu-1)^{-1} + N] \Delta E_c}{V_c \Delta H_c} \quad (7)$$

K now being designated the calibration constant.

For an unknown sample

$$E_o = KV_o J_o \quad (8)$$

where  $E_o$  is the coil voltage,  $V_o$ , the sample volume, and  $J_o$ , the sample magnetization. Rearranging (8) we obtain

$$J_o = \frac{E_o}{KV_o} \quad (9)$$

from which, in conjunction with equation (7), one can derive the magnetization of the unknown. The volumes are generally written in terms of the diameters ( $D_o^3, D_o^3$ ), since use of the volumes requires precise knowledge of the densities, which can only be accurately determined from nearly spherical samples. In using the diameters the calibration constant will be designated  $K_1$ , which differs by a factor  $\pi/6$  from K.



The above derivation assumes that there is no hysteresis. This assumption is essentially correct for high permeability materials like fairly pure iron; there being only a slight remanence at zero applied field.

It should also be noted that  $\Delta E_C$  in the present work is not the actual voltage induced in the coils but a value which depends on an unknown amplification factor.

The quantities  $\Delta E_C$  and  $\Delta H_C$  can be put in terms of quantities derived from the hysteresis curves. Since we are only concerned with the ratio of  $\Delta E_C / \Delta H_C$ , an arbitrary value on the horizontal field axis can be chosen for which to relate voltage and field values. If we call this value  $x$  divisions, the corresponding value on the vertical axis is  $y$  divisions related to  $x$  by means of the initial slope ( $s$ ) of the linear portion of the curve, that is

$$y = sx. \quad (10)$$

Now

$$\frac{\Delta E_C}{E_m} = \frac{y}{y_m} \quad (11)$$

where  $E_m$  is the maximum voltage reading, and  $y_m$  is the corresponding number of divisions. Substituting (10) into (11) and rearranging



$$\Delta E_c = \frac{E_m \times S}{Y_m} \quad (12)$$

These values are given in Table 19. Derivation of  $\Delta H_c$  is just a matter of converting the x divisions to a field value by means of the equation

$$\Delta H_c = xfg + h \quad (13)$$

where f, g and h are scale values given in Table 17. For calculating  $J_0$  for nickel, the values of  $D_0$  and  $E_0$  can be found in Table 20.

### Demagnetization Factor

For a nearly spherical oblate spheroid the approximate formula for the demagnetization factor is

$$N_a = 4\pi \left( \frac{1}{3} - \frac{1}{15} \epsilon^2 - \frac{4}{105} \epsilon^4 + \dots \right) , \quad (14)$$

where  $\epsilon^2 = 1 - \left( \frac{c}{a} \right)^2 \ll 1$  ,

a = the equatorial semi-axis along the applied field, and  
c = the polar semi-axis.

Values of 'a', 'c', and  $N_a$  are given in Table 19.



Table 19. Basic and derived data of the iron calibration samples and hysteresis curves

Parameter	FE 1	FE 2	FE 3
a <sup>1</sup> (cm)	0.1563 ±0.0012	0.1581 ±0.0009	0.1582 ±0.0009
C <sup>1</sup> (cm)	0.1510 ±0.0002	0.1488 ±0.0004	0.1547 ±0.0006
N <sub>a</sub> <sup>1</sup>	0.3288 ±0.0010	0.3253 ±0.0007	0.3304 ±0.0009
N <sub>C</sub> <sup>2</sup>	0.3311 ±0.0010	0.3293 ±0.0007	0.3318 ±0.0009
μ <sup>3</sup>	4000	4000	4000
ΔE <sub>m</sub> (mV) <sup>4</sup>	1.835 ±0.010	1.823 ±0.010	1.835 ±0.010
y <sub>m</sub> (div.) <sup>5</sup>	42.5 ±0.1	41.9 ±0.1	42.5 ± 0.1
s	0.811 ±0.002	0.794 ±0.003	0.806 ±0.001
x (div.) <sup>6</sup>	50	50	50
ΔE <sub>C</sub> (mV)	1.751 ±0.011	1.726 ±0.013	1.740 ±0.011
f (mV/div.)	0.998 ±0.003	0.998 ±0.003	0.998 ±0.003
g (Oe/mV)	105	105	105
h (Oe) <sup>7</sup>	76	76	76
ΔH <sub>C</sub> (Oe)	5300 ±20	5300 ±20	5300 ±20
D <sub>C</sub> (cm) <sup>8</sup>	0.3117 ±0.0037	0.3143 ±0.0058	0.3154 ±0.0030
D <sub>C</sub> <sup>3</sup> (cm <sup>3</sup> )	0.0303 ±0.0011	0.0311 ±0.0017	0.0314 ±0.0009
mass (g) <sup>9</sup>	0.125 ±0.000	0.130 ±0.001	0.130 ±0.000
ρ (g/cm <sup>3</sup> ) <sup>10</sup>	7.8748 ±0.0041	7.8748 ±0.0041	7.8748 ±0.0041
J (G) <sup>11</sup>	1714		

NOTES: Some symbols in the Table are defined elsewhere in this appendix. Errors are standard deviations.

<sup>1</sup> Demagnetization factor (N<sub>a</sub>) along the applied field





direction calculated from equation (14). The samples are almost spherical except for a slightly flattened spot marking the polar 'end', which is due to the elimination of a nipple during machining. Consequently the distribution of diameter determinations is skewed. 'a' and 'c' values are separate averages of high and low values; the distribution being divided in two using personal judgement.

- <sup>2</sup> The demagnetization factor used is an average of that for a sphere and  $N_a$ .
- <sup>3</sup> This is a rounded-off linearly interpolated value for  $\mu$  between 98.5% (2000) and 99.91% (5000) pure iron.
- <sup>4</sup>  $E_m$  is the average of the positive and negative maximum voltage readings on the hysteresis curves.
- <sup>5</sup>  $y_m$  is the average of the positive and negative distances (divisions) at the maximum voltage readings. The divisions (div.) along the vertical and horizontal axes are equal (0.1 inches = div.)
- <sup>6</sup>  $x$  is an arbitrary value.
- <sup>7</sup>  $h$  is an intercept value of a straight line fitted to a certain portion of the Hall probe calibration curve of voltage vs. field. The probe was calibrated with a Rawson-Lush gaussmeter.
- <sup>8</sup> Average calculated from 50 measurements.
- <sup>9</sup> Average calculated from 7 measurements.
- <sup>10</sup> X-ray density data at 25°C.
- <sup>11</sup> Value at 20°C.



## Appendix 6

Table 20. Basic data of nickel calibration samples

Parameter	NI 1	NI 2
$E_O$ (mV) <sup>1</sup>	0.658 ±0.010	0.645 ±0.010
$y_O$ (div.) <sup>2</sup>	41.2 ±0.1	40.0 ±0.1
$s$ <sup>3</sup>	2.160 ±0.011	2.071 ±0.022
$D_O$ (cm) <sup>4</sup>	0.3133 ±0.0029	0.3157 ±0.0038
$D_O^3$ (cm <sup>3</sup> ) <sup>5</sup>	0.03074±0.00086	0.03148±0.00112
mass(g) <sup>6</sup>	0.144 ±0.001	0.148 ±0.001
$\rho$ (g/cm <sup>3</sup> ) <sup>7</sup>	8.9117 ±0.0038	8.9117 ±0.0038
$J_S$ (G) <sup>8</sup>	484	

NOTES: Some symbols are explained in Appendix 5. Errors are standard deviations.

<sup>1</sup>  $E_O = E_m$  (Table 19, Appendix 5), and generally stands for the voltage induced by an unknown sample. Nickel was used for the unknown sample in order to test the VSM.

<sup>2</sup>  $y_O = y_m$ .

<sup>3</sup> Initial slope of the linear portion of the hysteresis curve.

<sup>4</sup>  $D_O$  is the average of 50 measurements of the sample diameter.

<sup>5</sup>  $D_O^3$  rather than  $V_O$  is used in equation (8).

<sup>6</sup> Average of 7 measurements.

<sup>7</sup> X-ray density data at 25°C.

<sup>8</sup> Value at 20°C.



## Appendix 7

Table 21. Resume of experimental work on olivines

Sample	Experiment (exp.)	Comments
FA30	Grinding <sup>1</sup> for 8 hrs.	Ground 2 yrs. prior to exp. by Hoyer.
FA30A	CRM <sup>2</sup> ( 6060 min.) <sup>14</sup> AFd <sup>3</sup> , IRMb <sup>4</sup>	dry test run of method. 240 min. run: 550°C for 2 min. 1000 min. run: O <sub>2</sub> and oven switched off. 6020 min. run: O <sub>2</sub> ran out. <sup>14</sup>
FA30B	IRM <sup>5</sup>  Cd <sup>6</sup> (for 16.8 hrs.) IRM <sup>5</sup> Cd <sup>6</sup> (tot. 35.8 hrs.), IRM <sup>5</sup> Bd <sup>7</sup> (-10 kOe) Cd <sup>6</sup> (tot. 83.3 hrs.) IRM <sup>5</sup> , Bd <sup>7</sup> (-0.8 kOe)	test run using DC <sup>6</sup> on sample of Hoyer and Evans (1975). Previous history: CRM <sup>2</sup> (2190 min.), AFd <sup>13</sup> , ARM <sup>8</sup> AFd <sup>9</sup> , IRMb <sup>4</sup> , AFd <sup>10</sup>
FA50	Grinding <sup>1</sup> for 8.5 hrs.	dry grinding for 8-10 min.
FA50A	IRMb <sup>4</sup> , Bd <sup>7</sup> (-0.58 kOe), AFd <sup>10</sup> CRM <sup>2</sup> (8015 min.)	sample packed 'normally'.
FA50B	IRMb <sup>4</sup> , Bd <sup>7</sup> , (-.58 kOe), AFd <sup>10</sup> CRM <sup>2</sup> (8015 min.)	sample packed tightly.
FA50C	IRM <sup>4</sup>  Bd <sup>7</sup> (-0.58 kOe), AFd <sup>10</sup>  CRM <sup>2</sup> (8015 min.)  After ea. oxid. step:  AFd <sup>3</sup> , IRMb <sup>4</sup> , Bd <sup>7</sup> , AFd <sup>10</sup> .  Cd <sup>11</sup> (7 min.) IRMb <sup>4</sup> , AFd <sup>12</sup>	sample packed 'normally'. C run with A and B after first oxidation step. 80 min. step: T may have reached 550°C for several min. 2120 min. run: 10.8 Oe field for unknown time. 4000 min. run: 100 Oe for 0.5 sec.





Cd <sup>11</sup> (15 min.)	tot. time: 22 min.
IRMb <sup>4</sup> , Bd <sup>7</sup> (-0.7 kOe)	
IRM <sup>5</sup> , AFd <sup>12</sup>	
Cd <sup>11</sup> (30 min.)	tot. time: 52 min.
IRM <sup>4</sup> , Bd <sup>7</sup> (-0.9 kOe)	
IRM <sup>4</sup> , AFd <sup>12</sup>	

---

FA90	Grinding <sup>1</sup> for 8 hrs. CRM <sup>2</sup> (8008 min.) Bd (-0.5 kOe), AFd <sup>10</sup> IRMb <sup>4</sup> , AFd <sup>12</sup> IRMb <sup>4</sup> , Bd <sup>7</sup> (-10 kOe)	>4320 min. step: 100 Oe
FA90A	Cd <sup>6</sup> (11.8 hrs.), IRMb <sup>4</sup> Cd <sup>6</sup> (3.3 hrs.), IRMb <sup>4</sup> Cd <sup>6</sup> (13.7 hrs.), IRMb <sup>4</sup>	piece of CRM sample. tot. time: 15.1 hrs. tot. time: 28.8 hrs.
FA90B	IRMb <sup>4</sup>	piece from CRM sample top(?)
FA90C	IRMb <sup>4</sup>	piece from CRM sample middle
FA90D	IRMb <sup>4</sup>	piece from CRM sample bottom(?)

---

- <sup>1</sup> Olivine pellets ground in dry acetone.
- <sup>2</sup> CRM by oxidation for different time periods at constant temperature (500°C) in O<sub>2</sub> gas (99.95%) with bias field of 10 Oe. Cooled in He<sub>2</sub> gas (99.995%) with bias field switched off.
- <sup>3</sup> AF demagnetization (AFd) of CRM in 1.8 kOe.
- <sup>4</sup> IRM build-up (IRMb) in fields to 10 kOe.
- <sup>5</sup> IRM produced in 10 kOe.
- <sup>6</sup> Chemical demagnetization by diammonium citrate (DC) solution.
- <sup>7</sup> Backfield demagnetization (Bd) of IRM in steps.
- <sup>8</sup> ARM produced in 10 Oe field and 1.8 kOe AF.
- <sup>9</sup> AF demagnetization (AFd) of ARM in steps to 1.8 kOe.
- <sup>10</sup> AF demagnetization (AFd) of IRM in 1.8 kOe.
- <sup>11</sup> Chemical demagnetization (Cd) by dithionite-citrate-bicarbonate method (Mehra and Jackson 1960).
- <sup>12</sup> AF demagnetization (AFd) of IRM in steps to 1.8 kOe.
- <sup>13</sup> AF demagnetization (AFd) of CRM in steps to 1.8 kOe.
- <sup>14</sup> Effective oxidation time is between 4920 and 6020 min. due to oxygen running out.

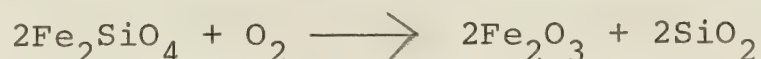


## Appendix 8

### Estimating the amount of single domain hematite in terms of the total possible hematite

#### Calculation of the Maximum Possible sd Hematite that could be Produced from a (Mg,Fe) Olivine

Only the fayalite component ( $\text{Fe}_2\text{SiO}_4$ ) will oxidize to produce hematite, and this according to the following formula:



The total mass of the fayalite component ( $M_{\text{fa}}$ ) present can be calculated from the molecular weights (MW) of the fayalite ( $MW_{\text{fa}}$ ) and forsterite ( $MW_{\text{fo}}$ ), the molar percentage of fayalite ( $x$ ), and the mass of the sample ( $M_s$ ) by the following formula:

$$M_{\text{fa}} = \frac{x \cdot MW_{\text{fa}} \cdot M_s}{x \cdot MW_{\text{fa}} + (1-x)MW_{\text{fo}}}$$

The total mass of hematite produced is just a proportion of  $M_{\text{fa}}$  according to the ratio of the MW's of fayalite and hematite ( $MW_{\text{h}}$ ) given in the chemical equation;



that is,

$$M_h = \frac{MW_h \cdot M_{fa}}{MW_{fa}}$$

### Calculation of the Actual Hematite Present

$M_h$  can be converted to a magnetic moment by multiplying it by the saturation remanence of hematite at room temperature. For present purposes this value will be taken as 0.12 e.m.u./g -- a value estimated from Roquet's (1954) curve at 30 kOe given in Irving (1964). The actual hematite remanence in the sample can be approximately determined by measuring the increase in moment in the IRM build-up curves between 3 and 10 kOe, and extrapolating this value by means of the slope to 0 and 30 kOe. The percentage of the actual moment to the total theoretical hematite moment can be taken as a measure of the proportion of actual stable sd hematite to the theoretical maximum sd hematite. It is assumed that all hematite mentioned above is in the form of non-interacting sd grains. In this case the ratio of saturation remanence to true saturation is 0.5, and the actual and maximum possible values are directly comparable.

















**B30217**